Doctoral Thesis

Wide-area Broadband Private Wireless Communication System

Kiminobu Makino

Graduate School of Informatics, Kyoto University

March 2024

Preface

Since radio waves are a limited, scarce, and public resource, they are shared and used for various purposes, such as communications and broadcasting. In recent years, since Internet traffic has increased explosively with the development of information and communication technology (ICT), in particular, the demand for wireless communication using radio waves is increasing. Conventionally, mobile terminals and base stations have often been connected through active user actions. However, wireless communication in various forms is increasing, such as connections with Internet of Things (IoT) devices, machine-to-machine (M2M) communication, vehicle-to-everything (V2X) communication, etc. Therefore, the design of wireless communication systems tailored to the application is needed.

In particular, R&D is actively underway in private communication systems that users can develop suitable for the application or install based on the desired standards ideal for the application. This thesis proposes the R&D of two private communication systems based on usage and frequency allocation conditions and evaluates their performance.

The first private communication system is the wireless regional area network (WRAN), a wide-area private communication system that uses the very-high-frequency (VHF) band. The VHF band is a lower frequency band than the UHF band, which is used for public (cellular) communications or field pick-up unit (FPU) systems described below. Wireless communications that use low-frequency bands have characteristics of relatively low power attenuation, making it easy to secure a wide coverage area. In addition, it is relatively less susceptible to the effects of Doppler shift, making it easier to ensure movement resistance. On the other hand, the power of delayed waves with long delay times is also not attenuated and affects the desired wave. Therefore, transmission performance tends to degrade due to frequency-selective fading caused by multipath waves.

Taking these characteristics into consideration, R&D of wide-area private communication systems is ongoing. It is assumed that it will be used in various conditions, such as in mountainous areas, where it is difficult to install a base station, and when it is difficult to install a base station during a disaster. In fact, it is being introduced in some government offices. However, performance evaluations under system-specific conditions, such as the strong influence of frequency-selective fading, have not been sufficiently conducted. Furthermore, for a single base station and mobile station pair, the maximum transmission distance that can be stably transmitted is about 10 km.

There is a multi-hop transmission technology that repeats relaying using relay stations to realize a wider area system; however, the throughput and coverage area of this system have not been sufficiently evaluated. This thesis proposed several receiver designs for this system and conducted a comparative evaluation through computer simulations in an environment with strong frequency-selective fading, which is unique to the VHF band. The thesis also evaluated its performance using a prototype equipped with the proposed method through laboratory experiments to simulate the same environment. Furthermore, the thesis evaluated the increasing transmission distance and decreasing transmission rate during multihop by combining the experimental results with theoretical values about the system.

The second private communication system is the next-generation FPU system that uses a wide-band of 17.18 MHz. Next-generation FPUs use high-frequency of 1.2 GHz/2.3 GHz and wide band. Since it uses a wide-band, it is expected to realize ultra-high capacity wireless communication. On the other hand, since it uses a high-frequency band, it is strongly affected by Doppler shift, and the propagation environment changes drastically in mobile transmission. Additionally, because it has a wide bandwidth, it is also affected by frequency selectivity within the band.

With its ultra-high capacity, next-generation FPUs are being R&D as a mobile transmission system for high-definition video for ultra-high-definition (UHD) broadcasts of marathons, road races, and other events. In particular, to increase capacity, singular value decomposition (SVD)-multiple-input multiple-output (MIMO) is used, which uses four antennas each for the base station and mobile station and spatially multiplexes the data for transmission. Furthermore, adaptive transmission control (ATC) is also used, which achieves both stable and high-speed transmission by changing transmission parameters according to the ever-changing propagation environment. In SVD-MIMO, transmitting (Tx) and receiving (Rx) weight matrices are used for transmission. These weight matrices have degradation that cannot be avoided due to system design. However, conventional ATC was based on the channel quality when transmitting with an ideal weight matrix, resulting in significant performance degradation. This thesis proposed a method to estimate degraded channel quality and perform ATC based on the estimated one and evaluated it using computer simulation.

Furthermore, the thesis proposed a method to compensate for degraded Tx weight matrices using machine learning (ML). Similarly, the thesis proposed simplified channel metrics to evaluate the compensation performance of ML and a method for creating training data. The validity of selecting optimal parameters using simplified metrics was evaluated by computer simulation. Furthermore, this thesis showed a computer

simulation evaluation using the parameters selected to be optimal.

This thesis described the prospects for platforms toward the use of various applications based on each private communication system's proposed methods and study results. First, this thesis described a cyber-physical system (CPS) platform that uses WRAN and other communication systems and applies them to various areas. In agriculture or disaster prevention, since the communication area is vast or there is often no need to connect to the Internet, WRAN, a wide-area private communication system, can be at the core system. Similarly, this thesis described a program production platform using next-generation FPUs and other communication systems. In the field of television (TV) program production, efforts of remote program production using Internet protocol (IP) lines or program production using the public cloud or the Internet lines have begun. Conventional FPUs are insufficient for wirelessly transmitting large amounts of video. Therefore, the program production platform is expected to be realized by combining the next-generation FPU with other communication systems.

The chapters of this thesis are listed as follows. Chapter 1 described the circumstances surrounding the research content for each private communication system covered in this thesis. Chapter 2 described the use cases and specifications of each private communication. Chapter 3 proposed methods for single-hop and multi-hop transmission for WRAN and evaluated the performance. Chapter 4 proposed improvement methods of ATC for the next-generation FPU and evaluated the performance. Chapter 5 similarly proposed a compensation method using ML for Tx weight matrices and evaluated the performance [5]. Chapter 6 discussed the prospects for wireless communication design toward the realization of platforms that can be used in various applications based on the study results in the previous chapters. Finally, Chapter 7 concluded this thesis.

Acknowledgement

First of all, I would like to express my sincere gratitude to my supervisor, Professor Hiroshi Harada, for his helpful guidance and support in my research. Without his persistent help and constructive instruction, this work would have never been completed.

I also express my deep appreciation to Professor Eiji Oki and Professor Ken Umeno at the Graduate School of Informatics and Professor Kimihito Nakamura at the Graduate School of Agriculture for their valuable advice and incisive comments on this thesis. Their advice and comments have been a great help in improving this thesis.

I express my great gratitude to Associate Professor Keiichi Mizutani for his strong support and guidance. Without his consistent and constructive guidance, I would not have reached the starting line of this thesis.

I would also like to thank Dr. Takeshi Matsumura for his helpful comments on my research.

I am deeply grateful to Mr. Takayuki Nakagawa and other former colleagues at NHK Science & Technology Research Laboratories for helpful discussions and advices on my research and to Mr. Taro Miyazaki for his excellent guidance in my mastering machine learning technologies.

I am also very grateful to Assistant Professor Yusuke Koda and other members of the Digital Communication Laboratory of the Graduate School of Informatics, Kyoto University.

I thank everyone at the Kyoto University School of Platforms Office for their exceptional support during my course studies.

I would also like to thank Dr. Hiroshi Abe and others at Toyota Motor Corporation and Dr. Kazuhiro Otsuki and others at NHK, for accommodating me about working hours, working location, etc., to take the doctoral course.

Finally, I would like to thank my family for their support and encouragement throughout my work.

Contents

List of Figures

List of Tables

Abbreviations

Abbreviation	Description
3GPP	third generation partnership project
4G	fourth-generation mobile communication systems
5G	fifth-generation mobile communication systems
ABPA	adaptive bit and power allocation
ARIB	Association of Radio Industries and Businesses
ATC	adaptive transmission control
AWGN	additive white Gaussian noise
BER	bit error rate
BS	base station
CP	cyclic prefix
CPS	cyber-physical system
DL	downlink
DSRCs	dedicated short-range communication systems
E_b/N_0	Energy per bit to Noise density ratio
EP	equal power
FFT	fast Fourier transform
FPGA	field programmable gate array
FPU	field-pickup units
GSM	global system for mobile communications
IAB	integrated access and backhaul
ICI	inter-carrier interference
ICT	information and communication technology
IEEE	Institute of Electrical and Electronics Engineers
IEICE	Institute of Electronics Information and Communication Engineers
i.i.d.	independent and identically distributed
ISI	inter-symbol interference
IFFT	inverse fast Fourier transform
IoT	Internet of Things
IP	Internet protocol
ITE	The Institute of Image Information and Television Engineers
ITS	intelligent transport system

Abbreviation	Description
JVET	Joint Video Experts Team
LPWA	low-power wide-area
MAC	medium access control
Mbps	megabits per second
MCS	modulation and coding scheme
MER	modulation error ratio
MGW	management gateway
MIMO	multiple-input multiple-output
ML	machine learning
MMSE	minimum mean square error
MRC	maximum-ratio combining
MS	mobile station
M2M	machine-to-machine
OFDM	orthogonal frequency-division multiplexing
OFDMA	orthogonal frequency division multiple access
PUSC	partial usage subchannelization
QAM	quadrature amplitude modulation
QPSK	quadrature phase-shift keying
RBF	radial basis function
RS	relay station
RTG	receive/transmit transition gap
Rx	receive
SHF	super-high-frequency
SHV	Super-Hi-Vision
SINR	signal-to-interference-plus-noise ratio
SNR	signal-to-noise ratio
SVD	singular value decomposition
SVR	support vector regression
TDD	time-division duplex
TTG	transmit/receive transition gap
TV	television
Tx	transmission
UE	user equipment

Abbreviation	Description
UHD	ultra-high-definition
UHF	ultra-high-frequency
UL	uplink
V2I	vehicle-to-infrastructure
V2N	vehicle-to-network
V2V	vehicle-to-vehicle
V2X	vehicle-to-everything
VHF	very-high-frequency
Wi-SUN	wireless smart ubiquitous network
WiMAX	worldwide interoperability for microwave access
WLAN	wireless local area network
WRAN	wireless regional area network
WSN	wireless sensor network
ZF	zero-forcing

Chapter 1
Introduction

1.1 Background

Since radio waves are a limited, scarce, and public resource, they are shared and used for various purposes, such as communications and broadcasting. In recent years, since Internet traffic has increased explosively with the development of ICT, in particular, the demand for wireless communication using radio waves is increasing [1, 2]. Conventionally, mobile terminals and BSs have often been connected through active user actions. However, wireless communication in various forms is increasing, such as connections with IoT devices, M2M communication, V2X communication, etc. Therefore, the design of wireless communication systems tailored to the application is needed.

Wireless communication is divided into two types: public communication, where operators prepare communication equipment to which user terminals can connect, and private communication, where users prepare communication equipment.

Public communications are being standardized worldwide by the 3GPP and other organizations. Therefore, public communications have the advantage that devices that comply with the same standard can be used worldwide just by signing a contract, without having to go through complex procedures such as obtaining a license. On the other hand, users can only use services the operators provide, and making connections with equipment other than the assumed equipment is not easy. Also, because it is shared, it has the characteristic of being a best-effort type service, except for a guaranteed bandwidth contract. Furthermore, when a disaster occurs, users can only wait for the provider to recover.

On the other hand, in private communication systems, users can develop a system suitable for the application or install one based on the desired standards suitable for the application. While there are degrees of freedom in system installation, the installers must select, evaluate, install, and operate the system at their own risk. Since it is possible to perform recovery at one's own risk during a disaster, rapid recovery of the system is possible. Furthermore, radio waves have characteristics depending on the assigned frequency band, and the use of various frequency bands is currently being

The part of this chapter is partially quoted from references [3, 4, 5, 6].

considered for wireless communications, from the VHF band below 300 MHz to the millimeter wave above 30 GHz. Therefore, it is necessary to decide the bandwidth according to the usage, or the usage according to the bandwidth. Because it is easy to meet this requirement, free research and system design for private communications is possible.

For these reasons, R&D of various private communication systems is underway. R&D is progressing on the WRAN system, which is a wide-area private communication system using the VHF band and is intended for use in various services, such as IoT and V2X. Similarly, R&D is progressing on the large-capacity next-generation mobile relay FPU system, which is a wide-band private communication system intended for use in the production of road race broadcasts for TV programs such as marathons and relay races in Japan. It is desirable to achieve wireless transmission as high throughput and wide coverage area as possible by using the same band and transmission power in all wireless communications, including private communications on both sides.

1.2 Overview of This Thesis

This thesis proposes and evaluates methods to achieve wireless transmission as high speed and wide-area as possible for private communications, based on the background from the previous section. Figure 1.1 shows the overview of this thesis. The following parts of this chapter discuss the circumstances surrounding the research content for each private communication system covered in this thesis. Chapter 2 describes the use cases and specifications of each private communication. In particular, a common system model for wide-band private communication systems used in Chapter 4 and Chapter 5 is described. Chapter 3 proposes methods for single-hop and multi-hop transmission for wide-area private communication systems and evaluates the performance through computer simulations and experiments. Finally, the performance evaluation results and theoretical values are combined to evaluate the limits of transmission speed and possible transmission distance for various specifications [3]. Chapter 4 proposes improvement methods of ATC for wide-band private communication systems and evaluates the performance [4]. Chapter 5 similarly proposes a compensation method using machine learning for quantization degradation of Tx weight matrices for wide-band private communication systems and evaluates the performance [5]. Chapter 6 discusses the prospects for wireless communication design toward the realization of platforms that can be used in various applications based on the study results in the previous chapters. Finally, Chapter 7 concludes this thesis.

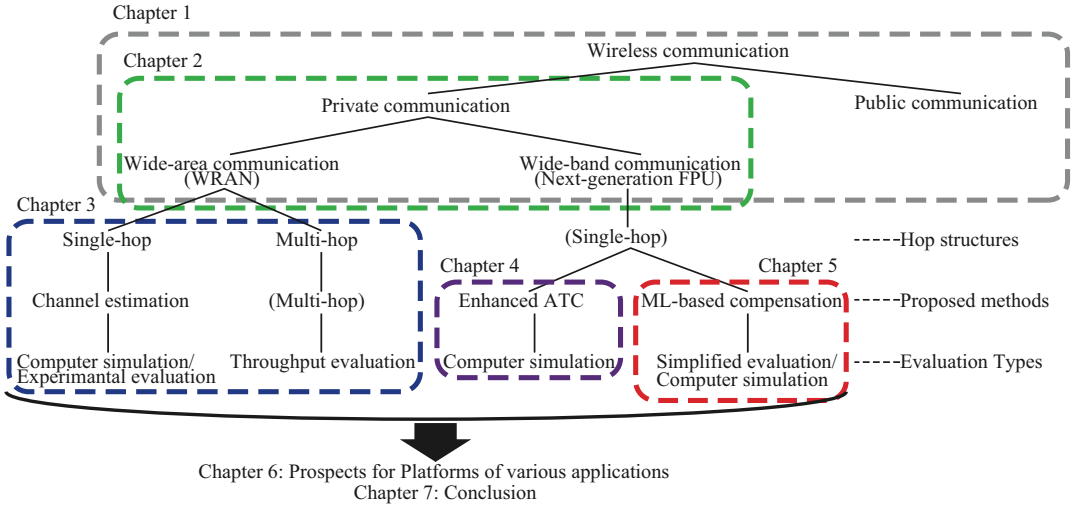

Figure 1.1: Overview of this thesis.

1.3 Private Communication Systems

This section describes the background surrounding wide-area and wide-band private communication systems and related works for them.

1.3.1 Wide-area Private Communication System in VHF band for IoT and V2X

The implementation of CPS platforms has significantly improved the IoT and V2X-based applications in recent years [7]. CPSs transmit sensor, metering, and monitoring information from physical space to cyberspace. This information is processed in the cyberspace through machine learning, and the results are then fed back into the physical space to form value. A wide-area communication system is required to collect data from a wide area to configure a CPS platform for the IoT and V2X applications. The communication distance must be more than 10 km to implement the platform in various applications, such as ITSs with V2X, positioning, marine sensing, and ship-to-ship communication. Furthermore, a high mobility environment requires a transmission rate of at least several Mbps since the information to be collected includes text and numerical data along with moving images.

These requirements can be satisfied by implementing the WRAN. WRAN is primarily employed for regional area communication over several tens of kilometers between wireless devices. It is mainly used in the VHF or UHF bands, such as the 200–400 MHz band, to secure a larger communication area per BS. One of the standardized WRAN systems is the IEEE 802.22 [8]. It was standardized in 2011; an initial prototype was developed [9] and demonstrated in the field [10]. However, IEEE 802.22 uses OFDMA with a bandwidth of 6 MHz per channel, which is highly

resistant to the frequency-selective fading that occurs in wide-area communications. This system is primarily intended for fixed communications and does not support mobile communications. Further research and development must be performed for commercialization in highly mobile environments [11] before it can be applied in ITSs.

IEEE 802.16 is a standard for broadband wireless communication systems based on OFDMA in higher UHF and SHF bands (recommended for application at 2.5, 3.5, and 5.8 GHz [12] in 2009). It was launched as WiMAX [13]. Extensive research has been conducted in this field, and various studies have been conducted on the channel estimation methods [14, 15, 16]. It has a maximum carrier frequency of 5.8 GHz and a maximum speed of 100 km/h; the Doppler frequency is 537 Hz, and the CP is set at approximately 10.0 μs [13]. Consequently, the system exhibits high resistance to movement speed (i.e., time fluctuation of the propagation channel) but not to the long-delayed waves (i.e., frequency selectivity).

ARIB STD-T103 was standardized for the WRAN system by the ARIB of Japan in 2011 to meet the formerly mentioned requirements [17, 18, 19]. In 2013, this standard was standardized as IEEE 802.16n (hereafter referred to as ARIB T103/IEEE 802.16n) [20]. This is a broadband mobile communication system that uses OFDMA in the VHF band for public usage. Wireless communication systems using the VHF band are characterized by less power attenuation over the same distance as compared to the UHF and higher bands. Therefore, a WRAN in the VHF band is expected to be used over a wide area of several tens of kilometers. Additionally, tolerance to the multipath fading that occurs in wide communication areas can be expected owing to the usage of OFDMA. In terms of the size of FFTs per channel, the number of ARIB T103/IEEE 802.16n (FFT size is 1024) is greater than or equal to that of IEEE 802.16-2009 because ARIB T103/IEEE 802.16n was developed based on IEEE 802.16-2019. Therefore, since the subcarrier spacing of ARIB T103/IEEE 802.16n is less than or equal to that of IEEE 802.16-2009, ARIB T103/IEEE 802.16n exhibits the same or higher resistance to frequency-selective fading as that exhibited by IEEE 802.16-2009. Furthermore, ARIB T103/IEEE 802.16n is specialized for the VHF band. Therefore, it is expected to have a longer transmission distance than IEEE 802.16-2009, which primarily uses frequencies above the UHF band. ARIB T103/IEEE 802.16n also requires a smaller FFT size than IEEE 802.22 (with an FFT size of 2048), making it relatively easy to build devices. Moreover, ARIB T103/IEEE 802.16n supports mobile communication with a transmission rate of several Mbps [17, 18, 20], which is not supported by IEEE 802.22, does not require a core network like IEEE 802.22, and is easier to install than 4G and 5G networks. Therefore, ARIB T103/IEEE 802.16n is expected to be an effective communication system for V2X to meet the requirement of super-large-coverage over 10 km and higher transmission rate over several Mbps.

1.3.1.1 Related Work

Some wireless communication systems are currently available for V2X applications, as shown in Table 1.1 [17, 21, 22, 23, 24, 25].

4G and 5G, which are public communication systems standardized by the 3GPP, can be considered for V2X communication systems. 4G and 5G primarily use the UHF band and SHF band, respectively, which facilitates a transmission distance of several kilometers per BS. However, each BS requires a connection to the core network. Additionally, the use of public communication systems presents various problems, such as the huge subscriber fees owing to the requirement of up-to-date information from all the roads for nationwide use of V2X, in the cases such as automated driving. Therefore, a private wireless communication system, such as a WLAN with wide-area communication and without connection to a core network, is suitable for collecting information with a small number of BSs. Moreover, wireless communication must be standardized by the international standards development organizations.

IEEE 802.11p is a standard based on OFDM for WLAN-based DSRCs for vehicular communication; it is designed to support safety applications via V2X in 2010 [25]. Multihop communication is required to achieve long-range multicasting for full-range vehicular networks owing to the limited communication coverage of the IEEE 802.11p system [26]. However, its operating frequency is the 5 GHz band, which requires multiple hops to support an area of several tens of kilometers.

Several LPWA communication systems for IoT devices have been analyzed in the sub-1 GHz band [21]. Additionally, private communications using licensed or unlicensed bands and 3GPP cellular-based public communications have also been analyzed. However, the bandwidth, associated transmission speed, mobility tolerance, and area range are restricted owing to the low power and wide area. In summary, no existing standardized system can ensure a communication distance of 10 km or more between BS and terminals; collect information from sensors, meters, and monitors, including moving images; and control them with transmission speeds above several Mbps in mobile environments, such as ITS and IoT.

There has been research about ARIB T103/IEEE 802.16n. In addition, they have been introduced as a public BB by the Ministry of Land, Infrastructure, Transport and Tourism and local governments [27, 28]. However, all the modulation schemes developed in previous studies [29], including uplink and downlink, with and without diversity, for ARIB T103/IEEE 802.16n were not comprehensively analyzed using computer simulations and experimental evaluations. Additionally, the transmission distance achieved using the ARIB T103/IEEE 802.16n has not been analyzed. This analysis of the transmission distance must also include an expansion of the transmission distance, assuming the relay between the RSs.

Table 1.1: Comparison among candidate technologies for IoT and V2X communications. [3] Table 1

	Tradisional V2X		LPWA				Proposed
Technology	Cellular [21, 24]	DSRC [21, 25]	LoRa [21, 23]	Sigfox [22, 23]	NB-IoT [21, 23]	eMTC [21]	WRAN [17]
Coverage	< 10 km	< 1.0 km	< 50 km	< 50 km	< 35 km	< 10 km	> 10 km
Data rate	20 Mbps	< 27 Mbps	250 kbps	100 bps	< 250 kbps	< 1 Mbps	< 8 Mbps
Mobility	Support	Support	Limited	Limited	Not support	Support	Support
Frequency band	UHF band	SHF band (5 GHz)	UHF band (Sub 1 GHz)	UHF band (Sub 1 GHz)	UHF band	UHF band	VHF band (200 MHz in Japan)
Band license	Licensed	Licensed	Unlicensed	Unlicensed	Licensed	Licensed	Licensed
Based standard	3GPP	IEEE 802.11p	Proprietary	Proprietary	3GPP	3GPP	ARIB STD-T103+119 IEEE 802.16n
Core network	Needed	Needed	Not Needed	Needed	Needed	Needed	Not Needed

1.3.2 Wide-band Private Communication System for Live Video Transmission

Currently, TV broadcasting in UHD [30] has started in some countries worldwide, and Japan, satellite broadcasting in both 4K resolution and 8K resolution has begun. 8K UHD is also called SHV in Japan. The main focus of the current TV programs is the recorded programs and the relay broadcasting of sports programs using wired lines. Furthermore, the start of UHD terrestrial broadcasting is being considered, and R&D of it is actively being carried out [31]. Although 4K relay using multiple cellular lines has been implemented [32], there are issues such as high delays and difficulty in stable transmission.

R&D on next-generation FPUs for mobile relay is underway to transmit higher-capacity video material such as at 4K/8K resolutions in mobile environments. FPUs are wireless communication equipment used by broadcasters to transmit video and audio program materials in Japan [33, 34, 35]. They are also used in other countries [36] under various names, such as wireless links, and research is also being conducted [37, 38]. Some FPUs are used for various purposes in the production of relay programs [39, 40, 41]. In particular, FPUs for mobile relay programs are used for real-time broadcasts of road racing programs such as marathons and long-distance relay races [39]. However, those FPUs used at current program production sites are restricted in terms of the transmission of higher quality video material because they were developed assuming video material equivalent to 2K-resolution transmission [42]. Therefore, R&D on next-generation FPUs for mobile relay is underway to transmit higher-capacity video material such as at 4K/8K resolutions in mobile environments [4, 43, 44, 45, 46, 49].

Furthermore, since video materials are videos used as raw materials for program production, encoding processing for broadcasting is further performed after they are transmitted and edited. Therefore, a higher quality video than the final broadcast one is required. Furthermore, in Japanese UHD satellite broadcasting, 8K broadcasting is broadcast at a transmission speed of 100 Mbps based on the ISDB-S3 standard. Additionally, even when using H.266/VVC [50], the latest video encoding technology standardized by the JVET, 8K video transmission requires a maximum transmission capacity of 180 Mbps depending on the situation was confirmed in subjective experiments [51]. Note that in video transmission, the required transmission capacity changes depending on the type of video. For these reasons, it is necessary to have as large a transmission capacity as possible, several tens to 100 Mbps or more for UHD video material transmission.

The channel environment for real-time broadcasts of road racing programs is a mobile environment because video material is transmitted while moving. In the mobile environment, the propagation channel changes over time. However, since conventional FPUs were designed for simplex communication, changing the transmission parameters dynamically is impossible. Therefore, these channel parameters, such as MCSs, were fixed to parameters with a high noise tolerance for stable transmission,

even over poor propagation channels. For this reason, even if most racing courses had a good propagation channel, the system design was fixed at low throughput, so the throughput could not be increased.

Next-generation FPUs under development combine three technologies to achieve "stable transmission" with low throughput over poor propagation channels and "high-speed transmission" with high throughput over good propagation channels. Elemental technologies include SVD-MIMO, which improves the transmission capacity by spatial multiplexing, two-way communication by TDD, and ATC by changing parameters in accordance with channel conditions. SVD-MIMO uses Tx and Rx weight matrices calculated by SVD and transmits over multiple equivalent independent channels called eigenmodes or streams [4, 43, 46, 47, 48, 52, 53, 54, 55, 56, 57]. This thesis calls these channels streams. In particular, an optimal transmission for the channel capacity can be expected when SVD-MIMO is combined with ATC algorithms [4, 43] that control the power allocation $\{p_i\}$ and modulation schemes for each stream i and coding rate R for all streams.

Next-generation mobile relay FPUs have standardized as ARIB STD-B75 [46]. In previous R&D involving this standard, studies assuming ideal SVD-MIMO transmission were conducted. However, in actual transmission, there are degradations of the weight matrix that cannot be avoided due to system design. Various parameters were not optimized for transmission with this degraded weight matrix. In particular, ATC assuming a degraded weight matrix and compensation for quantization degradation using machine learning have not been studied.

1.3.2.1 Related Work

Next-generation FPUs for mobile-relay broadcast programs have been actively researched, developed, and standardized [43, 46, 55]. In particular, a method using modulation schemes with a high modulation order and turbo codes achieved a maximum transmission rate of 180 Mbps and a frequency utilization efficiency of 10 bit/s/Hz in an experimental mobile environment [55].

Several improvements to the SVD-MIMO transmission method with incomplete Tx weight matrices have been proposed. In reference [54], an ATC method based on the BER without decoding was proposed. However, it does not compensate for the degradation of the Tx weight matrices. The compensation methods proposed in [56] used channel prediction at the Tx, and channel estimation at the Rx was proposed. However, these methods focus on compensating for the degradation caused by time-varying channels.

Estimating a scalar value from a vector is a regression problem. SVR, logistic regression, ridge regression, regression methods using NNs, etc., are used for solving regression problems [58]. Reference [59] applied regression into wireless communications. However, the method used therein targeted only channel estimation. Numerous other methods, such as decoding error correction code, channel estimation methods, and detecting MIMO signals, have been proposed as applications of ML to

wireless communication [60, 61]. Although NNs that operate equivalently to SVD have been researched [62], there is no research on using ML to compensate for the degradation of the Tx weight matrices for SVD-MIMO transmissions or generating a large amount of training data based on statistical distributions. There is no research on simplified channel metrics for evaluating the degradation in performance of the Tx weight matrices.

Chapter 2
Use Cases and Specifications

2.1 Wide-area Private Communication System: WRAN

2.1.1 Use Case of WRAN

Figure 2.1 presents an example of the CPS platform using a WRAN and other wireless communication systems. When not using WRAN, the public wireless communication systems, and local-area private communication systems collect various types of information. For example, a public mobile communication system standardized by the 3GPP such as 5G is used for public communication. A Wi-SUN standardized by IEEE 802.15.4g [63] or a WLAN by IEEE 802.11 is used for local-area private communication. However, the communication service area is only a public operator's service area, which expands through local communication. In addition, using these services incurs subscriber fees. These issues increase the difficulty of installing existing systems. On the contrary, the WRAN system conforming to ARIB STD-T103 can cover a wide range of 10 km or more with a transmission rate of several Mbps. Thus, this thesis envisions three use cases for WRAN: 1) IoT communications, 2) mobile communications, and 3) V2X communications.

1) IoT communications

   Various types of information, such as sensor data, are collected from the wide area with a distance of 10 km or more supported by the WRAN systems. The thesis assumes that the communication is performed directly using the sensor data with WRAN and the data is collected in the local area using another communication system (such as Wi-SUN or WLAN) and transmitted with WRAN via a MGW. In V2X, communication is categorized as V2I. It is expected to be used in various fields, such as a collection of information from both the environment and road monitoring sensors [21].

The part of this chapter is partially quoted from references [3, 4, 5, 6].

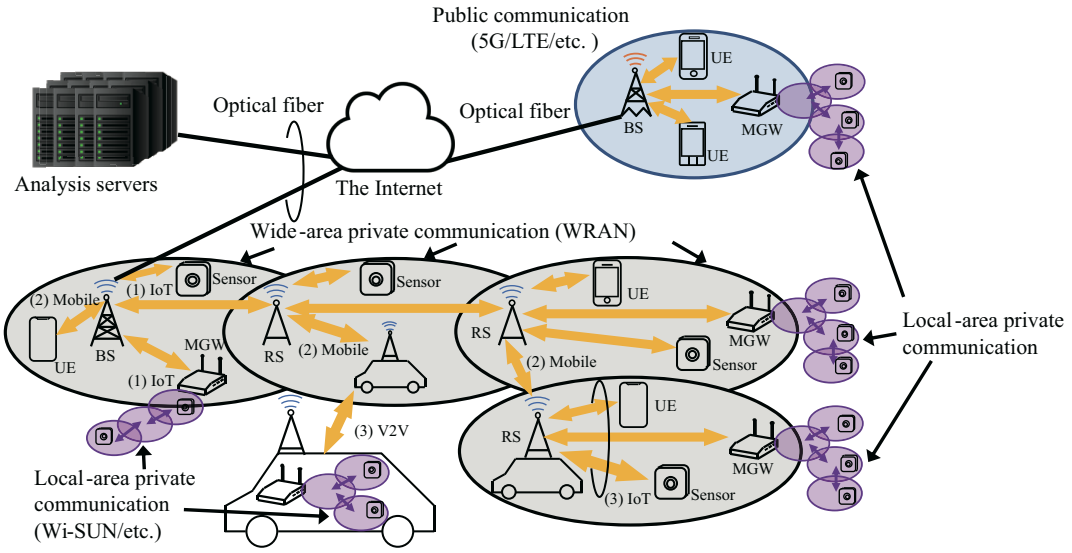

Figure 2.1: Example of public and private wireless communication systems on the CPS platform. [3] Fig. 1

2) Mobile communications

For mobile communications, the thesis assumes that communication is performed with moving UE, similar to general public cellular communication and communication with vehicles, such as cars. In the vehicle, various control information required for automatic driving and other actions, is collected locally via Wi-SUN or WLAN, etc., and this information is widely collected via WRAN. Conversely, WRAN can be used to remotely achieve the control required for automated driving. V2X communication is categorized as V2N.

3) V2X communications

When a vehicle is outside the WRAN communication area, the communication area is extended using multi-hop communication via V2V communication [64] based on the WRAN. Moreover, the communication area can be expanded as an IAB link by installing a WRAN BS, which functions as an RS in a vehicle. For example, it can function as a temporary BS in the event of a disaster. This RS can be connected to terminals using WRAN and can also transmit information collected by Wi-SUN and WLAN using the MGW function of RS.

2.1.2 Specifications of ARIB STD-T103 and IEEE 802.16n

The ARIB STD-T103 [18] was standardized for WRAN systems by the ARIB in Japan in 2011. The ARIB STD-T103 is a broadband mobile communication system which employs OFDMA in the VHF band for public usage. Wireless communication systems using the VHF band are characterized by less power attenuation for the same distance as the UHF and higher bands. Consequently, a WRAN in the VHF band is expected to be used over a wide area, such as several tens of kilometers. Table 2.1 lists the specifications of ARIB STD-T103. The ARIB STD-T103 operates with a bandwidth of 5 MHz per channel and has two modes: Mode 1 and Mode 2. Mode 1 has two FFT size options: 512 and 1024-point FFTs. The modulation schemes, duplex methods, multiple access schemes, maximum Tx power, and MAC layer protocol of Mode 1 are based on IEEE 802.16-2009 [15]. In IEEE 802.16-2009, 1024-point FFTs are not supported for the operation of a 5 MHz bandwidth. However, 1024 FFTs can be used even in operation with a 5 MHz bandwidth to compensate for signal variations due to severe frequency-selective fading in the VHF band.

The differences between the 512 and 1024-point FFT systems are in terms of the following: FFT size, frame length, OFDM symbol length, and CP length. This thesis focused only on the 1024-point FFT-applied Mode 1 owing to its widespread usage in Japan [29]. As the 1024-point FFT-applied systems achieve a CP of over 20 μs, they can support delayed paths of greater than 20 μs. In addition to the above differences, Mode 1 has unique pilot patterns between the DL and UL to compensate for signal variations that are caused by fading and the slot allocation ratio for the DL and UL in a TDD frame [18]. Mode 1, with a 512-point FFT, could support only 35:21 and 26:21, respectively. However, with a 1024-point FFT, Mode 1 supported a different ratio of 9:38. Mode 2 supported ratios of 37:10, 23:24, and 9:38. Therefore, Mode 1 with the 1024-point FFT, and Mode 2 can provide a higher ratio of UL and are effective in various cases, such as monitoring, metering, and surveillance. Figure 2.2 shows the TDD frame structure of the DL and UL used in Mode 1 with a 1024-point FFT. The pilot patterns of ARIB STD-T103 are roughly divided into the cluster and tile types [17, 18]. In the tile type, pilot subcarriers are placed at the four corners of each resource unit, whereas in the cluster type, they are not placed at the four corners. Cluster and tile types differ in transmission speed owing to the number of pilot subcarriers, resistance to frequency selectivity, and resistance to time fluctuations. Table 2.2 lists the average numbers of null, pilot, and data subcarriers for each OFDM symbol. The ARIB STD-T103 in 2011 and IEEE 802.16-2009 were standardized to IEEE 802.16n in 2013 [20].

Table 2.1: Specification of ARIB STD-T103. [3] Table 2

	Prameter							
Base standard	Wireless MAN-OFDMA (IEEE 802.16-2009)							
Channel bandwidth	5.0 MHz (4.9 MHz occupied)							
Modulation scheme	QPSK, 16QAM, and 64QAM							
Duplex method	Time division duplex (TDD)							
Multiple access	DL: OFDM/time division multiplexing (TDM), UL: OFDMA							
Tx power	5 W (37 dBm)							
Mode	Mode 1					Mode 2		
FFT size	512 point		1024 point					
Subcarrier spacing	10.94 kHz		5.47 kHz					
Frame length	5.0 ms		10.0 ms					
OFDM symbol length	102.8 μs		205.7 μs					
CP length (ratio:1/8)	11.4 μs		22.9 μs					
Symbol rate (T_s)	9.728 kHz		4.862 kHz					
Ratio of DL to UL symbols	35:12	26:21	35:12	26:21	9:38	37:10	23:24	9:38
Number of symbols for control	DL: 6 symbols, UL: 3 symbols							
Max. throughput (T_x^{max}) for DL[1] (Mbps)	6.3	4.3	6.3	4.3	0.65	5.9	3.2	0.57
Max. throughput (T_x^{max}) for UL[1] (Mbps)	1.5	3.0	1.5	3.0	5.9	1.5	4.5	7.6
Pilot pattern	IEEE 802.16-2009					ARIB STD-T103 original		
MAC	IEEE 802.16-2009					ARIB STD-T103 original		

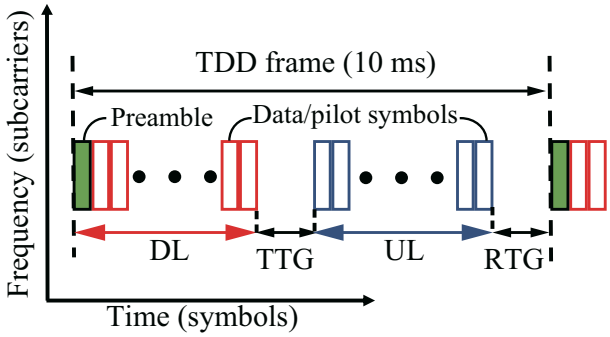

Figure 2.2: TDD frame configuration.

Table 2.2: Average number of subcarriers. [3] Table 3

	Mode 1		Mode 2	
	DL	UL	DL	UL
Null subcarriers	184			
Pilot subcarriers	120	280	210	120
Data subcarriers	720	560	630	720

2.1.3 Specifications of Transmitter

Figure 2.3 depicts the transmitter block diagram of the ARIB T103/IEEE 802.16n system and the process of each block is presented in [17]. The transmitter performs channel coding, modulation, frequency interleave using PUSC, IFFT, and OFDM processes, including CP. The frequency interleave and CP increased the resistance to long delay paths. Mode 1 uses pilot allocations standardized in IEEE 802.16-2009, as shown in Fig 2.4. DL uses cluster-type channel allocation combined with a high data symbol ratio, leading to the difficulty of estimation. Conversely, UL uses a tile-type channel allocation set with a low data symbol ratio, which makes channel estimation relatively easy.

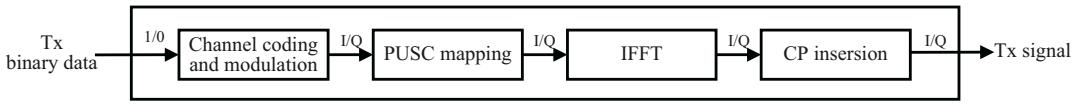

Figure 2.3: Structure of transmitter. [3] Fig. 2

[1] when 64QAM and coding rate of 1/2 are used.

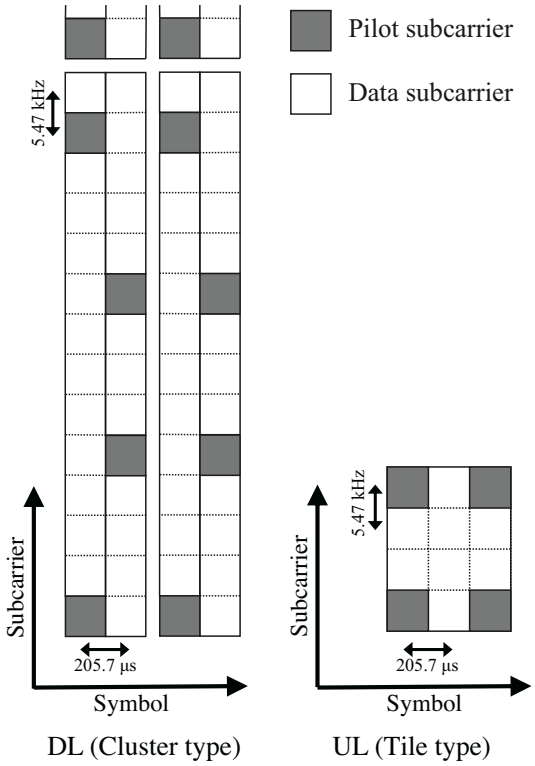

Figure 2.4: Pilot patterns. [3] Fig. 3

2.2 Wide-band Private Communication System: Next-generation FPU

2.2.1 Use Case of Next-generation FPU

Figure 2.5 presents an example of real-time production for road-racing programs using next-generation FPU. In actual video transmission, a 4K/8K video encoder is connected to the MS side, and a decoder is connected to the BS side. In particular, using a variable encoder [65], it is possible to transmit video materials with the highest-quality video according to the transmission capacity. Additionally, this method realizes two-way video transmission using TDD. Taking advantage of this feature, it can also be used for wireless IP remote production, where cameras on moving vehicles are remotely controlled from the switching center [66].

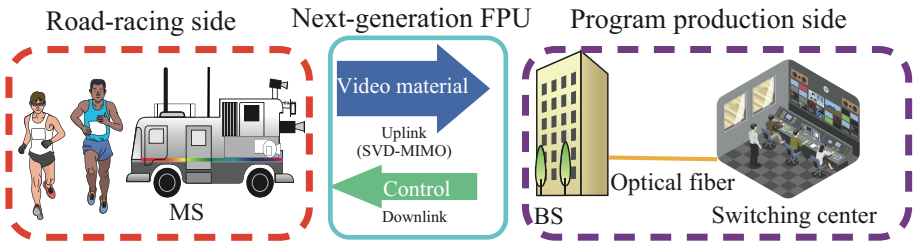

Figure 2.5: Example of real-time production for road racing program using next-generation FPU. ©2023 ITE, [6] Fig. 1

2.2.2 Specifications of ARIB STD-B75

The ARIB STD-B75 [46] was standardized for next-generation FPU systems by the ARIB in Japan in 2021. As mentioned above, the standard specifies two-way communication using TDD. Furthermore, different transmission methods are specified for DL and UL depending on the application. In addition to high line reliability, since UL requires high-capacity transmission speed, a transmission method that combines 4×4 SVD-MIMO, OFDM, and ATC is specified. While DL requires similar line reliability, it is expected to be used at a relatively low transmission speed. Therefore, 2×4 space-time trellis coded-MIMO, the transmission method used in conventional FPU [42], is specified. This thesis omits the transmission method of DL. Table 2.3 shows the UL specifications of STD-B75. Here, N^{mod} is the sum of the modulation orders n^{mod} of each stream i.

2.2.3 Overview of the System Model

This section gives an overview of next-generation FPU system model under development [46]. For next-generation FPUs for mobile relays, a method of switching between high speed and stability depending on the environment is being researched. In particular, since TDD enables two-way communication, the aim of these systems is to adaptively control parameters depending on changes in the propagation environment due to movement. The flow of the control is shown below.

Figure 2.6 shows a functional block diagram of the next-generation FPUs for mobile relays. On the BS side, the RF/OFDM process, channel estimation, signal detection, demodulation, and decoding are performed on the signal received from the MS, and parameters (deteriorated weight matrix $\boldsymbol{V}'$, $\{n_i^{\mathrm{mod}}\}$, R, and $\{p_i\}$) for the next frame are created and transmitted to the MS. On the MS side, coding, modulation, multiplication of Tx weight matrices, and the OFDM/RF process are performed using the received parameters. Figure 2.7 shows the TDD frame structure of the DL and UL used in this thesis. First, the channel matrix $\boldsymbol{H}$ is estimated on the basis of the pilot symbol included in the received signal for UL transmission from the MS at the BS. After that, control information such as the Tx weight matrices $\boldsymbol{V}$, power allocation $\{p_i\}$, and MCSs for UL transmission of the next TDD frame is created by SVD and

Table 2.3: Specifications of ARIB STD-B75 (UL). ©2023 IEICE, [5] Table 1

	Parameter					
Frequency band	1.2 GHz (1.24–1.30), 2.3 GHz (2.33–2.37)					
Spatial multiplexing	4×4 SVD-MIMO					
FFT size	1024			2048		
Subcarrier spacing (kHz)	19.97			9.99		
Mode	Half		Full	Half		Full
Occupied Bandwidth (MHz)	8.47		17.18	8.47		17.18
Total number of subcarriers	424		860	848		1720
Number of data subcarriers	408		816	844		1688
Sum of modulation orders (N^{mod})	10, 12, 14, 16, 18, 20, 22, and 24					
Modulation schemes (Modulation order)	BPSK (1), QPSK (2), 8QAM (3), ..., and 4096QAM (12)					
Inner code	Turbo codes (Code rate: $R = 0.33$–0.92)					
Outer Code	Reed-Solomon codes (204,188, $t = 8$)					
GI length (μs)	6.26	9.39	12.5	12.5	18.8	25.0
Sym. length (μs)	56.3	59.5	62.6	113	119	125

ATC algorithms (in Chapter 4). Finally, these parameters are transmitted to the MS via a DL.

OFDM is used for the FPUs. Four modes are standardized for the TDD frame structure [46], and the thesis uses a 1K-Full mode having the structure shown in Fig. 2.7. There are 816 data subcarriers and 28 data symbols in a UL subframe of one TDD frame, so there are 22,848 ($= 816 \times 28$) symbols for data transmission in total. SVD is performed on the representative (of a precoding block consisting of about eight subcarriers) 108 subcarriers of the final data symbol of the UL subframe. The created Tx weight matrices are used for all UL symbols per each precoding block in the TDD frame. ATC is performed after averaging the channel quality of all symbols and subcarriers in the UL subframe. After that, the same control information is used for all symbols and subcarriers in the UL subframe of the next TDD frame [46].

2.2.4 SVD-MIMO Transmission for UL

SVD-MIMO transmission used for UL transmission can be used with ATC to allocate optimal power to each stream, allowing for high communication channel capacity [52]. To implement optimal ATC, it is necessary to estimate transmission channel quality during control accurately. This thesis describes the undesired signals, such as noise power and interference power of “ideal SVD-MIMO transmission” where the Tx and Rx weight matrices are ideal and “actual SVD-MIMO transmission” where the Tx and Rx weights are imperfect in line with the actual transmission.

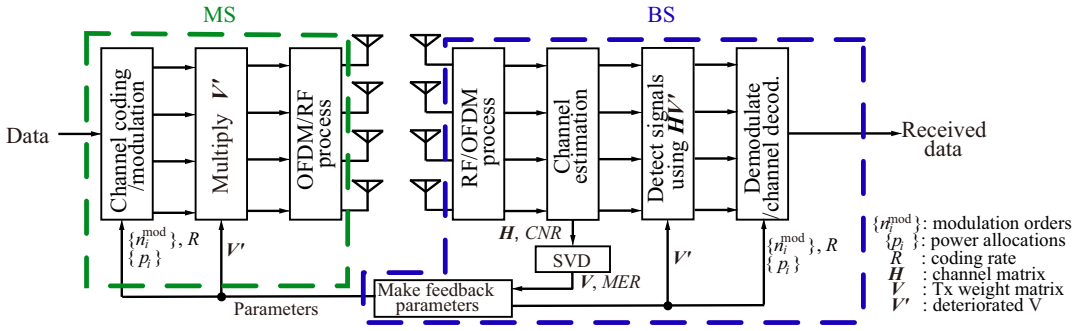

Figure 2.6: Block diagram of conventional transceiver. ©2023 ITE, [6] Fig. 2

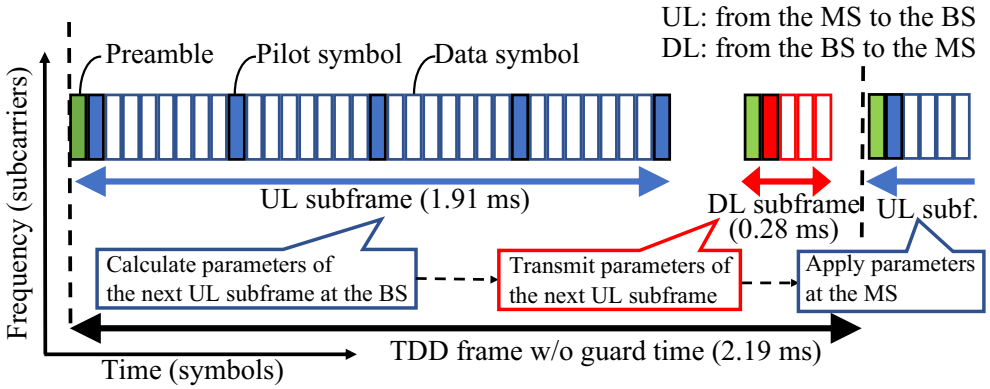

Figure 2.7: Example of TDD frame configuration. ©2023 IEICE, [5] Fig. 1

First, $\boldsymbol{H} \in \mathbb{C}^{4\times4}$ is decomposed by SVD:

$$\boldsymbol{H} = \boldsymbol{U}\boldsymbol{\Sigma}\boldsymbol{V}^{\mathrm{H}}, \tag{2.1}$$

where $\boldsymbol{U}, \boldsymbol{V} \in \mathbb{C}^{4\times4}$ are unitary matrices, $\boldsymbol{\Sigma} \in \mathbb{R}^{4\times4}$ is a diagonal matrix whose elements are the singular values $\{\xi_i\}$ of $\boldsymbol{H}$, and the superscript H means Hermitian transpose. $i = 0, 1, 2, 3$ is the stream index.

2.2.4.1 Procedure of Ideal SVD-MIMO Transmission

Figure 2.8 shows the procedure of ideal SVD-MIMO transmission. In the ideal SVD-MIMO transmission, $\boldsymbol{V}$, $\boldsymbol{U}^{\mathrm{H}}$, and $\boldsymbol{\Sigma}^{-1}$ are the Tx weight matrix, Rx weight (signal detection) matrix, and equalization matrix, respectively [52]. When being multiplied $\boldsymbol{V}$ and $\boldsymbol{U}^{\mathrm{H}}$, the weighted received signal $\boldsymbol{y}_0 \in \mathbb{C}^4$ is

$$\boldsymbol{y}_0 = \boldsymbol{U}^{\mathrm{H}}\left[\boldsymbol{H}(\boldsymbol{V}\boldsymbol{T}\boldsymbol{x}) + \boldsymbol{n}\right] = \boldsymbol{\Sigma}\boldsymbol{T}\boldsymbol{x} + \boldsymbol{U}^{\mathrm{H}}\boldsymbol{n}, \tag{2.2}$$

where $\boldsymbol{x} \in \mathbb{C}^4$ is the transmit signal, $\boldsymbol{T} \in \mathbb{R}^{4\times4}$ is a diagonal matrix whose elements are the amplitude components of power distribution $\{\sqrt{p_i}\}$, and $\boldsymbol{n} \in \mathbb{C}^4$ is an AWGN

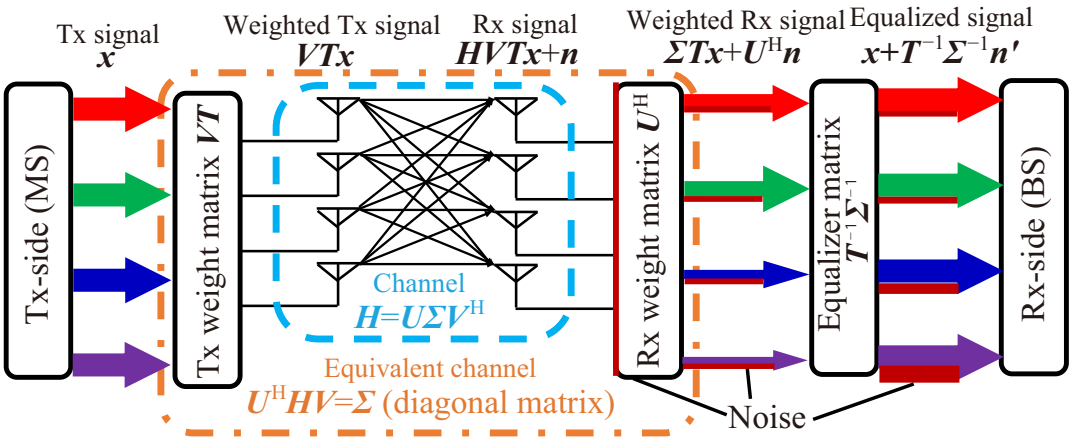

Figure 2.8: Procedure of ideal SVD-MIMO transmission. ©2023 IEICE, [4] Fig. 3

vector. Note that the Tx signal power is constrained to $\sum_i p_i = 1$ because the total of the four streams needs to be constant.

The final output, equalized signal $\boldsymbol{y}$, is multiplied by the equalization matrix $\boldsymbol{\Sigma}^{-1}$ and the power distribution inverse matrix $\boldsymbol{T}^{-1}$ with respect to $\boldsymbol{y}_0$:

$$\boldsymbol{y} = \boldsymbol{T}^{-1}\boldsymbol{\Sigma}^{-1}\boldsymbol{\Sigma}\boldsymbol{T}\boldsymbol{x} + \boldsymbol{T}^{-1}\boldsymbol{\Sigma}^{-1}\boldsymbol{U}^{\mathrm{H}}\boldsymbol{n} = \boldsymbol{x} + \boldsymbol{T}^{-1}\boldsymbol{\Sigma}^{-1}\boldsymbol{n}'. \tag{2.3}$$

At this time, since the rotated noise vector $\boldsymbol{n}'$ is $\boldsymbol{n}' = \boldsymbol{U}^{\mathrm{H}}\boldsymbol{n}$ and $\boldsymbol{U}^{\mathrm{H}}$ is a unitary matrix, the rotated noise vector becomes a noise vector with the same distribution as $\boldsymbol{n}$. Also, each element y_i of $\boldsymbol{y}$ is

$$y_i = x_i + n_i' / \left(\xi_i \sqrt{p_i}\right). \tag{2.4}$$

In other words, $1/\left(\xi_i\sqrt{p_i}\right)$ times more emphasized noise is added to the desired signal x_i as an undesired signal and received [52]. Also, for the sake of the next section, $\boldsymbol{U}^{\mathrm{H}}$ and $\boldsymbol{\Sigma}^{-1}$ are combined and defined into the signal detection matrix $\boldsymbol{W} = \boldsymbol{\Sigma}^{-1}\boldsymbol{U}^{\mathrm{H}}$.

2.2.4.2 Procedure of Actual SVD-MIMO Transmission

However, in actual SVD-MIMO transmissions, it is hard to use ideal weight matrices for various reasons described later [53, 54]. This section describes the actual SVD-MIMO transmission using the degraded Tx weight matrix $\boldsymbol{V}'$ and the signal detection matrix $\boldsymbol{W}'$ changed from the ideal matrix $\boldsymbol{W}$. Figure 2.9 shows the procedure of the actual SVD-MIMO transmission. The equalized signal $\boldsymbol{y}' \in \mathbb{C}^4$ is

$$\begin{aligned} \boldsymbol{y}' &= \boldsymbol{T}^{-1}\boldsymbol{W}'\left[\boldsymbol{H}(\boldsymbol{V}'\boldsymbol{T}\boldsymbol{x}) + \boldsymbol{n}\right] \\ &= \boldsymbol{x} + \boldsymbol{T}^{-1}\boldsymbol{W}'\boldsymbol{n} + \boldsymbol{T}^{-1}\boldsymbol{\Delta}\boldsymbol{T}\boldsymbol{x}, \end{aligned} \tag{2.5}$$

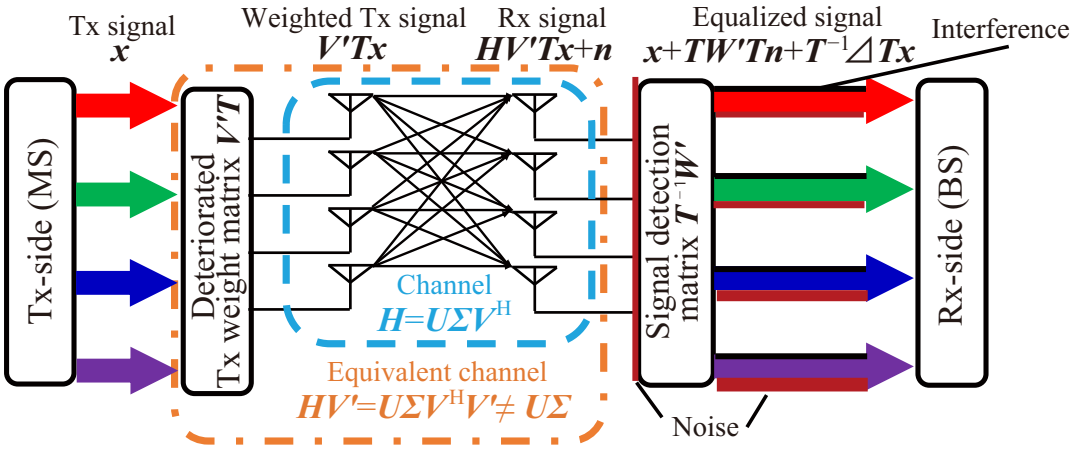

Figure 2.9: Procedure of actual SVD-MIMO transmission. ©2023 IEICE, [4] Fig. 4

where $\boldsymbol{\Delta}$ is interference component matrix. It is the difference between $\boldsymbol{W'HV'}$ and the identity matrix $\boldsymbol{I} \in \mathbb{C}^{4\times4}$:

$$\boldsymbol{\Delta} = \boldsymbol{W'HV'} - \boldsymbol{I}. \tag{2.6}$$

Same as ideal SVD-MIMO transmission, undesired signals are added to the desired signal x_i and received. The undesired components in the received signal are the emphasized noise component $\boldsymbol{T^{-1}W'n}$ and the interference component $\boldsymbol{T^{-1}\Delta Tx}$.

2.2.5 Degradation Factors in the Tx Weight Matrices

The system model conforms to the standard [46], wherein various factors degrade the Tx weight matrices. The degradation factors are described below.

2.2.5.1 Degradation Due to Quantization

As shown in Fig. 2.7, the Tx weight matrices are created at the BS and then transmitted to the MS via the DL. The Tx weight matrices $\boldsymbol{V}$ are generated with the number of bits depending on the hardware's computing power. Because the evaluation in this study used 64-bit floating-point arithmetic, the Tx weight matrices were also generated in this format. The Tx weight matrices are specified in the standard to transmit the minimum required one OFDM symbol per TDD frame. However, considering the transmission of the real and imaginary parts of the Tx weight matrices $\boldsymbol{V}$, the number of matrix elements, and the total number of subcarriers (860), 1.76 Mbits (64-bit $\times$ 2 $\times$ (4 $\times$ 4) $\times$ 860) must be transmitted. It is impossible to transmit all the Tx weight matrices because about 9 Kbits can be transmitted for the DL subframe in the configuration of Fig. 2.7. On the other hand, increasing the number of DL symbols causes a decrease in the UL transmission rate. For these reasons, the standard [46] specifies three-bit quantization for each element, which causes a quantization error

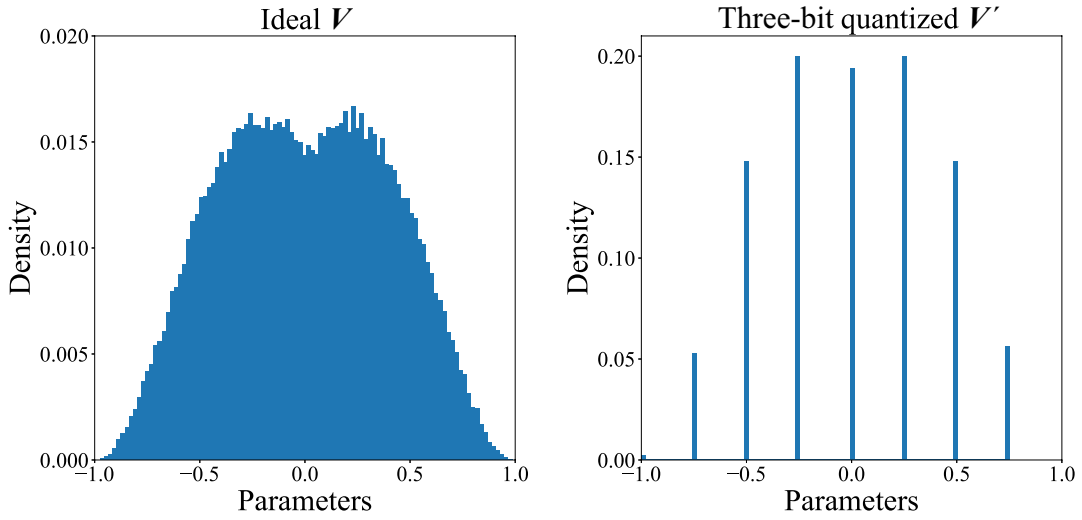

Figure 2.10: Quantization for each parameter of the Tx weight matrices. ©2023 IEICE, [5] Fig. 3

relative to the ideal value. Figure 2.10 shows an example of the degradation in each element of the real part caused by three-bit quantization. In Ideal $\boldsymbol{V}$, each parameter varies continuously between -1.0 and 1.0. On the other hand, in the three-bit quantized $\boldsymbol{V}'$, each parameter is limited to $2^3 = 8$ patterns.

2.2.5.2 Other Degradation Factors

The Tx weight matrices are also degraded by a) channel estimation errors and by b) the use of precoding blocks.

a) Degradation due to channel estimation error
This sort of degradation occurs because the estimated channel matrices $\widetilde{\boldsymbol{H}}$ for creating the Tx weight matrices are different from the ideal ones. In particular, delays due to feedback and the use of pilot symbols make a difference. Differences due to delays always occur when estimating channel matrices in time-varying channels. Furthermore, because the Tx weight matrices in this system are fed back to the MS via DL subframe as one of the transmission parameters of Fig. 2.7, especially long (sub) frames cause a large difference.

b) Degradation due to the use of precoding blocks
This sort of degradation occurs when precoding blocks are used to reduce the amount of feedback data in the Tx weight matrix, similar to degradation due to quantization in Section 2.2.5.1. Eight subcarriers are put together as a precoding block, for which one representative Tx weight matrix is used [46]. As a result, the transmission is reduced to about 9 Kbits, and it is possible to transmit the Tx weight matrix to the MS in the frame structure shown in Fig. 2.7. However, the Tx weight matrices are no longer ideal.

2.2.6 Change in Signal Detection Matrix

Other factors change the signal detection matrix in addition to a) degradation due to channel estimation error that was also a degradation factor of the Tx weight matrix described in Section 2.2.5.2. The signal detection matrix in the system model changes from $\boldsymbol{W}$ because the matrix obtained by the signal detection method is used instead of the Rx weight matrix $\boldsymbol{U}^{\mathrm{H}}$ and the equalization weight matrix $\boldsymbol{\Sigma}^{-1}$ generated by SVD.

As signal detection methods, in addition to ZF $\boldsymbol{W}_{ZF} = (\boldsymbol{HV})^{-1}$ which is the same matrix as $\boldsymbol{W} = \boldsymbol{\Sigma}^{-1}\boldsymbol{U}^{\mathrm{H}}$ under ideal conditions, MMSE, maximum likelihood, successive interference cancellation, etc. are proposed [67, 72]. ARIB STD-B75 exemplifies signal detection using an MMSE matrix due to its ability to suppress noise enhancement and ease of processing, so this thesis also uses the matrix ($\boldsymbol{W}' = \boldsymbol{W}_{\mathrm{MMSE}}$). $\boldsymbol{W}_{\mathrm{MMSE}}$ is defined using degraded Tx weight matrix $\boldsymbol{V}'$ and estimated channel matrix $\widetilde{\boldsymbol{H}}$ as

$$\boldsymbol{W}_{\mathrm{MMSE}} = \left[\left(\widetilde{\boldsymbol{H}}\boldsymbol{V}'\right)^{\mathrm{H}} \widetilde{\boldsymbol{H}}\boldsymbol{V}' + \frac{4}{SNR^{\mathrm{Av.}}}\boldsymbol{I} \right] \left(\widetilde{\boldsymbol{H}}\boldsymbol{V}'\right)^{\mathrm{H}}, \tag{2.7}$$

where $SNR^{\mathrm{Av.}}$ is the average SNR at the Rx antenna [46]. As a result, the signal detection matrix changes significantly compared to $\boldsymbol{W}$, especially at low SNR.

Chapter 3
Wide-area Communication Systems: WRAN

3.1 Introduction

This chapter proposes a channel estimation method for ARIB T103/IEEE 802.16n downlink in a highly mobile environment to reduce the memory required for reception [17]. The BER performance was evaluated using QPSK, 16QAM, and 64QAM-OFDM and MRC diversity via computer simulations. Moreover, a prototype of ARIB T103/IEEE 802.16n was developed, and the transmission performance of the downlink was evaluated in a radio propagation environment in the VHF band [29] Moreover, the thesis comprehensively evaluates the transmission performance of both downlink and uplink in a VHF-band radio propagation environment through computer simulations and experimental evaluation using our WRAN prototype. The thesis employed both conventional and our proposed channel estimation methods. Subsequently, the transmission distance achieved using the ARIB T103/IEEE 802.16n was calculated based on the evaluation results. The main contributions of this chapter are summarized as follows:

- The transmission performance of ARIB T103/IEEE 802.16n with all the modulation schemes, uplink and downlink, and with and without diversity was comprehensively evaluated through computer simulations and experimental analysis of the transmission characteristics of the VHF band. The results of the computer simulation were validated based on the experimental results obtained from our WRAN prototype. Subsequently, the SNR and input power at the receiver required to achieve the BER of 10^{-6} were determined.
- The transmission distance between the RSs of ARIB T103/IEEE 802.16n with and without the multihop relay was evaluated by using the required input power obtained from the experimental evaluation.

Section 3.2 proposes the receiver of ARIB T103/IEEE 802.16n Mode 1. Section 3.3 presents channel estimation and equalization schemes for DL and UL in ARIB T103/IEEE 802.16n Mode 1. Moreover, the enhanced scheme is proposed for DL. Sections 3.4 and 3.5 present the computer simulation results and experimental laboratory results of ARIB T103/IEEE 802.16n Mode 1. Section 3.6 describes the expected transmission distance based on the results. Lastly, Section 3.7 summarizes the conclusions drawn from this chapter.

3.2 Proposed Receiver

Figure 3.1 shows the proposed receiver block diagram of an ARIB T103/IEEE 802.16n system [17]. First, each CP is removed before obtaining the received subcarriers through FFT processing. If the CP length is sufficient for removing the effect of the delay paths, there is no ISI or ICI in the obtained subcarriers. Subsequently, the receiver performs channel estimation, equalization, demapping using PUSC, demodulation, and channel decoding. Figure 3.2 depicts the receiver block diagram of the MRC diversity [68]. It was assumed that the MRC diversity could be applied to two receiving antennas. By employing the received signal (r_1) and estimated effective channel ($\widetilde{h}_1$) of branch 1, and the received signal (r_1) and estimated effective channel ($\widetilde{h}_2$) of branch 2, the MRC-processed and equalized signal, r', can be obtained as follows:

$$r' = \frac{\widetilde{h}_1^* r_1 + \widetilde{h}_2^* r_2}{\left|\widetilde{h}_1\right|^2 + \left|\widetilde{h}_2\right|^2}, \tag{3.1}$$

where * denotes complex conjugate.

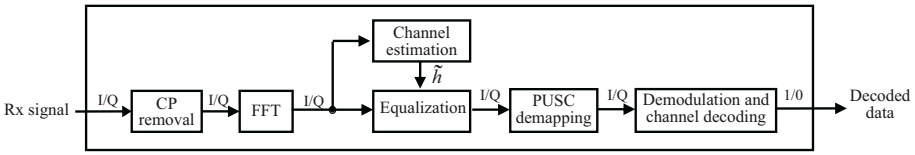

Figure 3.1: Structure of proposed receiver.

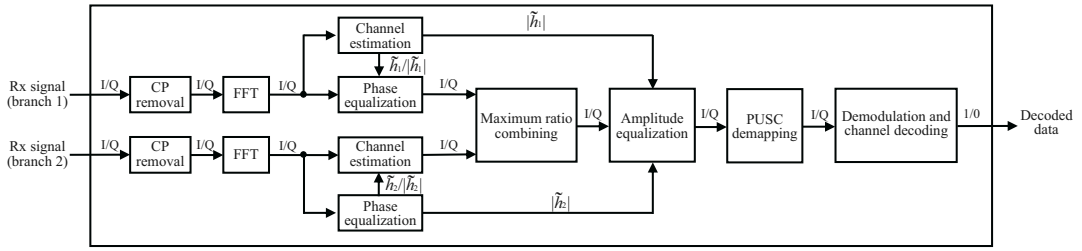

Figure 3.2: Structure of receiver with MRC diversity. [3] Fig. 4

3.3 Channel Estimation and Equalization

This section presents the basic channel estimation and equalization schemes for DL and UL in ARIB T103/IEEE 802.16n Mode 1. Moreover, the enhanced scheme is proposed for DL. The received subcarriers are expressed as follows:

$$r_{i,j} = h_{i,j}s_{i,j} + n_{i,j}, \tag{3.2}$$

where $s_{i,j} \in \mathbb{C}$, $r_{i,j} \in \mathbb{C}$, $h_{i,j} \in \mathbb{C}$, and $n_{i,j} \in \mathbb{C}$ represent the transmitted signal, received signal, effective channel, and noise signal of the j-th subcarrier in the i-th OFDM symbol, respectively. The effective channels, $\widehat{h}_{p,q_p}$, can be obtained by employing the transmitted and received signals of the pilot subcarriers, as follows:

$$\widehat{h}_{p,q_p} = \frac{r_{p,q_p}}{s_{p,q_p}} = h_{p,q_p} + \frac{n_{p,q_p}}{s_{p,q_p}}, \tag{3.3}$$

where q_p represents the pilot subcarrier index in the p-th OFDM symbol. The transmitted signals are known from both the transmitter and receiver. The effective channel, $\widetilde{h}_{i,j}$, of the data subcarriers is estimated by using the obtained effective channels of the pilot subcarriers, $\widehat{h}_{p,q_p}$. To equalize the effective channel and obtain the transmitted signals $s_{i,j}$, the received signals, $r_{i,j}$, were divided by the estimated effective channel, $\widetilde{h}_{i,j}$. The following sections present the schemes used to estimate the channels of data symbols from the estimated channels of pilot symbols per pilot allocation.

3.3.1 Channel Estimation Schemes for DL (Cluster type)

The three pilot subcarriers were not arranged at the corner of the cluster type in DL, as shown in Fig. 2.4. Therefore, the effective channels of the data subcarriers that were not allocated between the pilot subcarriers were estimated using the incomplete scheme using pilots of the adjacent clusters in the conventional scheme [14, 15], as shown in Fig. 3.3 (a). However, storing information other than the subcarriers of the

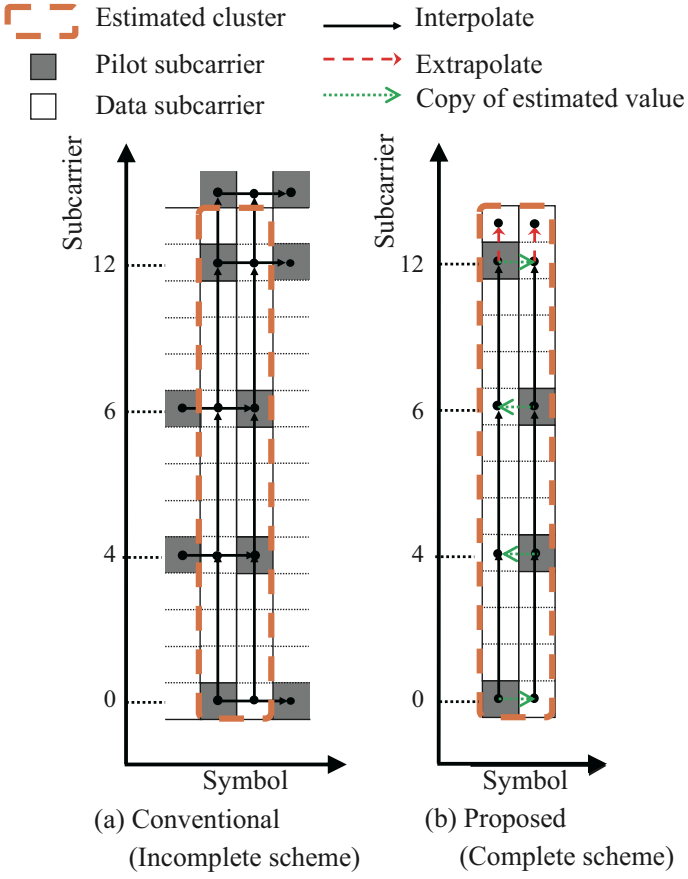

Figure 3.3: Channel estimation schemes for DL (Cluster type). [3] Fig. 5

user cluster is necessary to use the pilot subcarriers of the adjacent clusters, thereby squeezing the hardware memory. Therefore, a complete scheme for the DL cluster structure was proposed, as shown in Fig. 3.3 (b) [17]. The conventional and proposed schemes were applied in the time and frequency-domain estimation stages.

Let the effective channel in each cluster be defined as $\widetilde{h}_{s,t}^{x,z} = \widehat{h}_{i,j}$, where $s = i \bmod 2$ and $t = j \bmod 14$ are the symbol and subcarrier indices, respectively, and $x = \lfloor i/2 \rfloor$ and $z = \lfloor j/14 \rfloor$ are the cluster symbol and subcarrier indices.

First, this section describes the time-domain estimation stage. In the conventional scheme, the effective channels of two adjacent symbols in one cluster are estimated by interpolating those of both the pilots of the cluster and the adjacent cluster, as follows:

$$\begin{aligned} \widetilde{h}_{1,t}^{x,z} &= \frac{1}{2}\{\widetilde{h}_{0,t}^{x,z} + \widetilde{h}_{0,t}^{x+1,z}\} \quad (t = 0, 12), \\ \widetilde{h}_{0,t}^{x,z} &= \frac{1}{2}\{\widetilde{h}_{1,t}^{x,z} + \widetilde{h}_{1,t}^{x-1,z}\} \quad (t = 4, 8). \end{aligned} \tag{3.4}$$

However, the thesis assumed these effective channels were identical in the proposed scheme. The adjacent effective channels of the pilots in the time domain were esti-

mated by copying the estimated effective channels of the pilots as follows:

$$\begin{aligned} \widetilde{h}_{1,t}^{x,z} &= \widetilde{h}_{0,t}^{x,z} \quad (t = 0, 12), \\ \widetilde{h}_{0,t}^{x,z} &= \widetilde{h}_{1,t}^{x,z} \quad (t = 4, 8). \end{aligned} \tag{3.5}$$

Next, the thesis describes the frequency-domain estimation stage. In both the schemes, all the effective channels of the data subcarriers, except the 13th subcarrier, were estimated by interpolating between the pilots of their cluster, as follows:

$$\widetilde{h}_{s,t}^{x,z} = \frac{1}{4}\left\{t_{\mathrm{mod}}\widetilde{h}_{s,4(\lfloor t/4 \rfloor+1)}^{x,z} + (4 - t_{\mathrm{mod}})\widetilde{h}_{s,4\lfloor t/4 \rfloor}^{x,z}\right\} \quad (t = 13), \tag{3.6}$$

where $t_{\mathrm{mod}} = t \bmod 4$.

In the proposed scheme, the effective channel of the 13th subcarrier is estimated by extrapolating from the estimated effective channels of the 8th and 12th subcarriers, as follows:

$$\widetilde{h}_{s,13}^{x,z} = \frac{1}{4}\{5\widetilde{h}_{s,12}^{x,z} - \widetilde{h}_{s,8}^{x,z}\}. \tag{3.7}$$

However, in the conventional scheme, the effective channel of the 13th subcarrier was estimated by interpolating the estimated effective channels of the 12th subcarrier of the cluster and the 1st subcarrier of the adjacent cluster as follows:

$$\widetilde{h}_{s,13}^{x,z} = \frac{1}{2}\{\widetilde{h}_{s,0}^{x,z+1} - \widetilde{h}_{s,12}^{x,z}\}. \tag{3.8}$$

3.3.2 Channel Estimation Scheme for UL (Tile type)

There are few channel estimation considerations for the tile type because the pilot subcarriers are arranged at the four corners and bracket all the data subcarriers. An estimation scheme equivalent to the complete scheme was proposed in IEEE 802.16-2009 [16].

As all the pilot subcarriers are allocated to the corners, the effective channels of the data subcarriers can be estimated by interpolating those of the pilot subcarriers, as shown in Fig. 3.4. Therefore, the incomplete scheme is not useful for the tile type, regardless of DL/UL. The number of symbols per tile is defined as k. The effective channel in each tile is defined as $\widetilde{h}_{s,t}^{x,z} = \widehat{h}_{i,j}$, where $s = i \bmod k$ and $t = j \bmod 4$ are the symbol and subcarrier indices in each tile, respectively, and $x = \lfloor i/k \rfloor$ and $z = \lfloor j/4 \rfloor$ are the tile symbol and subcarrier indices. All the effective channels of the data subcarriers were estimated by interpolating between those of the pilot subcarriers

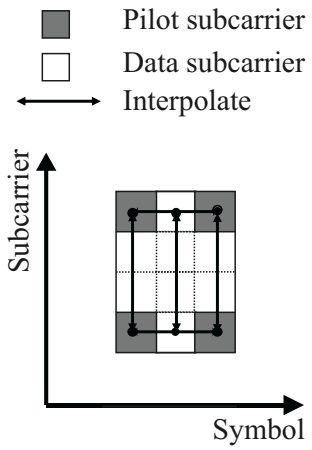

Figure 3.4: Channel estimation schemes for UL (Tile type). [3] Fig. 6

in the frequency and time domains as follows:

$$\begin{aligned}\widetilde{h}_{s,t}^{x,z} &= \frac{1}{3(k-1)}\Big\{(k-s-1)(3-t)\widetilde{h}_{0,0}^{x,z} + st\widetilde{h}_{2,3}^{x,z} \\ &\quad +s(3-t)\widetilde{h}_{2,0}^{x,z} + (k-s-1)t\widetilde{h}_{0,3}^{x,z}\Big\}. \end{aligned} \tag{3.9}$$

3.4 Performance Analysis by Computer Simulation

The transmission performance of Mode 1 in the ARIB T103/IEEE 802.16n was evaluated through computer simulation in terms of E_b/N_0 to BER. The proposed and conventional channel estimation schemes were compared and evaluated. The computer simulation codes were developed from scratch using MATLAB [69], and no communication-specific toolbox was used. Table 3.1 lists the simulation parameters. The AWGN environment, typical GSM urban model, and IEEE 802.22 Profile A model were used for the evaluation. Tables 3.2 and 3.3 list the models. The IEEE 802.22 Profile A model is a multipath fading channel model with a long delay path for a service distance of 10 km, standardized by the IEEE 802.22 working group. The required BER was set to 10^{-6} on ARIB STD-T103 [18].

3.4.1 Performance Analysis in AWGN Environment

Figure 3.5 depicts the BER performance of Mode 1 in an AWGN environment for each modulation scheme. The DL and UL exhibited nearly identical performances. Table 3.4 lists the E_b/N_0 and SNR of each modulation scheme that achieved the required BER $= 10^{-6}$. The difference in the E_b/N_0 is up to 6 dB. The performance

Table 3.1: Configurations of evaluation parameters. [3] Table 4

	Computer simulation	Experimental evaluation
Standard	ARIB STD-T103 (Mode 1)	
Channel model	AWGN Environment GSM Typical Urban model IEEE 802.22 Profile A model	
Encoding and decoding	Convolutional turbo codes (coding rate: 1/2) and Max-Log MAP algorithm	
Moving speed	80 km/h ($f_{\mathrm{D}}T_{\mathrm{s}} = 3 \times 10^{-3}$)	
DL:UL ratio	N/A	9:38
Max Tx power		37 dBm (BS), 30 dBm (MS)
Frequency		192.5 MHz–197.5 MHz

Table 3.2: GSM Typical Urban model. [3] Table 5

Path number	1	2	3	4	5	6
Delay time [μs]	-0.2	0	0.3	1.4	2.1	4.8
Relative power [dB]	-3.0	0	-2.0	-6.0	-8.0	-10

Table 3.3: IEEE 802.22 Profile A model. [3] Table 6

Path number	1	2	3	4	5	6
Delay time [μs]	0	3.0	8.0	11	13	21
Relative power [dB]	0	-7.0	-15	-22	-24	-19

difference for each mode was caused by the difference between the number of data subcarriers and boost of the pilot subcarriers.

3.4.2 Comparison of Channel Estimation Schemes in Multipath Fading Environment

Figure 3.6 depicts the BER performance of the receiver using two channel estimation schemes for DL and a channel estimation scheme for UL when compared to the ideal case with 64QAM in a typical GSM urban model. The BER degradation of the proposed scheme is up to 3.0 dB when compared to the ideal case in terms of E_{b}/N_0 at BER $= 10^{-6}$. Consequently, the channel estimation error slightly degrades the BER performance of a typical GSM urban model. In addition, the complete DL scheme exhibited almost no deterioration when compared to the conventional scheme.

Figure 3.7 shows the BER performance of the receiver using the channel estimation schemes in the IEEE 802.22 Profile A model. An error floor was observed both the DL estimation schemes. The proposed scheme showed a slightly higher error floor

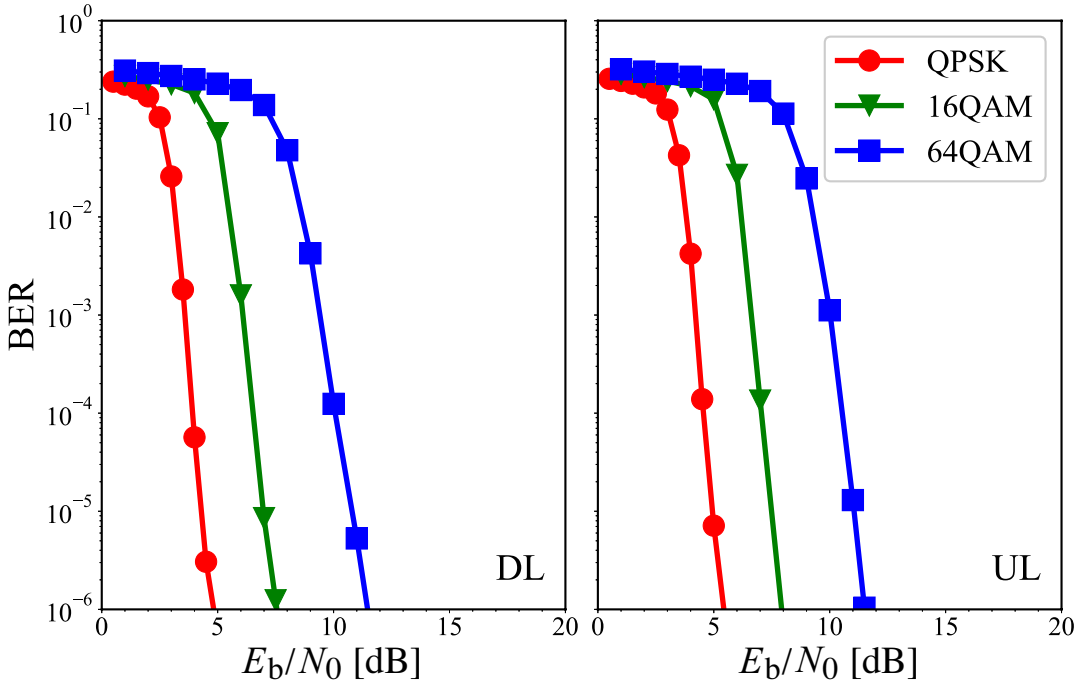

Figure 3.5: Performance evaluation in AWGN environment. [3] Fig. 7

Table 3.4: Required E_b/N_0 and SNR [dB] to achieve the required BER $= 10^{-6}$ in computer simulation. [3] Table 7

	AWGN		TU		Profile A		Profile A w/ div.	
	DL	UL	DL	UL	DL	UL	DL	UL
QPSK	5.0/3.3	5.5/2.7	18/16	18/15	26/27	22/20	14/12	14/11
16QAM	7.5/8.8	8.0/8.2	20/21	21/21	N/A	26/26	17/19	16/16
64QAM	12/15	11.5/14	22/25	24/26	N/A	N/A	28/31	20/22

than the conventional scheme and was adopted as the most straightforward scheme in the following discussion. Similarly, UL showed an error floor. This is because a wider pilot subcarrier interval induces a more significant channel estimation error owing to the severe frequency selectivity of fading caused by a long delay.

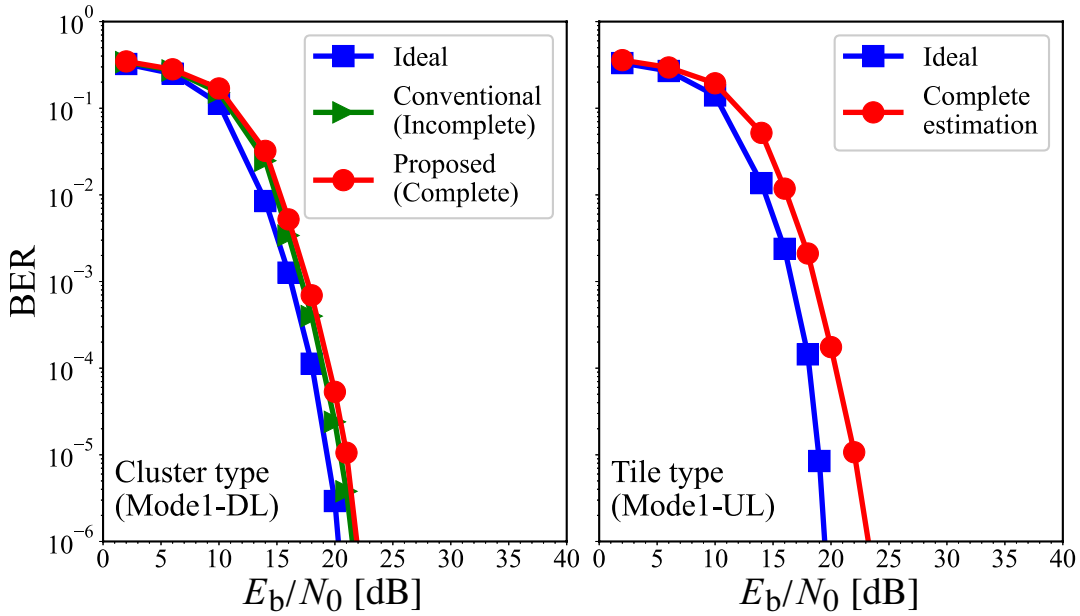

Figure 3.6: Performance evaluation of channel estimation schemes with 64 QAM in Typical Urban model. [3] Fig. 8

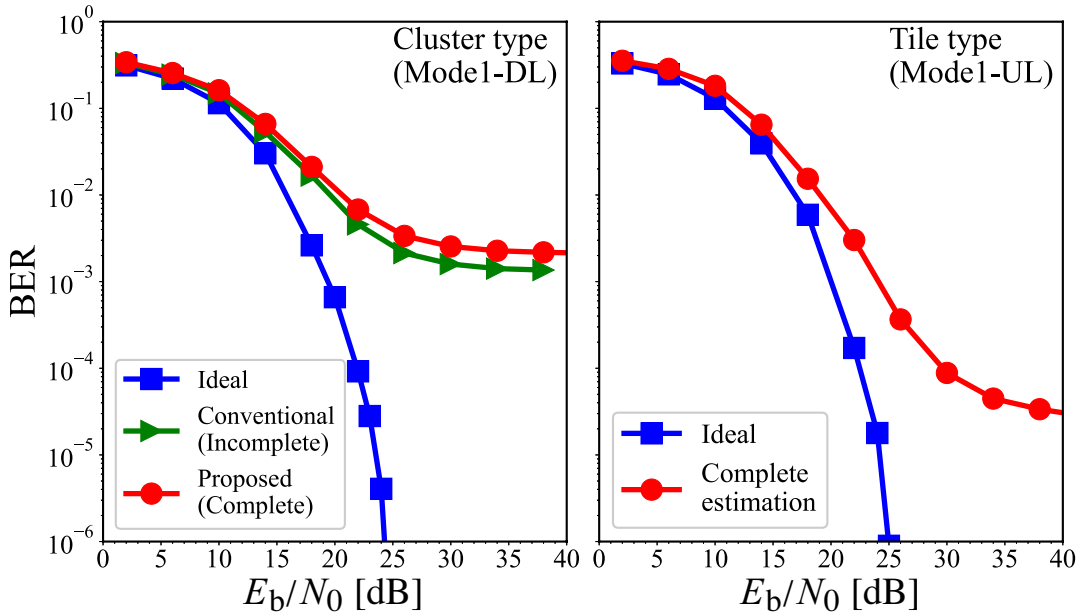

Figure 3.7: Performance evaluation of channel estimation schemes with 64 QAM in 802.22 Profile A model. [3] Fig. 9

3.4.3 Comparison of Modulation Schemes in Multipath Fading Environment

Figure 3.8 depicts the BER performance of Mode 1 in a typical GSM urban model for each modulation scheme based on the proposed channel estimation scheme. Similar characteristics are observed in DL and UL owing to the relatively high channel estimation accuracy. Table 3.4 also lists the E_b/N_0 and SNR of each modulation scheme that achieved the required BER $= 10^{-6}$ in multipath fading environment. Similar to the AWGN environment, the difference for each modulation scheme of the E_b/N_0 that achieves the required BER $= 10^{-6}$ is up to 6 dB.

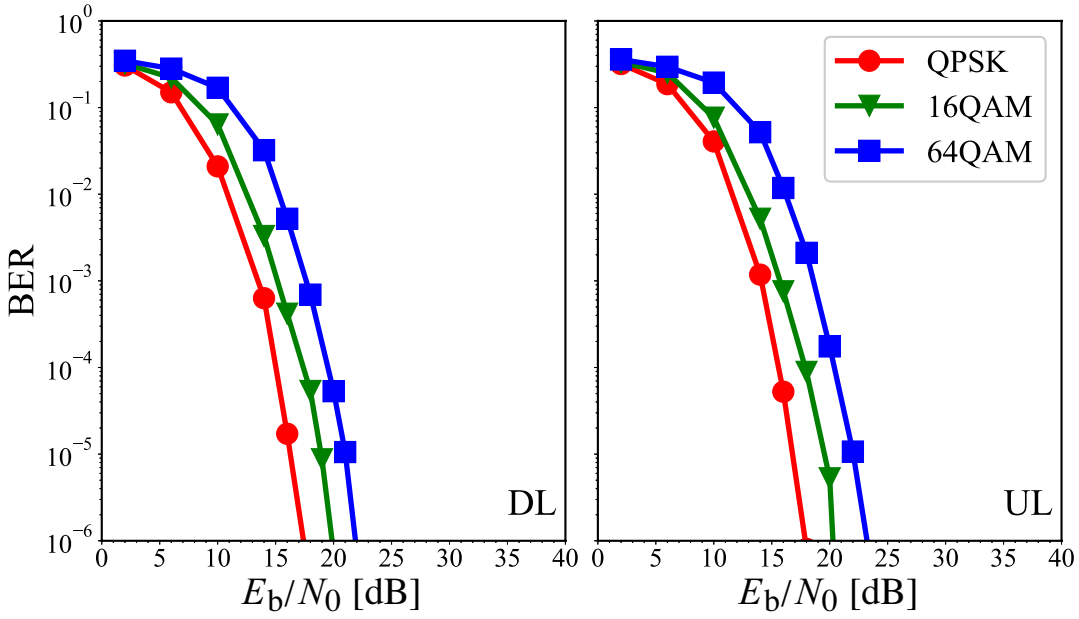

Figure 3.8: Performance evaluation in Typical Urban model. [3] Fig. 10

Figure 3.9 depicts the BER performance of the IEEE 802.22 Profile A model obtained through computer simulation for each modulation scheme. An error floor occurs under all conditions in 64QAM, as explained earlier. In DL, an error floor also occurs in 16QAM, and the performance in QPSK is significantly degraded when compared to UL. Therefore, the UL affords several advantages in a VHF-band transmission environment when using a single antenna. Additionally, 16QAM and 64QAM transmissions are difficult in the VHF transmission environments with long delay paths.

3.4.4 Comparison of MRC Diversity in Multipath Fading Environment

Figure 3.10 depicts the BER performance using the MRC diversity in the IEEE 802.22 Profile A model. The tendency of the error floor appears slightly in 64QAM with

DL (cluster type); however, high-quality transmission can be achieved with the tile types. These tendencies demonstrate that high-speed transmission can be achieved using the two branches of MRC diversity. Table 3.3 also lists the E_b/N_0 and SNR of each modulation scheme that achieved the required BER $= 10^{-6}$.

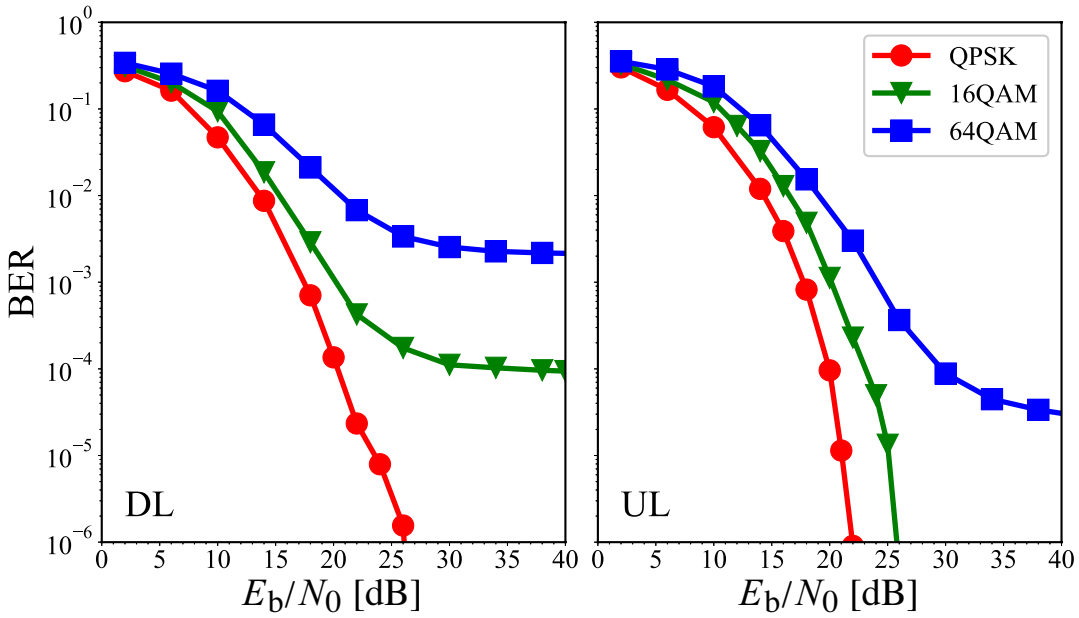

Figure 3.9: Performance evaluation in 802.22 Profile A model. [3] Fig. 11

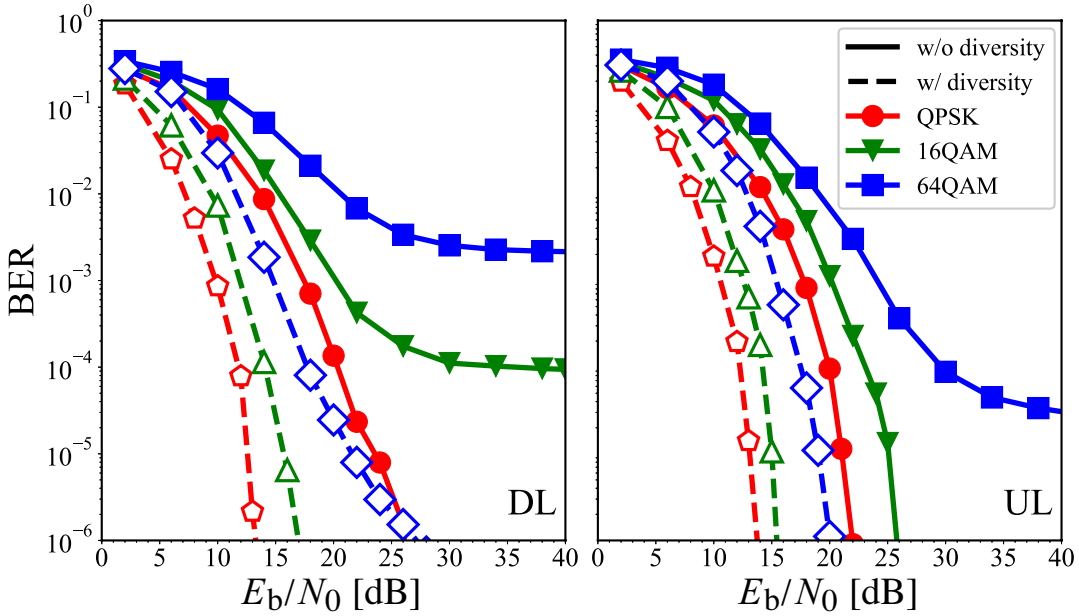

Figure 3.10: Performance evaluation in 802.22 Profile A model with MRC diversity. [3] Fig. 12

3.5 Experimental Performance Analysis by Prototype

The transmission performances of the transceivers using Mode 1 were evaluated through laboratory experiments using prototypes in terms of the input power to the BER. The experimental evaluation used parameters shown in Tables 2.2 and 3.1 and Fig. 3.11 shows our developed prototype and the experimental evaluation setup [29]. In the developed prototype, the proposed channel estimation method for downlink is implemented. The AWGN environment, typical GSM urban model, and IEEE 802.22 Profile A model were used for the evaluation.

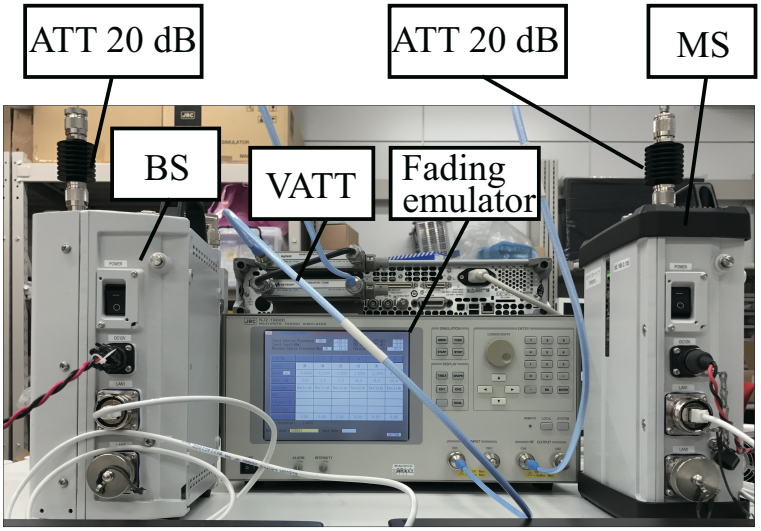

Figure 3.11: Developed prototype and experimental evaluation setup [29]. [3] Fig. 13

3.5.1 Performance Analysis in AWGN Environment

This section presents the evaluation of the prototype in the AWGN environment. Figure 3.12 depicts a diagram of the experimental evaluation of the prototype. The DL and UL were evaluated using different diagrams. The device was equipped with the 1st antenna for transmission and reception and the 2nd antenna for reception.

Figure 3.13 displays the BER performance in the AWGN environment obtained in the experimental evaluation for each modulation scheme. Both the receiving antennas were evaluated. The BER of the 1st antenna was degraded by 1.5–2.0 dB in terms of SNR at BER = 10^{-6} compared to the 2nd antenna because the signal power required to reach the processing unit is different due to power attenuation by the circulation processing of 1st antenna, even if the power input to the antenna is identical. Only the 2nd antenna was used for the subsequent evaluation with a single antenna. The BER characteristics exhibited an almost identical slope for both the experiments and computer simulations.

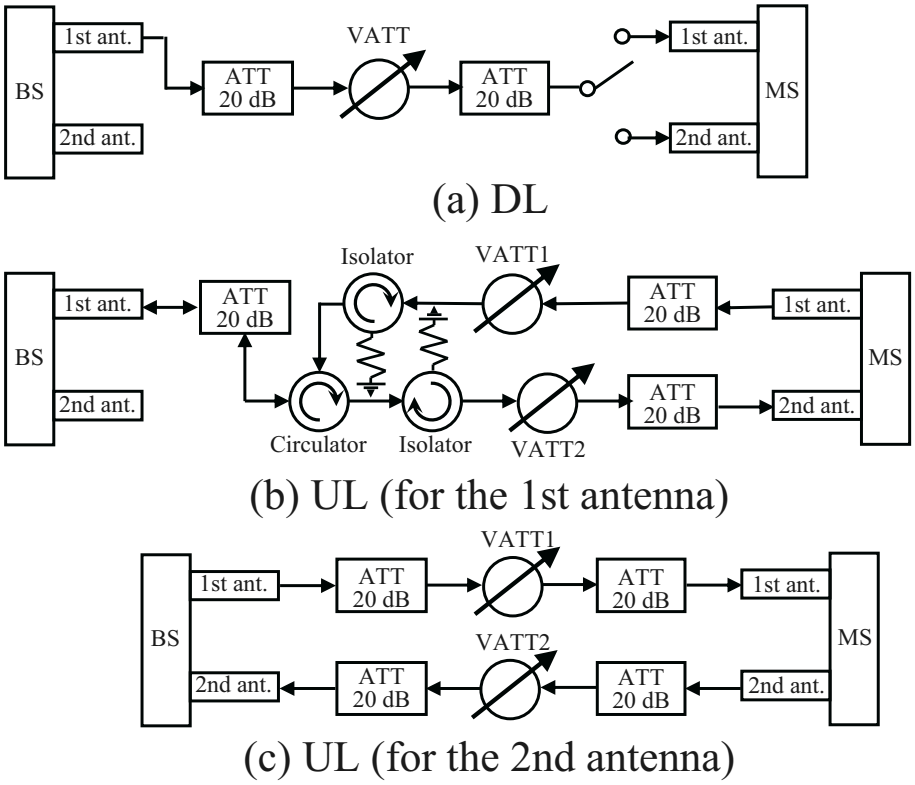

Figure 3.12: Experimental evaluation in AWGN environment. [3] Fig. 14

Table 3.5 lists the input power required to achieve the required BER = 10^{-6}. In the AWGN environment, the performance of DL and UL was nearly identical. The difference for each MCS in the input power that achieves the required BER = 10^{-6} is approximately 5–6 dB and is almost identical to that of a computer simulation. These results demonstrate the validity of the computer simulation in this environment.

3.5.2 Comparison of Modulation Schemes in Multipath Fading Environment

This section presents an evaluation of the performance of the prototype in a multipath fading environment through laboratory experiments by using a fading emulator (JRC, NJZ-1600D). Figure 3.14 presents a diagram of the experimental evaluation performed using the prototype and fading emulator. The prototype used in this experiment was installed using the complete proposed scheme for channel estimation.

Figure 3.15 depicts the BER performance in a typical GSM urban model obtained through experimental evaluation for each modulation scheme. Table 3.5 also lists the input power required to achieve the required BER = 10^{-6} in the multipath fading environment. The difference between each MCS of the input power, which achieves the required BER = 10^{-6}, is almost identical to that of a computer simulation. These results demonstrate the validity of the computer simulation in this environment. Sim-

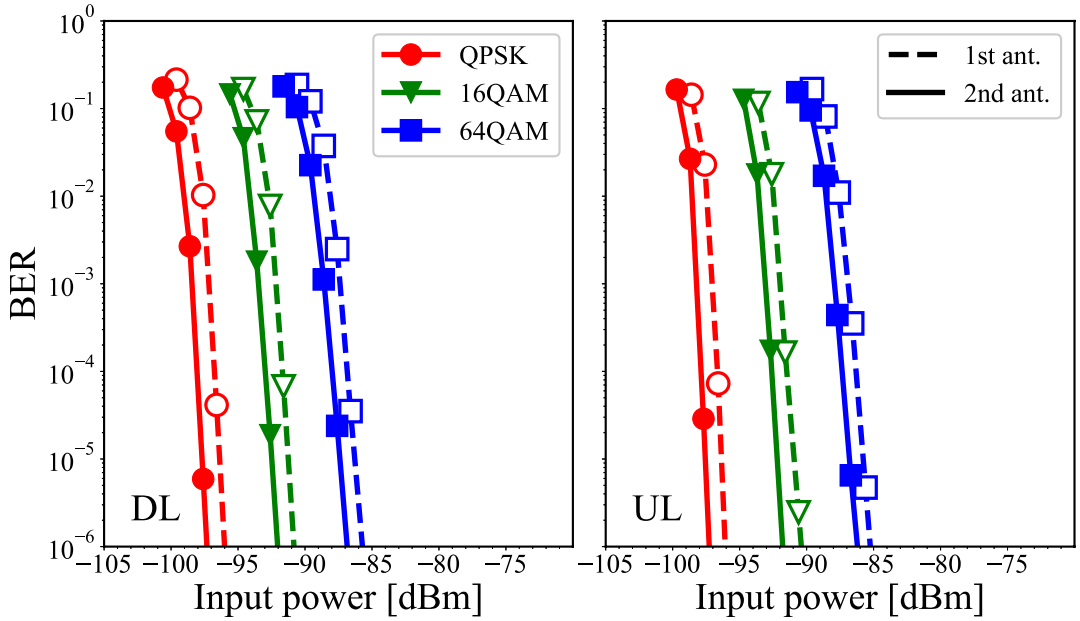

Figure 3.13: Experimental evaluation in AWGN environment. [3] Fig. 15

Table 3.5: Required input power [dBm] to achieve the required BER = 10^{-6} by experimental evaluation. [3] Table 8

	AWGN		TU		Profile A		Profile A w/ div.	
	DL	UL	DL	UL	DL	UL	DL	UL
QPSK	−97	−97	−87	−87	N/A	−74	−87	−86
16QAM	−92	−91	−81	−83	N/A	N/A	−83	−81
64QAM	−87	−86	−74	−77	N/A	N/A	N/A	−74

ilarly, Fig. 3.16 depicts the BER performance of the IEEE 802.22 Profile A model through an experimental evaluation for each modulation scheme. The tendency of the error floor is observed slightly in all the modulation schemes with DL (cluster type) and in 16QAM and 64QAM with UL (tile type). Table 3.5 also lists the input power required to achieve the required BER of each modulation scheme's required BER = 10^{-6} in the multipath fading environment. In the experimental evaluation, the performance was slightly degraded when compared to the computer simulation. However, a similar tendency is observed when DL (cluster type) performs better than UL (tile type). These results verify the validity of the computer simulation in this environment.

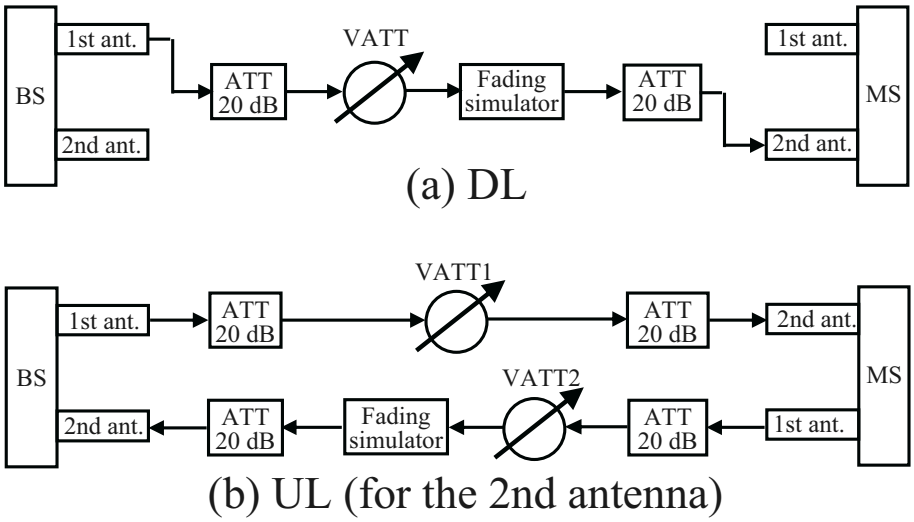

Figure 3.14: Experimental evaluation in multipath fading environment. [3] Fig. 16

3.5.3 Comparison of MRC Diversity in Multipath Fading Environment

This section evaluates the performance of the prototype in multipath fading environments based on laboratory experiments using MRC diversity. Figure 3.17 presents a diagram of the experimental evaluation performed using MRC diversity. Figure 3.18 depicts the BER performance using MRC diversity in the IEEE 802.22 Profile A model through an experimental evaluation. The error floor disappeared in most modulation schemes and appeared slightly in 64QAM with DL (cluster-type). Based on these tendencies, it was confirmed that high-speed transmission can be achieved using two branches of MRC diversity. Table 3.5 also lists the input power required to achieve the required BER = 10^{-6} for each modulation scheme in this evaluation.

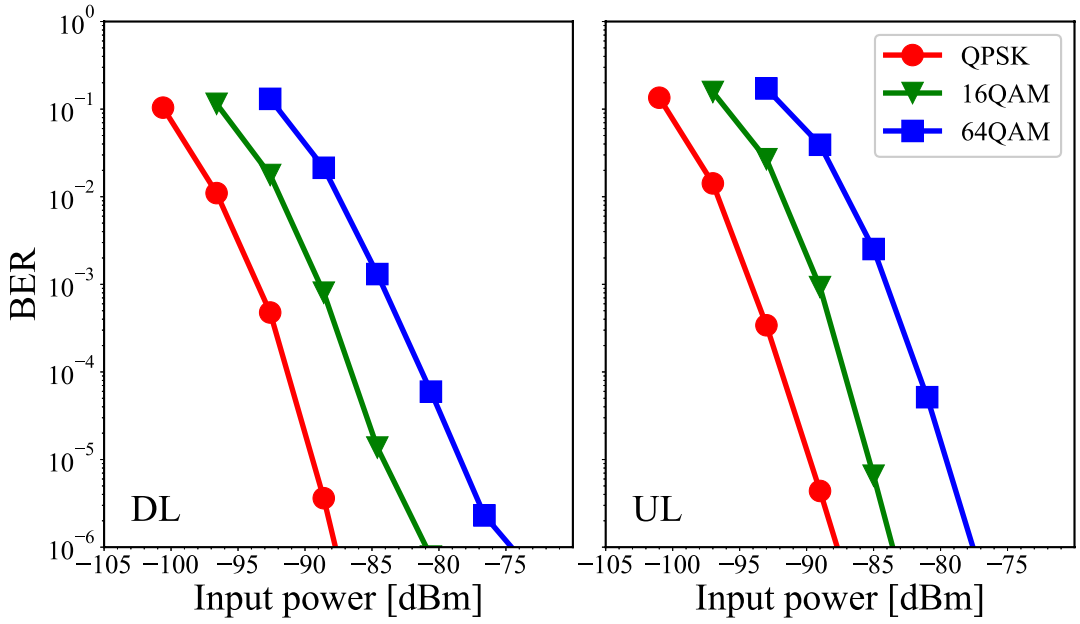

Figure 3.15: Experimental evaluation in Typical Urban model. [3] Fig. 17

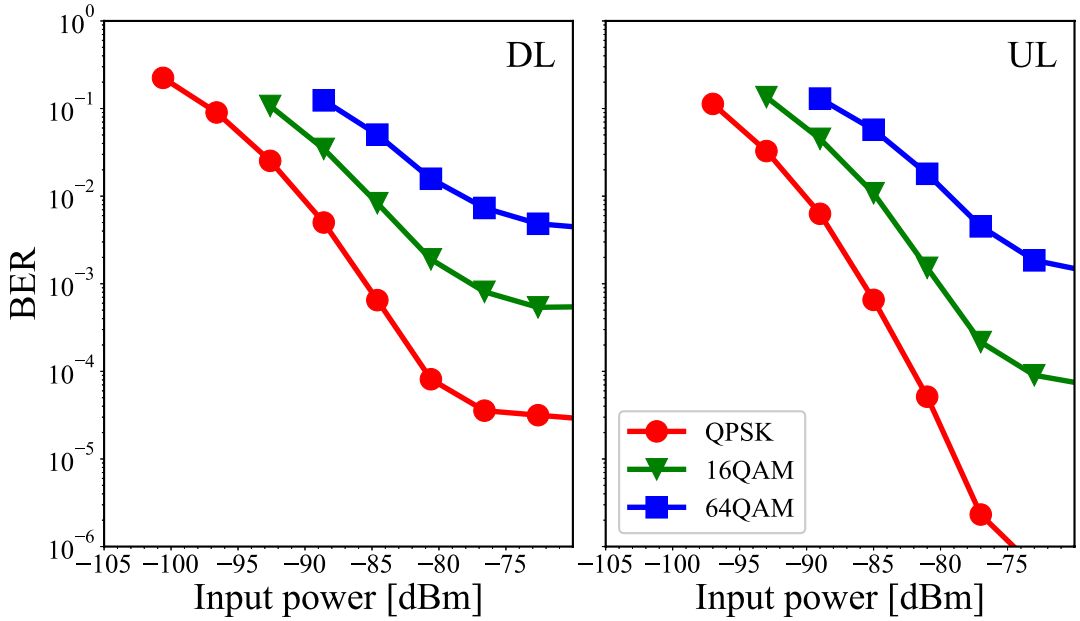

Figure 3.16: Experimental evaluation in 802.22 Profile A model. [3] Fig. 18

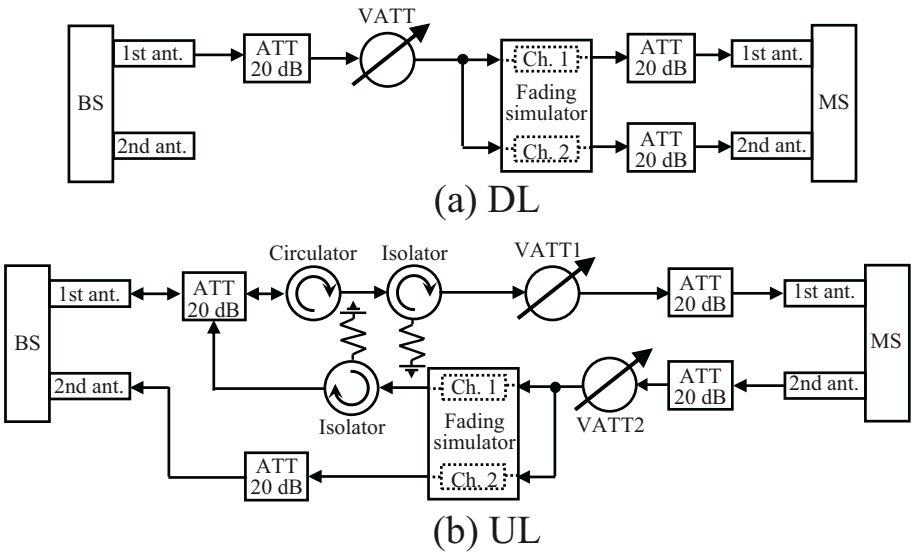

Figure 3.17: Experimental evaluation with MRC diversity in multipath fading environment. [3] Fig. 19

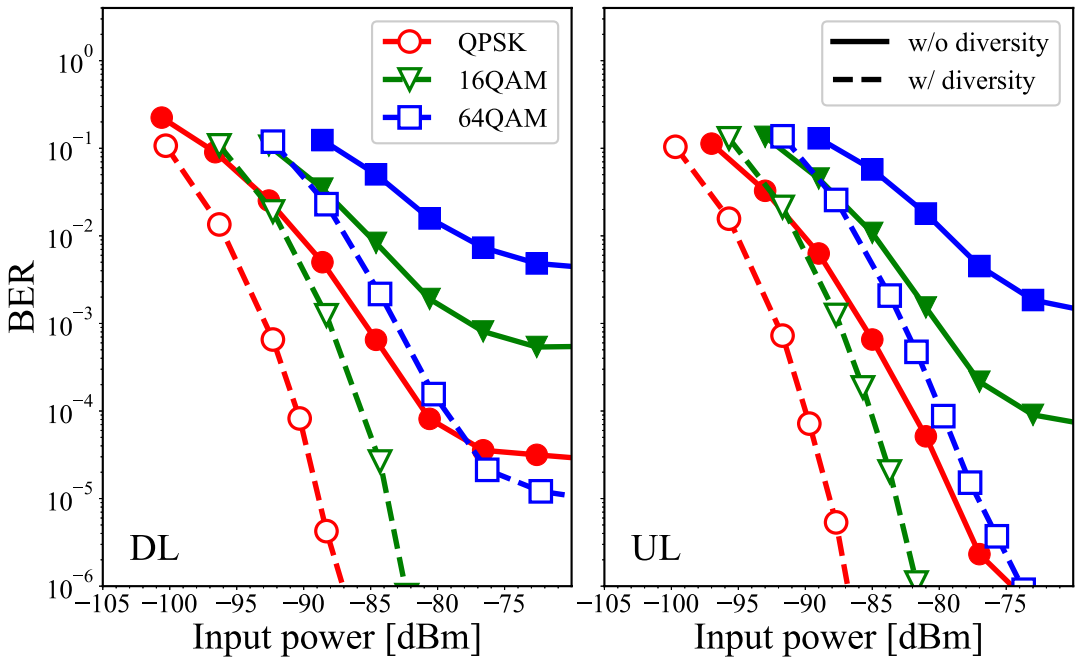

Figure 3.18: Experimental evaluation in 802.22 Profile A model with MRC diversity. [3] Fig. 20

3.6 Transmission Capability

This section evaluated the transmission capacity by evaluating throughput based on the experimental results presented in Section 3.5. The section evaluated both the single- and multihop transmissions.

3.6.1 Definition of Throughput

First, the throughput (T) of a single-hop transmission is defined as follows:

$$T = T^{\max}(1 - PER), \tag{3.10}$$

where $T^{\max}$ represents the maximum throughput as show in Table 2.1 and PER is defined as $PER = 1 - (1 - BER)^{11200}$. The size of the maximum transmission unit that is used for WiMAX is 11,200 [13]. Based on this equation, the input power versus T is evaluated using the evaluation results in Section 3.5. Similarly, this clause defines the throughput of multi-hop transmission. Ideal regenerative repeaters were assumed, and the input power versus T was evaluated. It is assumed that the relay is repeated with the required input power, as shown in Table 3.5, where there is no degradation in the throughput and transmission can be achieved between terminals using $T^{\max}$. When transmitted by n-hop one to one relay as shown in Fig. 3.19, the transmission speed T^n is expressed as follows [70]:

$$T^n = \frac{T^{\max} n}{\sum_{k=1}^{n} k} = \frac{2T^{\max}}{n+1}, \tag{3.11}$$

where the time slot configuration during multi-hop is as shown in Fig. 3.20.

3.6.2 Evaluation of Throughput

This section evaluated the transmission distance versus throughput with the assumption of an actual operation. In this evaluation, the single-hop or multihop communication between RSs illustrated in Fig. 2.1 is considered as a use case. The RS antenna height, H_{RS}, is set to 3.0 m because the antenna is to be installed on the roof of a car. Table 3.1 lists the transmission powers, and the DL:UL ratio was assumed to be 9:38. This is because the control and sensor information from the car is transmitted to the cloud. In the evaluation, the Extended Hata model [71] is used as a path model. The path loss, L_d, at a transmission distance (d) of more than 0.1 km and less than 20 km is expressed as follows:

Figure 3.19: Structure of multi-hop relay model.

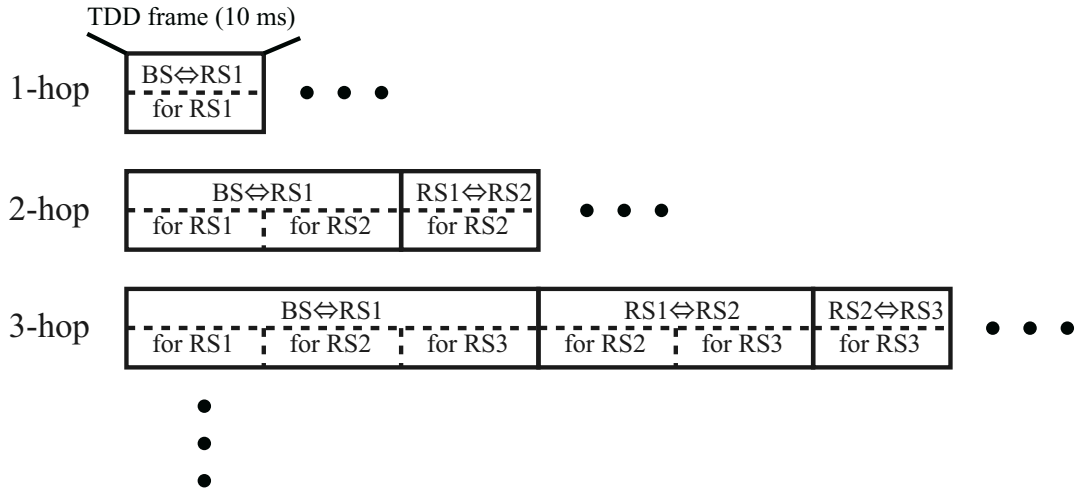

Figure 3.20: Time slots of multi-hop relay model.

$$
\begin{aligned}
L_d &= \begin{cases} L_d^{\text{urban}} & (\text{for TU model}) \\ L_d^{\text{suburban}} & (\text{for Prof. A model}) \end{cases}, \qquad (3.12)\\
L_d^{\text{urban}} &= 69.6 - 2a(H_{\text{RS}}) + 26.2\log(200) - 13.82\log\left(\max\{30, H_{\text{RS}}\}\right) \\
&\quad + [44.9 - 6.55\log\left(\max\{30, H_{\text{RS}}\}\right)]\log(d), \\
a(H_{\text{RS}}) &= (1.1\log(200) - 0.7)\min\{10, H_{\text{RS}}\} - (1.45\log(200) - 0.8) \\
&\quad + \max\left\{0, 20\log\left(\frac{H_{\text{RS}}}{10}\right)\right\}, \\
L_d^{\text{suburban}} &= L_d^{\text{urban}} - 2\left\{\log\left[\frac{\min\{\max\{150, 200\}, 2000\}}{28}\right]\right\}^2 - 40.94.
\end{aligned}
$$

The path loss for the urban and suburban environments is used in the GSM Typical Urban model and IEEE 802.22 Profile A model, respectively. The input power at the receiver ($P_{\text{R}}^{\text{input}}$) in dBm is expressed as follows:

$$P_{\text{R}}^{\text{input}} = P_{\text{T}} + G_{\text{T}} + G_{\text{R}} - L_d, \qquad (3.13)$$

where P_{T}, G_{T}, and G_{R} represent the transmit power, transmitter antenna gain, and receiver antenna gain, respectively, and both G_{T} and G_{R} are 10 dB. The single-hop throughput is calculated by applying Eqs. (3.10) and (3.13) and based on Figs. 3.15

and 3.18. Similarly, the multihop throughput is calculated by applying Eqs. (3.11) and (3.13) and based on Table3.5.

Figure 3.21 shows the transmission distance versus throughput in a typical GSM urban model. This result indicates that single-hop transmission was achieved up to approximately 9.0 km, even when QPSK was used. Conversely, when using multihop transmission, although the transmission speed is approximately 1/2 to 1/6 (almost 1.0 Mbps for UL and 0.1 Mbps for DL), the maximum transmission distance is approximately 50 km. Because UL transmission has a throughput of 1.0 Mbps, 10,000 sensors with a throughput of 100 bps can be accommodated. More sensors can also be accommodated by bundling multiple channels or by repeatedly using the same channel. It is also expected to be used in V2X based on the application. A large UL ratio primarily is set for collection purposes. Conversely, it is possible to change the DL:UL ratio based on the use cases.

Figure 3.22 shows the transmission distance versus throughput with MRC diversity reception in the IEEE 802.22 profile A model. Under these conditions, the multihop relay is not evaluated because an error floor occurs in the DL-64QAM, and the input power required to achieve the required BER does not exist. In addition, the same tendency as the typical GSM urban model without MRC diversity was obtained for the transmission distance. The BS is expected to have higher antennas, particularly in a suburban environment.

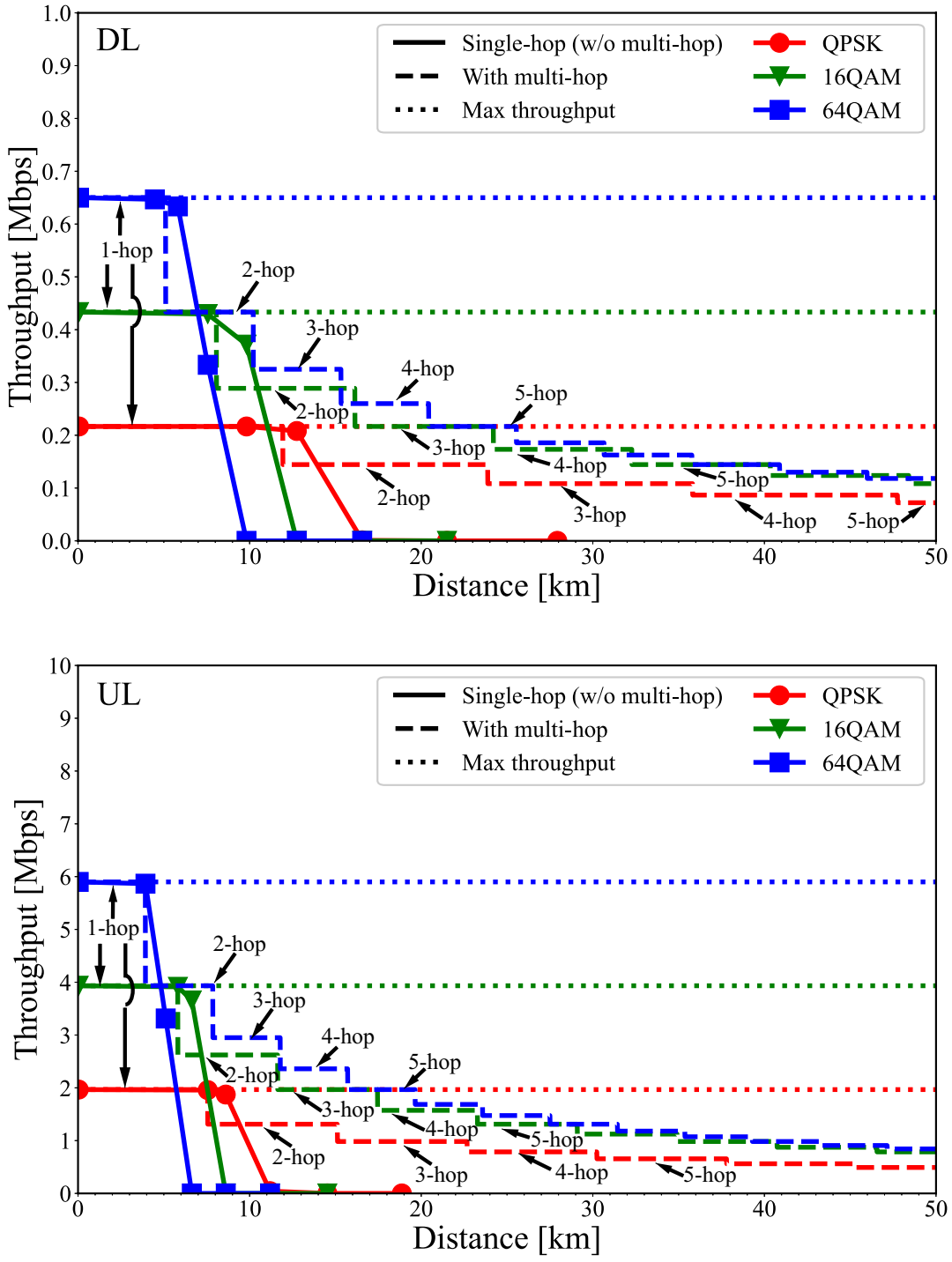

Figure 3.21: Transmission distance between RSs to throughput in Typical Urban model (DL:UL=9:38). [3] Fig. 21

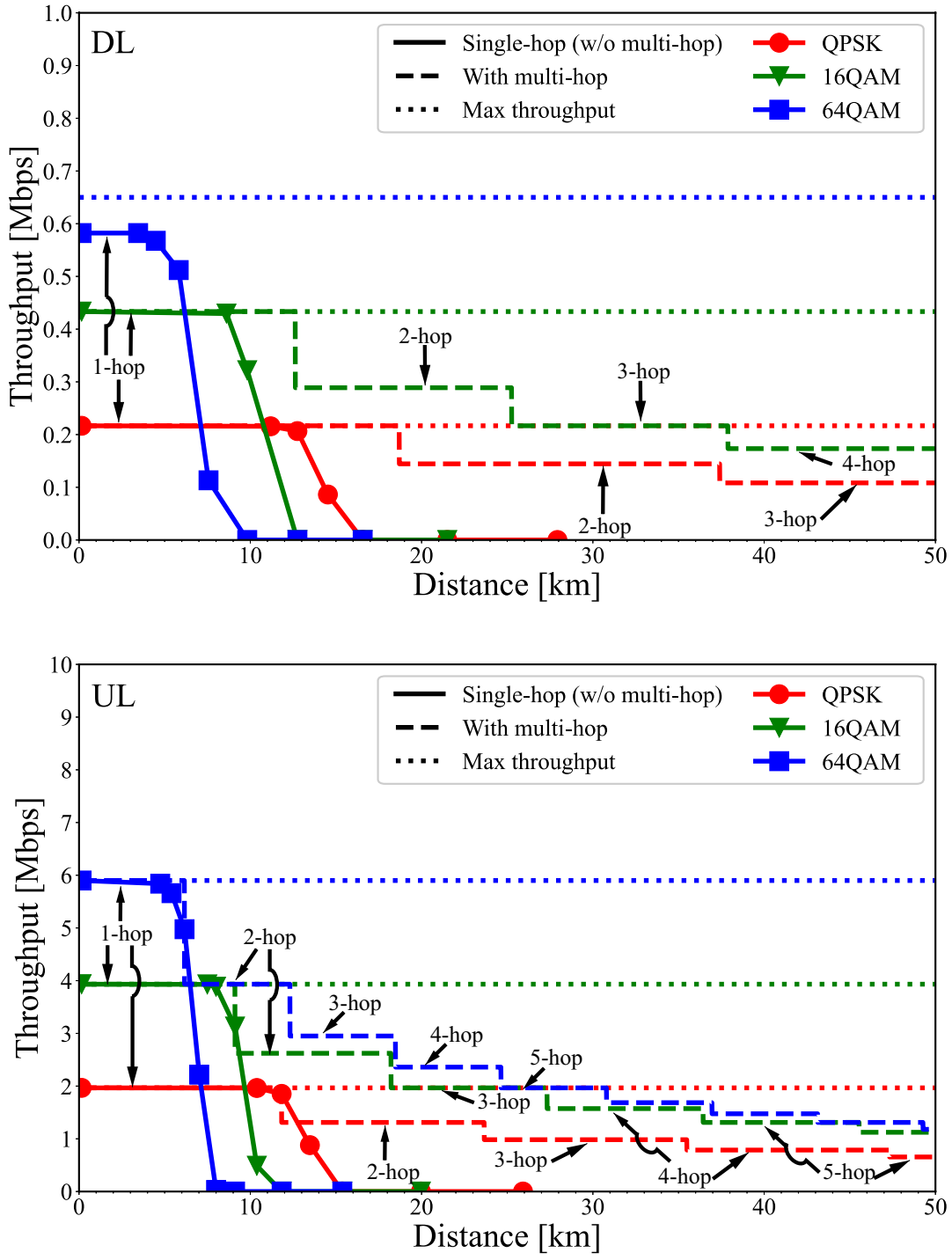

Figure 3.22: Transmission distance between RSs to throughput in Profile A model with MRC diversity (DL:UL=9:38). [3] Fig. 22

3.7 Conclusion

This chapter comprehensively evaluated the transmission performance using the proposed methods in a VHF-band radio propagation environment through computer simulation and experimental evaluation by using the prototype. The experimental evaluation results confirmed the validity of computer simulations in this environment. Single-hop transmission reaches up to approximately 10 km while maintaining transmission speeds of several Mbps on the UL, when QPSK is used. Conversely, by using multihop transmission, although the transmission speed is approximately 1/2 to 1/6 (almost 1.0 Mbps for UL and 0.1 Mbps for DL), the maximum transmission distance is approximately 50 km. These results indicate that the ARIB T103/IEEE 802.16n is expected to be a WRAN communication system for IoT and V2X-based applications.

Chapter 4
Adaptive Transmission Control for SVD-MIMO

4.1 Introduction

As mentioned in Chapter 2, a method using SVD-MIMO and ATC is being considered for next-generation FPUs. By using ATC assuming SVD-MIMO transmission, the aim is to control the optimal transmission method from the perspective of communication channel capacity. The MER is used as an index to express the channel quality in the conventional ATC method for the next-generation FPUs. MER is defined as the average value of the transmitted signal power divided by the error power between the transmitted signal and the received one. The standard is the "monitored MER," which is calculated from the transmitted and received signals of each stream and directly represents the channel quality. It is the same as the SINR for each stream. It is desirable to perform ATC using this monitored MER as the channel quality of each stream, but it is impossible to obtain this value before transmission. Therefore, a "calculated MER" estimated from the received SNR and estimated channel matrix of the previous frame is used for ATC.

In previous studies, calculated MER, which takes noise enhancement into account and is determined from singular values that are the output of SVD, has been used. From now on, this thesis calls it "conventional-calculated MER." The conventional-calculated MER matches the monitored MER of the ideal SVD-MIMO using ideal Tx and Rx weight matrices with high accuracy. As described in Section 2.2.4.2, the system model conforms to the standard [46], wherein various factors degrade the Tx weight matrices. In addition, an incomplete weight matrix that deviates from the ideal Rx weight matrix is used. These deviations change the amount of noise enhancement and also generate interference components. Therefore, in the actual transmission, the conventional-calculated MER deviates significantly from the monitored MER. Additionally, the use of the MER with ABPA, which is an ATC algorithm that does

This chapter is based on "Methods of adaptive transmission control for SVD-MIMO using incomplete weight matrices" [4], by the same author, which appeared in the IEICE Transactions on Communications (Japanese Edition),

not take interference into account, degraded transmission performance. On the other hand, there is no proposal or consideration about ATC using error correction codes or modulation schemes with high modulation order (such as 4096QAM) for the actual SVD-MIMO transmission, which uses incomplete weight matrices in a mobile environment.

This chapter proposes two methods. First, this chapter proposes a new calculated MER (the thesis call it "proposed-calculated MER"). The MER is an index that expresses the channel quality, which includes the amount of the changed noise enhancement and interference components when transmitting with incomplete weight matrices. This chapter also proposes a new ABPA algorithm as an ATC algorithm that takes changed noise enhancement and interference components into account. By conducting computer simulations of SVD-MIMO transmission using these proposed methods, this chapter will confirm the effectiveness of the proposed ATC in improving transmission performance. The sections of this chapter are listed as follows. Section 4.2 defines the monitored MER, conventional-calculated MER, and proposed-calculated MER using mathematical formulas as indexes of channel quality for ATC. Section 4.3 describes the ATC algorithm using calculated MER, which is ABPA and the equal power allocation-based method for comparative method. Section 4.4 evaluates the estimation performance of each calculated MER of Section 4.2 by computer simulation. Section 4.5 evaluates the required SNR for each method and each condition using computer simulation to evaluate ATC performance. Finally, Section 4.6 concludes this chapter.

4.2 Methods of Estimating Channel Quality

In actual SVD-MIMO transmission, such as system models described in Section 2.2.3, ATC is performed based on the estimated channel quality of each stream. Especially in the system model, channel quality is represented by MER, which is the ratio of the desired signal to the undesired signal in the received signal.

4.2.1 Monitored MER

The "monitored MER" $MER^{\text{monit.}}$ calculated by known-transmitted and -received signals is defined by

$$MER^{\text{monit.}} = \Sigma_s \left(|t_s|^2 \right) / \Sigma_s \left(|r_s - t_s|^2 \right), \tag{4.1}$$

where t_s and $r_s \in \mathbb{C}$ represent the transmitted and received signals at sample index s, respectively. The monitored MER expresses the channel quality and is synonymous with the SINR of the entire sample. However, measuring monitored MER before transmission and using it for ATC is impossible. Therefore, the use of the "calculated MER," which estimates the monitored MER from the estimated channel matrix $\boldsymbol{H}$

and $SNR^{\mathrm{Av.}}$, has been studied [43]. On the other hand, an equivalent MER can be calculated from the received SNR and channel matrix $\boldsymbol{H}$. It is called the "calculated MER" [43]. Correctly expressing the monitored MER by the calculated MER is synonymous with accurately estimating the channel quality.

4.2.2 Conventional-calculated MER

The definition of conventional-calculated MER considered only the noise enhancement in 2.2.4.1:

$$MER_i^{\mathrm{Conv.}} = SNR^{\mathrm{Av.}} \xi_i^2 p_i. \tag{4.2}$$

4.2.3 Proposed-calculated MER

This section proposes the proposed-calculated MER that considers the variation of the emphasized noise and interference components. First, the noise enhancement component $\boldsymbol{T}^{-1}\boldsymbol{W}'\boldsymbol{n}$ in Eq. (2.5) is

$$\begin{aligned} \boldsymbol{T}^{-1}\boldsymbol{W}'\boldsymbol{n} &= \boldsymbol{T}^{-1}\left(\Sigma_k w_{0,k} n_k, \cdots, \Sigma_k w_{3,k} n_k\right)^{\mathrm{T}} \\ &= \boldsymbol{T}^{-1}\left(\sqrt{\Sigma_k |w_{0,k}|^2}, \cdots, \sqrt{\Sigma_k |w_{3,k}|^2}\right)^{\mathrm{T}} \boldsymbol{n}'', \end{aligned} \tag{4.3}$$

where $w_{i,k}$ is the element at the i-th row and k-th column of $\boldsymbol{W}'$, $k = 0, 1, 2, 3$ is the stream index, $\boldsymbol{n}''$ is the noise vector, and the subscript T means the transpose. The sum of Gaussian distributions n_k is a Gaussian distribution. Since $\sqrt{\Sigma_k |w_{i,k}|^2}$ is the amount of amplitude variation from n_k of $\Sigma_k w_{i,k} n_k$, $\boldsymbol{n}'' = \{n_i''\}$ has the same distribution as $\boldsymbol{n}$. Similarly, by calculating Eq. (4.3), the noise component of each stream is $n_i'' \sqrt{\Sigma_k |w_{i,k}|^2} / \sqrt{p_i}$. From a comparison with the noise enhancement component in the ideal SVD-MIMO transmission (defined in Eq. (2.4)), this thesis defined the equivalent singular value ξ_i' as

$$\xi_i' = 1 / \sqrt{\Sigma_k |w_{i,k}|^2}. \tag{4.4}$$

This value is treated in the same way as the singular value ξ_i in Section 4.2.2.

Similarly, the interference component $\boldsymbol{T}^{-1}\boldsymbol{\Delta}\boldsymbol{T}\boldsymbol{x}$ in Eq. (2.5) is

$$\begin{aligned} &\boldsymbol{T}^{-1}\boldsymbol{\Delta}\boldsymbol{T}\boldsymbol{x} \\ &= \left[\left(\Sigma_k \delta_{0,k} \sqrt{p_k} x_k\right) / \sqrt{p_0}, \cdots, \left(\Sigma_k \delta_{3,k} \sqrt{p_k} x_k\right) / \sqrt{p_3}\right]^{\mathrm{T}}, \end{aligned} \tag{4.5}$$

where $\delta_{i,k}$ is the element at the i-th row and k-th column of $\boldsymbol{\Delta}$. Each transmitted signal x_i is normalized to have an average power of one. Therefore, the proposed-calculated

MER from the expected value of the undesired power is

$$MER_i^{\text{prop.}} = \left[\left(SNR^{\text{Av.}} \xi'^2_i p_i \right)^{-1} + \left(\Sigma_k \delta^2_{i,k} p_k \right) / p_i \right]^{-1}. \tag{4.6}$$

4.2.3.1 Correction Term of Interference Component

$\boldsymbol{W}'$ in Eqs. (4.4) and (4.5) was calculated only from the estimated channel. However, the difference between $\boldsymbol{W}$ and $\boldsymbol{W}'$ is also due to the error between the estimated channel matrix and the actual channel matrix. Therefore, the difference to be considered was insufficient. This thesis proposes a method to estimate channel quality using a corrected channel matrix, which is the estimated channel matrix $\widetilde{\boldsymbol{H}}$ plus a correction term. The channel estimation error includes elements caused by AWGN and elements unrelated to AWGN caused by subcarrier placement or control delay. The MMSE weight matrix $\boldsymbol{W}^{\text{Cor.}}_{\text{MMSE}}$ for channel quality estimation considering both elements is

$$\begin{aligned} &\widetilde{\boldsymbol{H}^{\text{Cor.}}} = \widetilde{\boldsymbol{H}} + \boldsymbol{D}_{SNR} + d \cdot \boldsymbol{1} \\ &\boldsymbol{W}^{\text{Cor.}}_{\text{MMSE}} \\ &= \left[\left(\widetilde{\boldsymbol{H}^{\text{Cor.}}} \boldsymbol{V}' \right)^{\text{H}} \widetilde{\boldsymbol{H}^{\text{Cor.}}} \boldsymbol{V}' + \frac{4}{SNR^{\text{Av.}}} \text{I} \right]^{-1} \left(\widetilde{\boldsymbol{H}^{\text{Cor.}}} \boldsymbol{V}' \right)^{\text{H}}, \end{aligned} \tag{4.7}$$

where $\boldsymbol{D}_{SNR}$ is AWGN with the same distribution as the received noise, d is a constant parameter that does not depend on AWGN, and $\boldsymbol{1}$ is a matrix with all elements one ($\in \mathbb{R}^{4\times4}$). This $\boldsymbol{W}^{\text{Cor.}}_{\text{MMSE}}$ is used as $\boldsymbol{W}'$ instead of $\boldsymbol{W}_{\text{MMSE}}$ which is used in Eqs. (4.4) and (4.5) ($\boldsymbol{W}' = \boldsymbol{W}^{\text{Cor.}}_{\text{MMSE}}$).

4.3 Adaptive Transmission Control Algorithm

As an ATC algorithm in SVD-MIMO, the water-filling algorithm and equal power allocation are power distribution methods that maximize the total channel capacity based on noisy-channel coding theorem [52]. When the power distribution p_i is fixed, the channel capacity C_i per unit bandwidth of each stream i is calculated using each stream MER MER_i

$$C_i = \log_2(1 + MER_i) \fallingdotseq \log_2(MER_i). \tag{4.8}$$

Here, as showned in Section 4.2, in the ideal environment $MER_i^{\text{Conv.}} = SNR^{\text{Av.}} \xi_i^2 p_i$. Also, when MER_i is sufficiently high compared to one, the approximation of Eq. (4.8) holds. Power allocation that maximizes the total channel capacity $\sum_i C_i$ without approximation is the water-filling algorithm, and power allocation when approximation is a precondition is the equal power allocation [73]. In the SNR region used for actual transmission, since MER_i is sufficiently high, the difference in channel capacity

between when using the water-filling algorithm and using the equal power distribution in SVD-MIMO is tiny. Therefore, this thesis uses equal power distribution as a comparison method for simplicity.

On the other hand, even with power distribution optimized for channel capacity, optimizing the modulation method according to the difference in channel capacity under certain N^{mod} conditions is another problem. BER-based methods for optimizing modulation schemes that do not use error correction codes are being considered under conditions of using power allocation based on the water-filling algorithm or equal power allocation [53, 54]. However, the paper [53] does not consider interference, and N^{mod} is less than 10. On the other hand, the paper [54] does not use modulation schemes with a high modulation order. Furthermore, since the method in that paper determines the modulation scheme independently for each stream, N^{mod} also changes significantly.

For the system model, an ABPA algorithm that optimizes the power allocation and modulation scheme for each stream under a fixed N^{mod} condition has been proposed [43]. This chapter compares and evaluates ABPA and an allocation method based on channel capacity using equal power distribution under various environments, including environments that consider interference. Since the same ATC is needed to be applied to all subcarriers in the TDD frame due to implementation, each of $MER_i^{\mathrm{conv.}}$ and $MER_i^{\mathrm{prop.}}$ is averaged at first. After that, the following ATC algorithm using the averaged MERs will be performed.

4.3.1 Equal Power Distribution and Modulation Scheme Determination

In equal power distribution, the power distribution p_i becomes $p_i = 1/l$ when the number of used streams is l. This section shows how to select the number of streams l and determine the modulation schemes $\{n_i^{\mathrm{mod}}\}$ according to the fixed N^{mod}. Figure 4.1 shows the process of it. First, equal power distribution requires a process to select the number of streams to be used that maximizes the approximate channel capacity. The number of used streams $l_{\max}$ is calculated by

$$
\begin{aligned}
l_{\max} &= \max_{l=\{1,2,3,4\}} \left\{C_l^{\mathrm{sum.}}\right\}, \\
\left\{C_l^{\mathrm{sum.}}\right\} &= \sum_{i=0}^{l-1} \left[\log_2\left(MER_i^l\right)\right],
\end{aligned}
\tag{4.9}
$$

where MER_i^l is the MER of i-th stream when equal power distribution $p_i = 1/l$ is used. The conventional method uses Eq. (4.2), and the proposed method uses Eq. (4.6).

Since the total channel capacity $\left\{C_l^{\mathrm{sum.}}\right\}$ does not match N^{mod}, it is necessary to determine the allocation of each capacity according to the difference in optimized channel capacity between the streams. The allocated capacity $n_i^{\mathrm{mod},0}$ of each stream

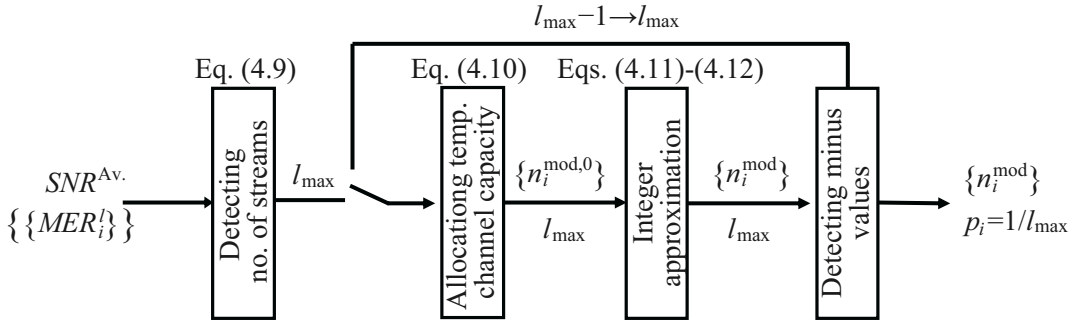

Figure 4.1: Process of equal power allocation and determination of modulation methods. ©2023 IEICE, [4] Fig. A·1

that gives an equal margin to the channel capacity is

$$n_i^{\mathrm{mod},0} = \log_2\left(MER_i^{l_{\max}}\right) + \left(N^{\mathrm{mod}} - C_l^{\mathrm{sum.}}\right)/l_{\max}. \tag{4.10}$$

However, $n_i^{\mathrm{mod},0}$ can not be an integer value. Therefore, under certain N^{mod} conditions, integer approximation is performed so that each modulation order becomes an integer. First, n_i^{mod} is calculated by rounding down to the decimal point:

$$n_i^{\mathrm{mod}} = \left\lfloor n_i^{\mathrm{mod},0} \right\rfloor. \tag{4.11}$$

Then, i_{add} was added one at a time to the surplus stream until the total allocated capacity n_i^{mod} matches the total modulation order N^{mod} $\left(N^{\mathrm{mod}} = \sum n_i^{\mathrm{mod}}\right)$:

$$\begin{aligned} i_{\mathrm{add}} &= \mathrm{argmax}_i\left(n_i^{\mathrm{mod},0} - n_i^{\mathrm{mod}}\right) \\ n_{i_{\mathrm{add}}}^{\mathrm{mod}} &= n_{i_{\mathrm{add}}}^{\mathrm{mod}} + 1. \end{aligned} \tag{4.12}$$

Since such approximation processing is essential, the allocated capacity will not be optimal for the channel capacity. However, these calculations can be expected to be a semi-optimal allocation method to channel capacity.

When the SNR is sufficiently high and $C_l^{\mathrm{sum.}}$ is well higher than N^{mod}, the allocated capacity of the stream with the minimum allocated capacity may be less than zero. In this method, the stream whose allocated capacity is less than 0 is discarded, and the number of streams is reduced by one ($l_{\max} = l_{\max} - 1$). Then, the process of Eqs. (4.10)-(4.12) is performed again. This $n_{i_{\mathrm{add}}}^{\mathrm{mod}}$ is each modulation order for output. This is the output of this method together with the power allocation $p_i = 1/l_{\max}$. This method determines the optimal power allocation and the modulation scheme based on it under ideal conditions where channel capacity is directly linked to channel quality. On the other hand, since the water-filling algorithm and equal power distribution do not take interference into account, there is a problem that the power distribution is not optimal under conditions where there is interference [73, 74]. In addition, as

far as the author knows, in SVD-MIMO, the method that determines the modulation orders according to the water-filling algorithm and equal power distribution and takes interference into account under certain N^{mod} conditions in a mobile environment has not been considered.

4.3.2 Adaptive Bit and Power Allocation (ABPA)

ABPA is an algorithm that matches and maximizes the "MER margin" between streams. Note that the MER margin is the value obtained by dividing the MER of each stream by the "reference MER" depending on the modulation method [43]. When setting an appropriate standard MER according to the channel capacity, this method maximizes the channel capacity of each stream while keeping the difference between the channel capacity of each stream and the channel capacity according to each standard MER (reference capacity) equal.

4.3.2.1 Conventional ABPA

Figure 4.2 shows the flow of the conventional ABPA algorithm based on the conventional-calculated MER of Section 4.2.2, which does not take interference into account. First, the provisional MER margin $Margin^{0}_{j,i}$ under the condition without power allocation is

$$\begin{aligned} MER_i^{\mathrm{conv.},0} &= SNR^{\mathrm{Av.}\xi_i^2} \\ Margin^{0}_{j,i} &= MER_i^{\mathrm{conv.},0} / MER^{\mathrm{thre.}}_{j,i}, \end{aligned} \tag{4.13}$$

where j is the modulation scheme allocation index and $MER^{\mathrm{thre.}}_{j,i}$ is the reference MER of the i-th stream. In this method, the value obtained from the required SNR value that achieves 10^{-4}, which is the required BER for pseudo-error-free RS decoding in an AWGN environment [43], is used as the reference MER. For example, when the modulation method of each stream of $j = 0$ is {64QAM, 64QAM, 16QAM, 16QAM}, each reference MER is set to $\{MER_{0,i}^{mathrmthre.}\} = \{24.3\,\mathrm{dB}, 24.3\,\mathrm{dB}, 18.3\,\mathrm{dB}, 18.3\,\mathrm{dB}\}$. Also, the modulation order under that condition is $\{n^{\mathrm{mod}}_{j,i}\} = \{6, 6, 4, 4\}$. In this method, determining j is equivalent to deciding the modulation scheme for each stream.

For each modulation method, the power allocation $p^{\mathrm{cal.}}_{j,i}$ of each stream is determined based on the provisional MER margin of the allocation j.

$$p^{\mathrm{cal.}}_{j,i} = \left[Margin^{0}_{j,i} \cdot \sum_i \left(Margin^{0}_{j,i} \right)^{-1} \right]^{-1} \tag{4.14}$$

Using $MER_i^{\mathrm{conv.}}$ which is obtained by substituting $p^{\mathrm{cal.}}_{j,i}$ into p_i of Eq. (4.2), the MER

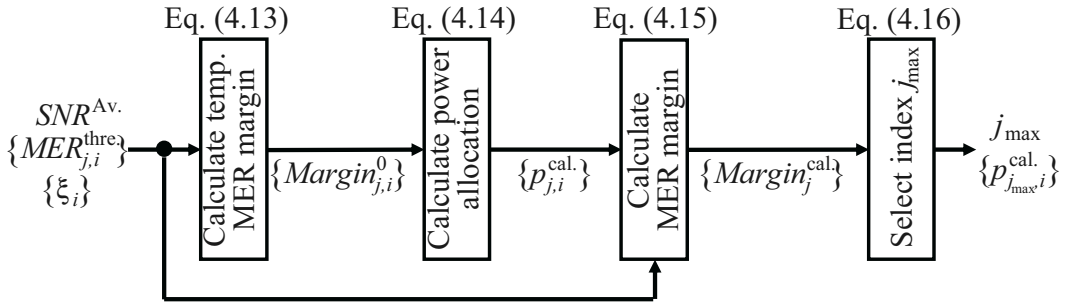

Figure 4.2: Process of conventional ABPA algorithms. ©2023 IEICE, [4] Fig. 5

margin of each stream $Margin^{\mathrm{cal.}}_{j}$ is

$$Margin^{\mathrm{cal.}}_{j} = MER^{\mathrm{conv.}}_{i} / MER^{\mathrm{thre.}}_{j,i}. \tag{4.15}$$

At this time, $Margin^{\mathrm{cal.}}_{j}$ matches regardless of the stream index i due to the effect of power allocation. By making this MER margin the same, the difference between the channel capacity obtained from the average MER of each stream and the reference capacity is made the same. The modulation scheme allocation index $j_{\max}$ that obtains the maximum MER margin is

$$j_{\max} = \mathrm{argmax}_{j} \left\{ Margin^{\mathrm{cal.}}_{j} \right\}. \tag{4.16}$$

$j_{\max}$ and $\{p_i\} = \left\{ p^{\mathrm{cal.}}_{j_{\max},i} \right\}$ will be output of the conventional ABPA. In addition, in an example of the simulation conditions evaluated with Section 4.4.1, $\left\{ p^{\mathrm{cal.}}_{j_{\max},i} \right\}$ deviates by 3 dB at most compared to the result of equal power distribution that is optimized for channel capacity in ideal SVD, under the same number of stream usage conditions. This value is sufficiently small compared to the maximum MER difference between streams, which is 40 dB. In other words, although conventional ABPA optimizes not only power allocation but also the modulation method, the power distribution is semi-optimal to the channel capacity under conditions that do not consider interference. Furthermore, by making the MER margin the same, the difference between the channel capacity of each stream and the reference capacity is made the same. Therefore, from the perspective of channel capacity, the modulation scheme was determined so that the same level of transmission performance can be expected between streams.

4.3.2.2 Proposed ABPA

This section proposes an ABPA algorithm based on the proposed-calculated MER of Section 4.2.3. Figure 4.3 shows the flow of it, which takes interference into account. First, the provisional power allocation $p_{j,i}^{\text{cal.}}$ is calculated using Eqs. (4.13) and (4.14). In this calculation, the equivalent singular value ξ'_i of Eq. (4.4) is used instead of the singular value ξ_i. After that, $p_{j,i}^{\text{cal.}}$ is used as $p_{j,i}^{\text{in}}$ and the provisional MER margin $Margin_{j,i}^{0}$ is updated as follows:

$$\begin{aligned} MER_{j,i}^{\text{Prop.},0} &= \left[\left(SNR^{\text{Av.}} \xi'^{2}_{i} p_{j,i}^{\text{in}} \right)^{-1} + \left(\Sigma_k \delta_{i,k}^{2} p_{j,k}^{\text{in}} \right) / p_{j,i}^{\text{in}} \right] \\ Margin_{j,i}^{0} &= MER_{j,i}^{\text{Prop.},0} / \left(MER_{j,i}^{\text{thre.}} p_{j,i}^{\text{in}} \right). \end{aligned} \tag{4.17}$$

Equation (4.14) gives the power allocation $p_{j,i}^{\text{cal}}$ that optimizes the MER margin $MER_{j,i}^{\text{Prop.},0}$ when using $p_{j,i}^{\text{in}}$ as the power allocation. However, changing $p_{j,i}^{\text{in}}$ changes the interference power, and the MER changes in turn; that is, the appropriate $p_{j,i}^{\text{cal.}}$ changes. The optimal power allocation considering interference can be obtained by repeatedly substituting $p_{j,i}^{\text{cal}}$ into $p_{j,i}^{\text{in}}$ and solving Eqs. (4.17) and (4.14). Figure 4.4 shows an example of how $p_{j,i}^{\text{cal.}}$ changes with repetition at j, which takes the maximum MER margin for each number of streams under the computer simulation conditions of Section 4.4.2. Note that the allocated amount in EP distribution is shown as a line segment without a marker. Regardless of the number of streams used, $p_{j,i}^{\text{cal}}$ converges sufficiently in less than three iterations. Because sufficient convergence is required not only in this example, four iterations were used in this study with a margin. In addition, in the proposed ABPA, there is a significant deviation from EP even under the same stream number usage conditions, especially at a maximum of just under 20 dB in 4-stream transmission. Under the conditions of Section 4.4.2, the maximum MER difference between streams is about 30 dB, so this power distribution difference is considered to have a strong impact on performance. Therefore, if the proposed ABPA achieves semi-optimal power distribution for the channel capacity under these conditions like the conventional ABPA, the EP optimized in the ideal environment deviates greatly from optimal power distribution in the degraded environment. The final output of the MER margin $Margin_{j,i}^{\text{cal}}$ using the post-convergence power allocation is calculated as

$$\begin{aligned} MER_{j,i}^{\text{prop.}} &= \left[\left(SNR^{\text{Av.}} \xi'^{2}_{i} p_{j,i}^{\text{cal.}} \right)^{-1} + \left(\Sigma_k \delta_{i,k}^{2} p_{j,k}^{\text{cal.}} \right) / p_{j,i}^{\text{cal.}} \right] \\ Margin_{j,i}^{\text{cal.}} &= MER_{j,i}^{\text{Prop.},0} / MER_{j,i}^{\text{thre.}}. \end{aligned} \tag{4.18}$$

When $p_{j,i}^{\text{cal.}}$ converges perfectly, $Margin_{j,i}^{\text{cal.}}$ is expected to be the same value regardless of i. In the case of insufficient convergence, the modulation scheme allocation index

$j_{\max}$ is determined on the basis of the stream having the lowest MER margin.

$$j_{\max} = \mathrm{argmax}_j \left\{ \min_i Margin_{j,i}^{\mathrm{cal.}} \right\} \tag{4.19}$$

$j_{\max}$, and $\{p_i\} = \left\{ p_{j_{\max},i}^{\mathrm{cal.}} \right\}$ are the outputs of the P-ATC.

4.3.3 Correction Methods Based on Transmission Performance

Both the equal power allocation and ABPA algorithms are methods that use average-calculated MER to optimize power allocation and modulation scheme determinations based on the noisy-channel coding theorem. On the other hand, in reality, it is not possible to obtain transmission performance that perfectly follows the channel capacity calculated by the average-calculated MER. Due to the difference in diversity order between streams and the ratio of interference components, significant performance differences occur even if the same channel capacity of the averaged MER is obtained. Because the ideal diversity order for SVD-MIMO in an i.i.d. environment is $\{16, 9, 4, 1\}$ for each stream [48], performance degradation is expected, especially for the third stream. This thesis considers two methods to quickly reflect this performance difference in ATC: a maximum 3-stream transmission method and a MER correction method.

1) Maximum three-stream transmission method
In this method, the maximum number of streams used is limited to three for all processing. Because transmission using four streams is no longer possible regardless of the conditions, scalability of ATC decreases.

2) MER correction method
ATC is performed by biasing the MER of a specific stream using the BER performance difference based on the diversity order of each stream. Performance can be expected to improve by setting an appropriate bias value based on transmission quality.

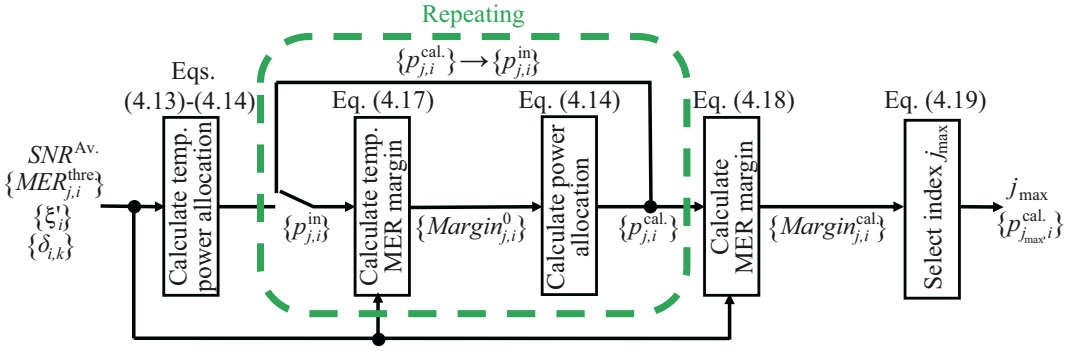

Figure 4.3: Process of proposed ABPA algorithms. ©2023 IEICE, [4] Fig. 6

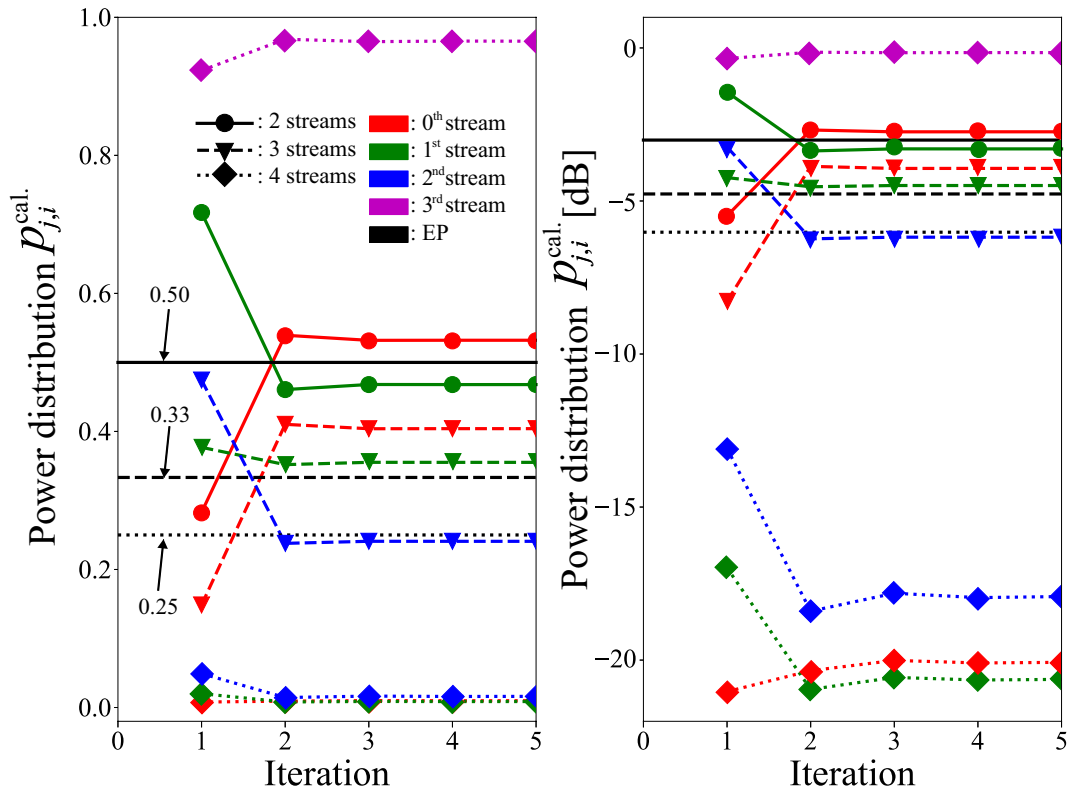

Figure 4.4: Example of power distribution convergence for proposed ABPA. ©2023 IEICE, [4] Fig. 7

4.4 Performance Evaluation of Channel Quality Estimation

This section evaluates the performance of the estimation method for channel quality of Section 4.2 by computer simulation. The channel model was an 11-path one obtained from outdoor experiments [55]. The Doppler frequency f_{D} was set to 43 Hz; the simulation assumed a mobile relay in the 2.3 GHz band and a mobile speed of 20 km/h. The Kronecker model [75] was used for the channel matrices $\boldsymbol{H}$:

$$\boldsymbol{H} = \sqrt{\boldsymbol{\Pi}_{\mathrm{r}}}\boldsymbol{G}\sqrt{\boldsymbol{\Pi}_{\mathrm{t}}}, \tag{4.20}$$

where $\boldsymbol{\Pi}_{\mathrm{t}}$ and $\boldsymbol{\Pi}_{\mathrm{r}}$ are the correlation matrices of transmission and reception. $\boldsymbol{G}$ is a 4×4 i.i.d. fading channel matrix created by the Jakes model [76] having a time variation and frequency selectivity. Note that the procedure assumes that the antennas are arranged at equal intervals, and the element of the i-th row and j-th column of the correlation matrix is defined using the nearest correlation value, as $\rho_{i,j} = \rho_0^{|i-j|^2}$ [77].

The section evaluates the performance of the estimation method by comparing the average MER of each stream using each index described in Section 4.4 against the average received SNR (SNR-MER evaluation). In the section, for simplicity, 32QAM with $n_i^{\mathrm{mod}} = 5$ is used for the modulation scheme for all streams, and the equal power distribution ($\forall i : p_i = 0.25$) is used. The section uses the medium correlation, which is the standard condition used for evaluation in ARIB STD-B75: nearest neighbor Tx correlation value $\rho_{\mathrm{t}} = 0.7$, same Rx correlation value $\rho_{\mathrm{r}} = 0.3$.

4.4.1 Ideal SVD-MIMO transmission

First, this section performs an SNR-MER evaluation of SVD-MIMO transmission under conditions where the Tx weight matrix $\boldsymbol{V}$ is not subject to degradation, such as estimation errors shown in Section 2.2.5. The signal detection matrix is also ideal ($\boldsymbol{W} = \boldsymbol{\Sigma}^{-1}\boldsymbol{U}^{\mathrm{H}}$). Furthermore, in this evaluation, the Tx and Rx weights were ideally created using the channel matrix used in the simulation rather than the estimated channel matrix based on pilot symbols.

Figure 4.5 shows the results of a comparative evaluation of the conventional-calculated MER (Conv.) obtained from the Eq. (4.2) and the monitored MER (Monit.). The section confirmed that by using the conventional converted MER, the monitored MER can be estimated correctly with an error within 1 dB under ideal conditions.

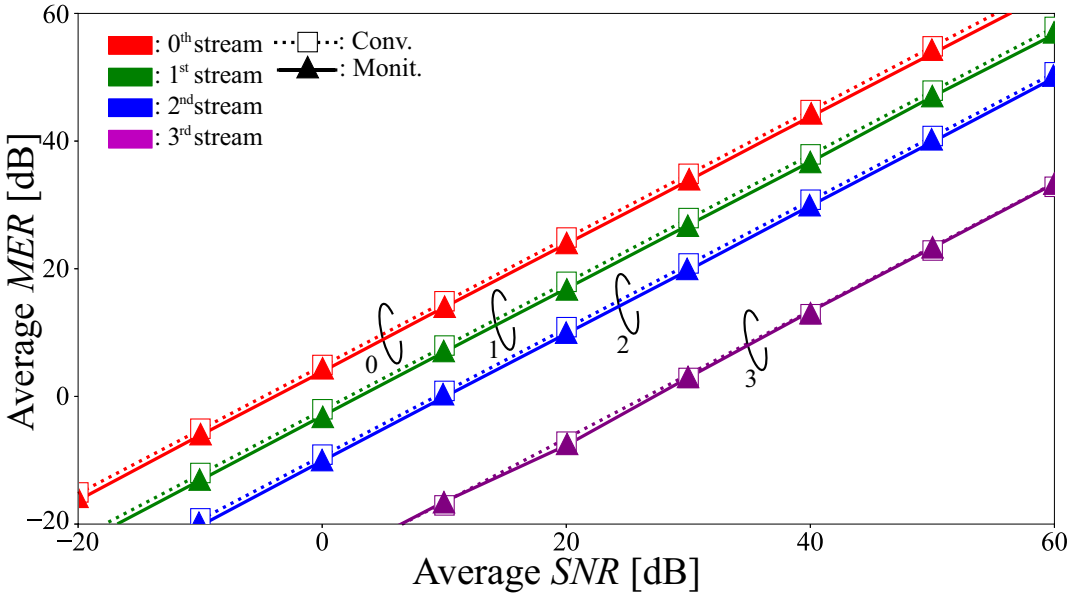

Figure 4.5: SNR-MER characteristics of the ideal environment. ©2023 IEICE, [4] Fig. 8

4.4.2 Actual SVD-MIMO transmission

Next, the section performs an SNR-MER evaluation of the actual SVD-MIMO transmission under conditions where the Tx weight matrix $\boldsymbol{V}$ is degraded by various factors described in Section 2.2.5 and signal detection matrix is changed by factors described in Section 2.2.6.

Figure 4.6 shows the results of comparative evaluation of the proposed-calculated MER (Prop. w/o correc.) without the correction term obtained from Eq. (4.6), Conv., and Monit.. Conv. deviates from Monit. by at most 20 dB or more. On the other hand, Prop. w/o correc. estimates Monit. with high accuracy and an error of 5 dB or less, except for low SNR below 0 dB or high SNR above 40 dB.

Here, Monit. converges to a constant value at low SNR below 0 dB ($SNR^{\mathrm{Av.}} \to 0$) and at high SNR above 50 dB ($SNR^{\mathrm{Av.}} \to +\infty$). This is because the signal detection matrix $\boldsymbol{W}_{\mathrm{MMSE}}$ converges to values that are not affected by SNR, and the equalized signal also converges to ones that are not affected by SNR. $\boldsymbol{W}_{\mathrm{MMSE}}$ are calculated as using Eq. (2.7),

$$\begin{aligned} \lim_{SNR^{\mathrm{Av.}} \to 0} \boldsymbol{W}_{\mathrm{MMSE}} &= \boldsymbol{O} \\ \lim_{SNR^{\mathrm{Av.}} \to +\infty} \boldsymbol{W}_{\mathrm{MMSE}} &= (\widetilde{\boldsymbol{H}}\boldsymbol{V}')^{-1} = \boldsymbol{W}_{\mathrm{ZF}}, \end{aligned} \tag{4.21}$$

where $\boldsymbol{O} \in \mathbb{R}^{4\times4}$ is the zero matrix and $\boldsymbol{W}_{\mathrm{ZF}}$ is the signal detection matrix when using the ZF method [67]. From Eqs. (4.21) and (2.5), the received signal converges to zero for all streams at low SNR. Therefore, from Eq. (4.1), Monit. converges to one

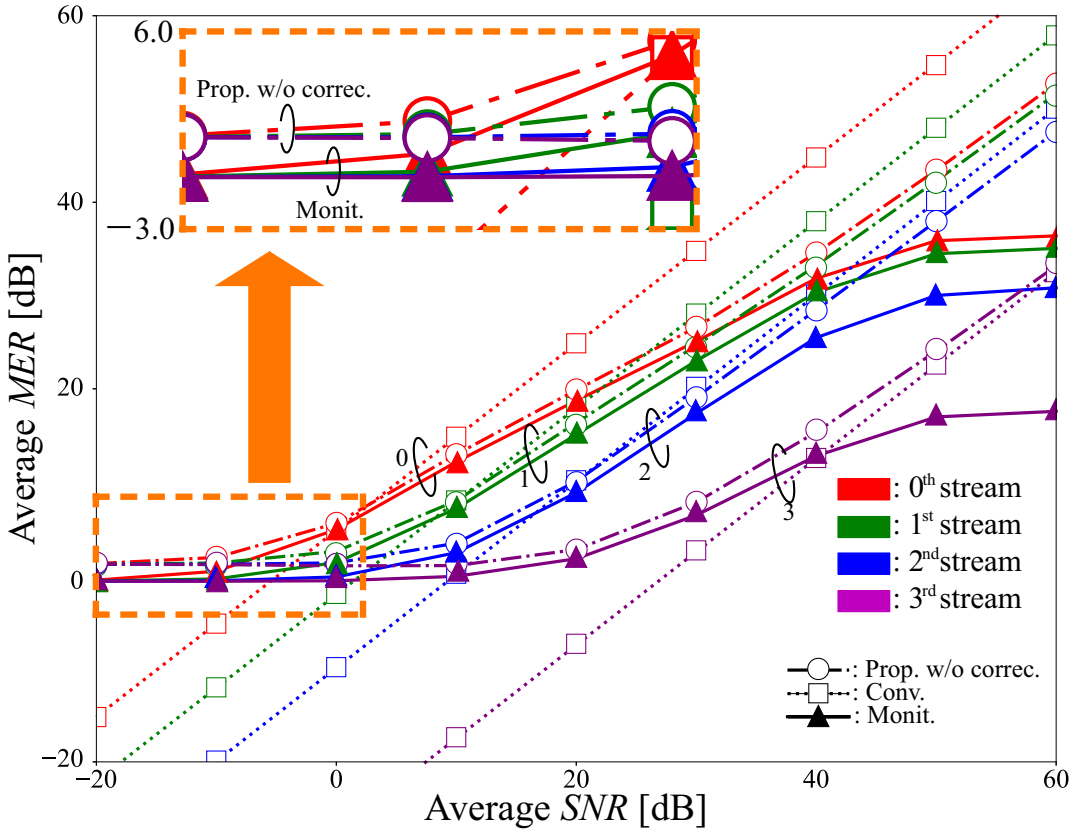

Figure 4.6: SNR-MER characteristics of the actual environment (without correction terms). ©2023 IEICE, [4] Fig. 9

(0 dB). From Eq. (2.5), the noise component in the received signal decreases, and the undesired signal becomes an interference component $\boldsymbol{T}^{-1}\boldsymbol{\Delta T}\boldsymbol{x}$ only. Therefore, Monit. converges to a constant.

Figure 4.7 shows the results of the comparative evaluation of the proposed MER obtained from Eq. (4.6) which adds the correction term described in the Eq. (4.7) (Prop.), in addition to Monit. and Prop. w/o correc.. In this evaluation, the constant correction term d was set to 0.006 ($\approx 0.0062\cdots$) based on the estimation error. To consider the influence of channel estimation errors, d is an approximate value from the average absolute difference ($|\boldsymbol{H}-\widetilde{\boldsymbol{H}}|$) between the ideal channel matrix in the computer simulation $\boldsymbol{H}$ and the estimated channel matrix $\widetilde{\boldsymbol{H}}$ in a noise-free environment. Prop. estimates Monit. with high accuracy for low SNR below 0 dB and high SNR above 40 dB. In particular, at an SNR of 0–50 dB, which is the practical operating range, Monit. is estimated with high accuracy and an error of less than 2 dB. Therefore, in the evaluation of Section 4.5, Prop. is used as the proposed method.

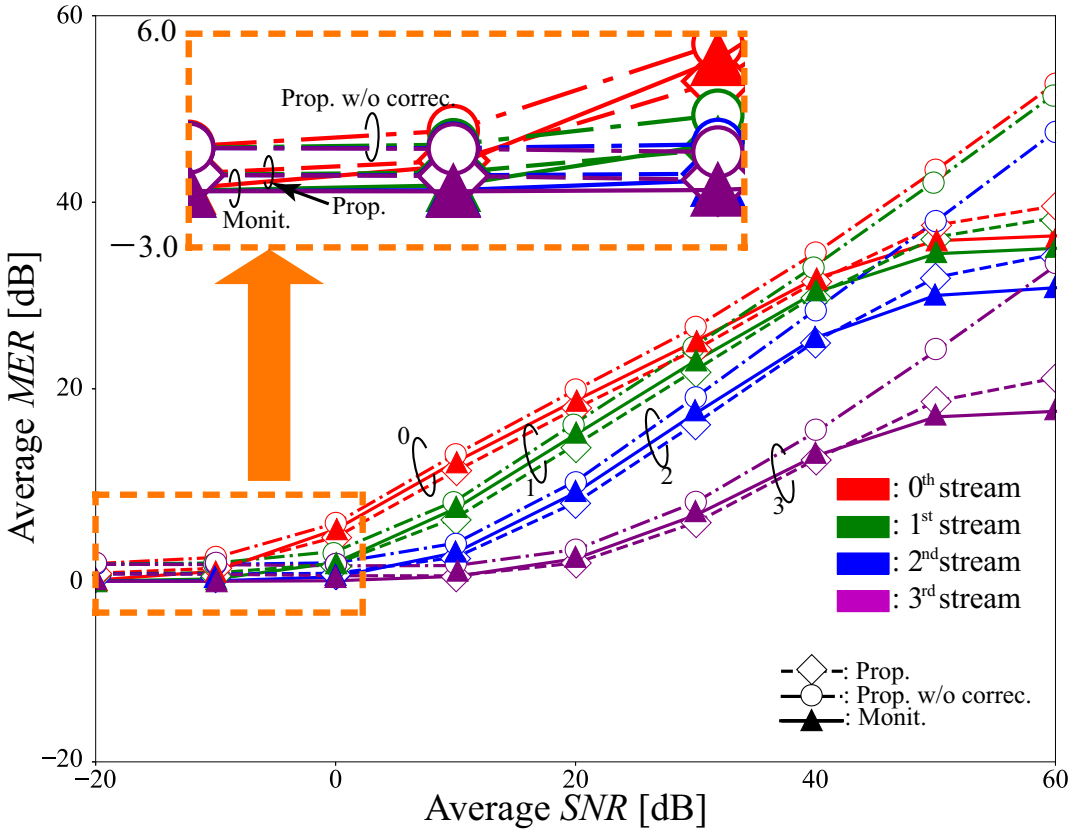

Figure 4.7: SNR-MER characteristics of the actual environment (with correction terms). ©2023 IEICE, [4] Fig. 10

4.5 Performance Evaluation of ATC algorithm

This section evaluates the ATC performance by comparing the BER against the average received SNR (SNR-BER evaluation). The required BER for pseudo-error-free operation was set to 1.0×10^{-4} [46], and the required SNR to achieve that BER was used for the evaluation. The basic evaluation conditions such as the channel model are the same as the evaluation conditions in Section 4.4. For the nearest neighbor correlation value of the transmitting and receiving antennas, in addition to the medium correlation (Med.: $\rho_t/\rho_r = 0.7/0.3$) used in Section 4.4, i.i.d. ($\rho_t = \rho_r = 0$) and high correlation (High: $\rho_t = \rho_r = 0.7$) are used. For reference, the section also partially evaluates the performance without error correction decoding of turbo codes (w/o dec.).

4.5.1 Comparison of Methods

This section compares the performance difference between the conventional method (Conv.) and the proposed method (Prop.) for EP distribution (EP) and ABPA. The conditions for performance comparison are $N^{\mathrm{mod}} = 20$, $R = 0.92$ and w/o dec., and

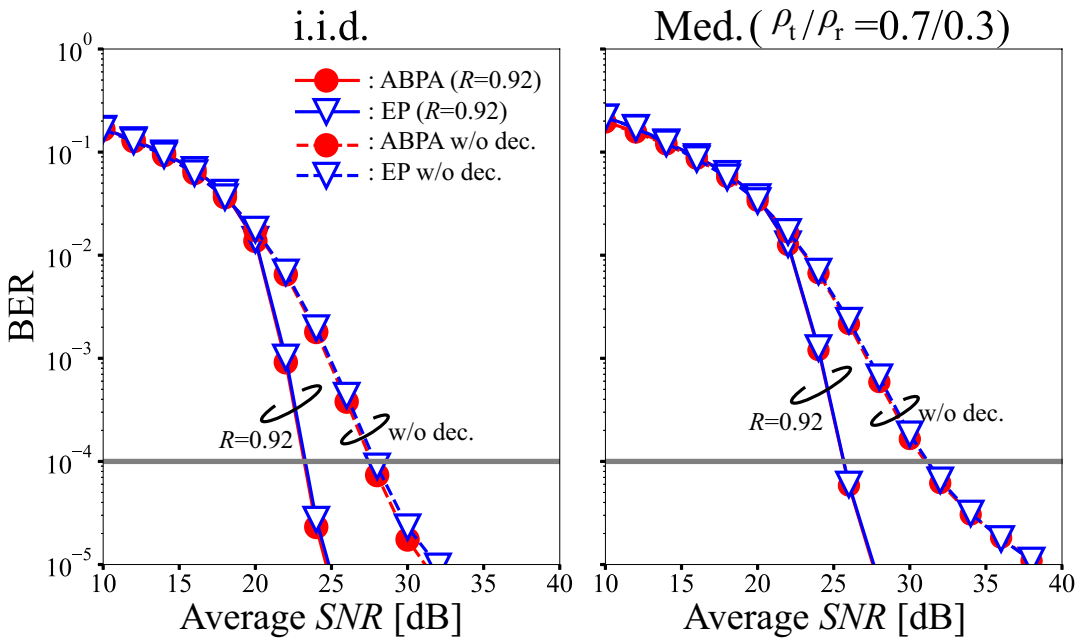

Figure 4.8: SNR-BER performances of the ideal environment. ©2023 IEICE, [4] Fig. 11

correlation is evaluated using i.i.d. and medium correlation (Med.).

4.5.1.1 Ideal SVD-MIMO Transmission

Similar to Section 4.4, this section performs SNR-BER evaluation using conventional-calculated MER for EP and conventional ABPA in ideal SVD-MIMO transmission to evaluate the original transmission performance of SVD-MIMO.

First, Fig. 4.8 shows the comparative SNR-BER evaluation results of ABPA or EP under each correlation condition and coding rate. There is almost no difference in the required SNR between the two methods, regardless of the conditions.

Next, the section evaluates the performance of each stream to compare the differences in performance between streams. Figure 4.9 shows the comparative evaluation results of each average MER margin performance obtained from the monitored MER against the average received SNR of each stream (SNR-MER margin). The MER margins are almost the same for both methods and both correlation conditions. From this, the section confirmed that the purpose of ATC can be achieved in an ideal environment. The purpose is to make the MER margin the same between streams, as described in section 4.3.2 that is, to equally control the difference between channel capacity and reference capacity between streams.

Next, Fig. 4.10 shows the comparative evaluation results of the BER without decoding against each average MER margin (MER margin-BER). Based on the results in Fig. 4.9, the MER margin-BER between streams was expected to be equivalent regarding channel capacity; however, in Fig. 4.10, the performance is not equal. The

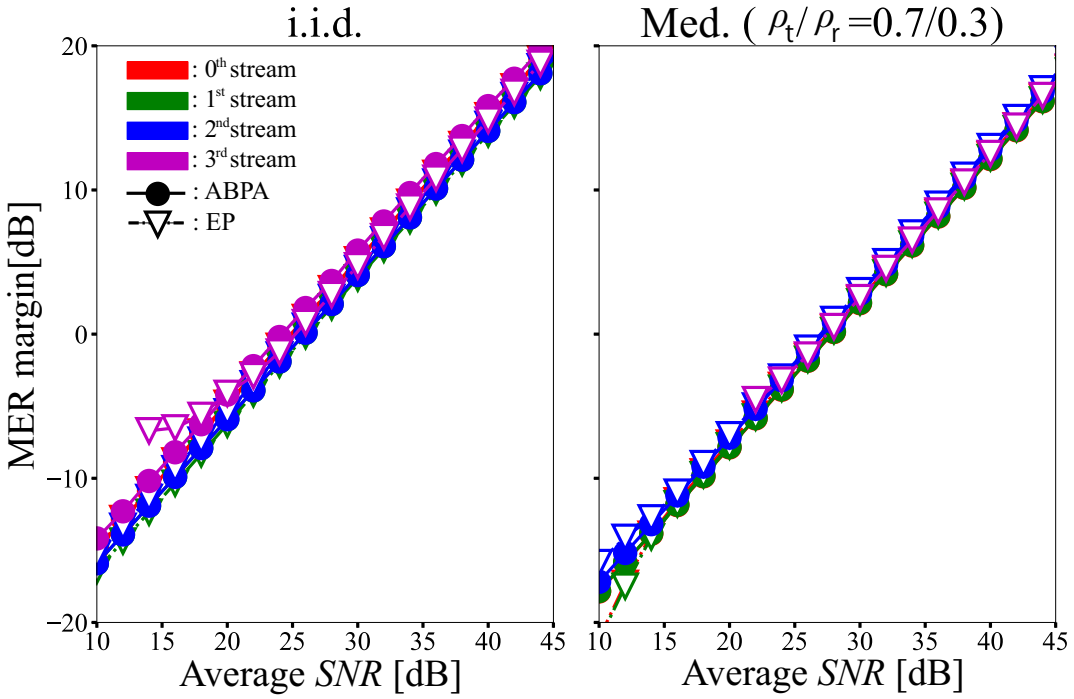

Figure 4.9: SNR-MER margin performances for each stream of the ideal environment. ©2023 IEICE, [4] Fig. 12

reason for this is the diversity order difference between streams in SVD-MIMO, which was mentioned in Section 4.3.3. In particular, in i.i.d., the third stream has a BER slope without any diversity gain. On the other hand, in the medium correlation, the diversity order difference between streams decreases, and the BER performance difference becomes relatively small. Also, due to the influence of diversity order, the slope becomes slower for all streams below $BER = 10^{-4}$. Furthermore, the third stream degrades compared to the other streams, similar to i.i.d. As shown in Fig. 4.5, the third stream has a low MER, and the modulation order of the used modulation scheme is small. Furthermore, because the singular value difference between streams is significant in the medium correlation, the third stream is not used with the ABPA algorithm and is rarely used with EP. Since there is also an effect of the error correction code, the difference between streams, including the third stream, and the slowing of the slope of the BER curve have a limited effect on the overall performance. For these reasons, ABPA and EP have similar performance in Fig. 4.8. However, by considering these performance differences, it is expected that a more optimal ATC will be realized.

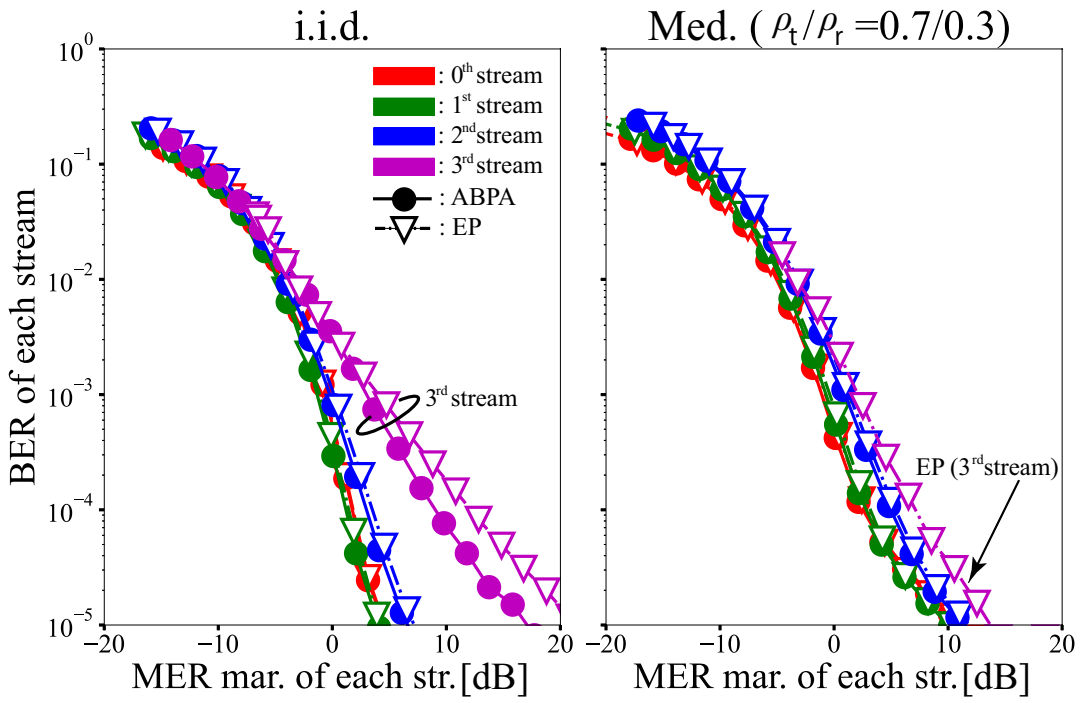

Figure 4.10: MER margin-BER performances for each stream without turbo decoding of the ideal environment. ©2023 IEICE, [4] Fig. 13

4.5.1.2 Actual SVD-MIMO Transmission

Similar to Section 4.4.2, this section evaluates the performance in SVD-MIMO, which degraded in the system model. Figure 4.11 shows the comparative evaluation results of each combination of EP and ABPA, and Prop. and Conv.. First, in i.i.d., when error correction decoding is used, the EP using the proposed-calculated MER degrades by 4 dB at the required SNR compared to the EP using the conventional-calculated MER. Note that in ABPA there is no difference between Prop. and Conv.. Similarly, in the medium correlation, while EP+Prop. deteriorates compared to EP+Conv., the proposed ABPA (ABPA+ Prop.) that uses proposed-calculated MER improves the required SNR by about 3 dB compared to conventional ABPA (ABPA+Conv.) that uses conventional-calculated MER. To investigate the cause of this, the section evaluates the performance of each stream.

Figure 4.12 shows the SNR-MER margin with EP or ABPA. For both ABPA and EP, Conv. does not match regardless of correlation; however, Prop. does match. From this, Prop. fulfills the purpose of equally controlling the difference between channel capacity and reference capacity between streams, even in degraded environments, regardless of ABPA or EP.

Figure 4.13 shows the MER margin of each stream-BER without decoding with EP or ABPA. In ABPA, the MER margin for the third stream to achieve the same BER is about 5 dB worse than the other three streams, regardless of correlation. This is mainly due to the difference in diversity order, as in the ideal environment.

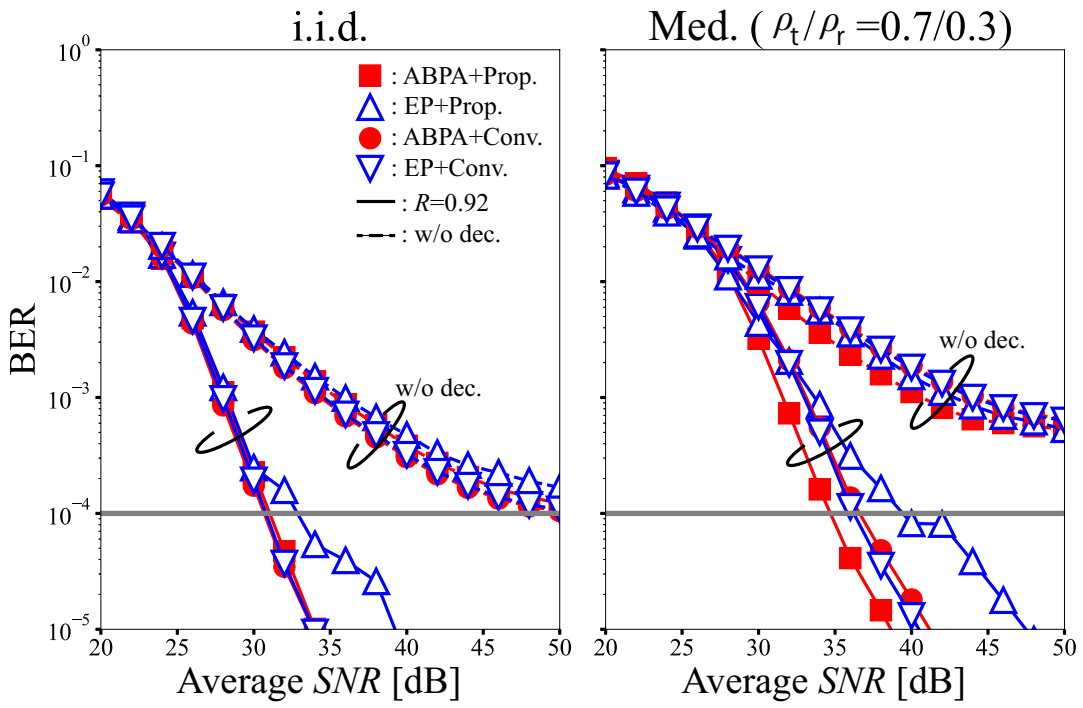

Figure 4.11: SNR-BER performances of the actual environment. ©2023 IEICE, [4] Fig. 14

Furthermore, various factors, such as interference components specific to the degraded environment, are acting in a complex manner. In addition, with Prop. in medium correlation, a tendency close to a floor error appears in the zeroth stream. In addition to the tendency that the third stream is inferior by about 5 dB with EP, as shown by the double arrow in the graph, the floor error of the zeroth stream is about one power higher than the first and second streams only with Prop..

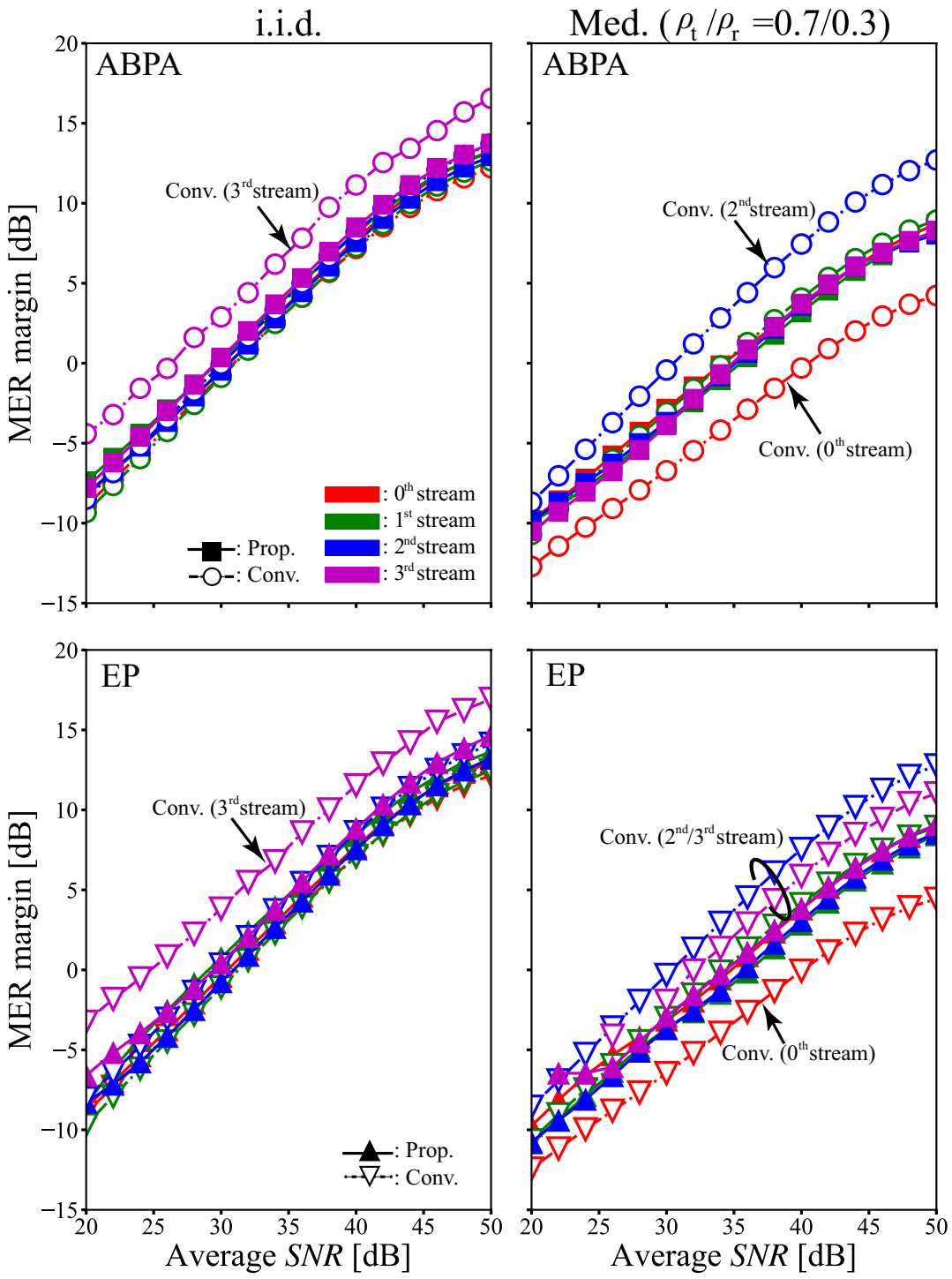

Figure 4.12: SNR-MER margin performances for each stream of the actual environment. ©2023 IEICE, [4] Fig. 15

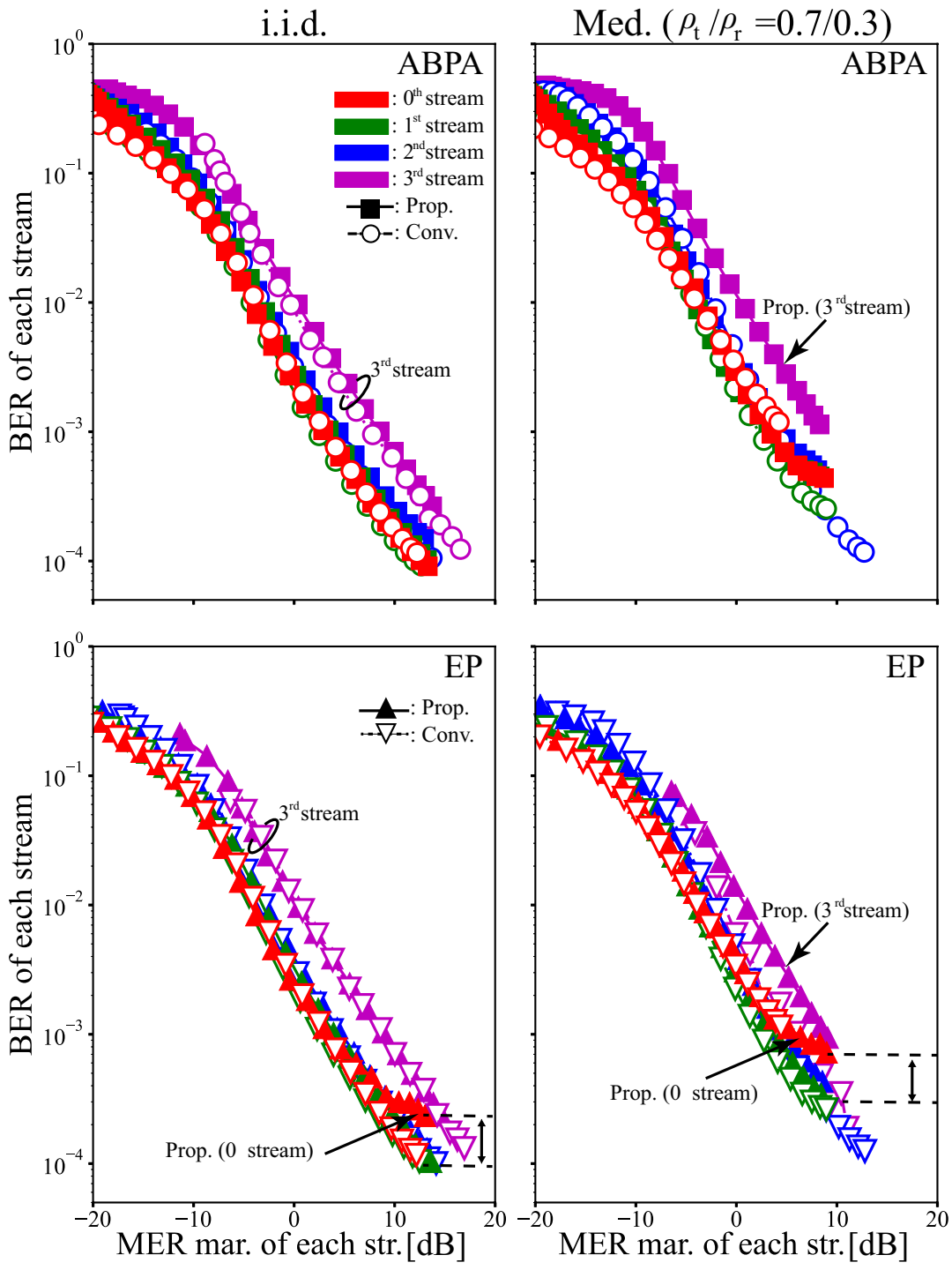

Figure 4.13: MER margin-BER performances for each stream without turbo decoding of the actual environment. ©2023 IEICE, [4] Fig. 16

In Figs. 4.12 and 4.13, the zeroth stream of Prop. has the same tendency in EP and ABPA; there was a significant performance difference in Fig. 4.11. To further investigate the cause of this, Fig. 4.14 shows the average received SNR-BER without decoding and of each stream in Prop. with EP or ABPA. In i.i.d., EP degraded compared to ABPA in the second stream with a received SNR of 35 dB or less and in the 0th stream with a received SNR of 35 dB or more. In a medium correlation environment, it degraded in the second stream with a received SNR of 40 dB or less and the 0th stream with a received SNR of 30 dB or more. This performance difference is thought to be influencing the performance difference between Prop. in Fig. 4.11. This degradation is caused by the fact that EP does not consider interference in power allocation, thus, the influence of interference power on the zeroth and second streams is significant. In addition, due to the influence of quantization, the equivalent singular values and MER differences between streams decrease, and the conditions for transmitting with four streams in Prop. increase compared to Conv.. This is thought to be why the zeroth stream particularly degrades with Prop.. One possible method is to use power distribution that is optimal for the channel capacity while taking interference into account; however, in that case, it is also necessary to separately determine the modulation scheme. For these reasons, below, the thesis uses ABPA+Prop., which semi-optimizes power allocation as well as determining the modulation scheme.

On the other hand, it is also possible that the poor performance of the third stream leads to the degradation of the overall performance. Therefore, this section compares and evaluates correction methods based on the transmission performance described in Section 4.3.3. As mentioned earlier, the third stream is about 5 dB worse in MER margin-BER than the other three streams. For each condition of ABPA+Prop. and Conv., the section compares and evaluates $R = 0.92$, without correction (W/o correc.)/maximum three-stream transmission (Max 3 str.)/MER 5 dB correction transmission that estimates the MER margin of the third stream to be 5 dB lower (5 dB biased).

Figure 4.15 shows the evaluation results. In i.i.d., the improvement due to correction is slight; however, in medium correlation, Prop. has an improvement effect of about 0.5 dB for both Max 3 str. and 5 dB biased. The reason why there is no difference between the two correction methods is that only a maximum of three streams are used, even with 5 dB biased. Due to its high scalability, the thesis will use 5 dB biased as a correction method based on transmission performance in following evaluations.

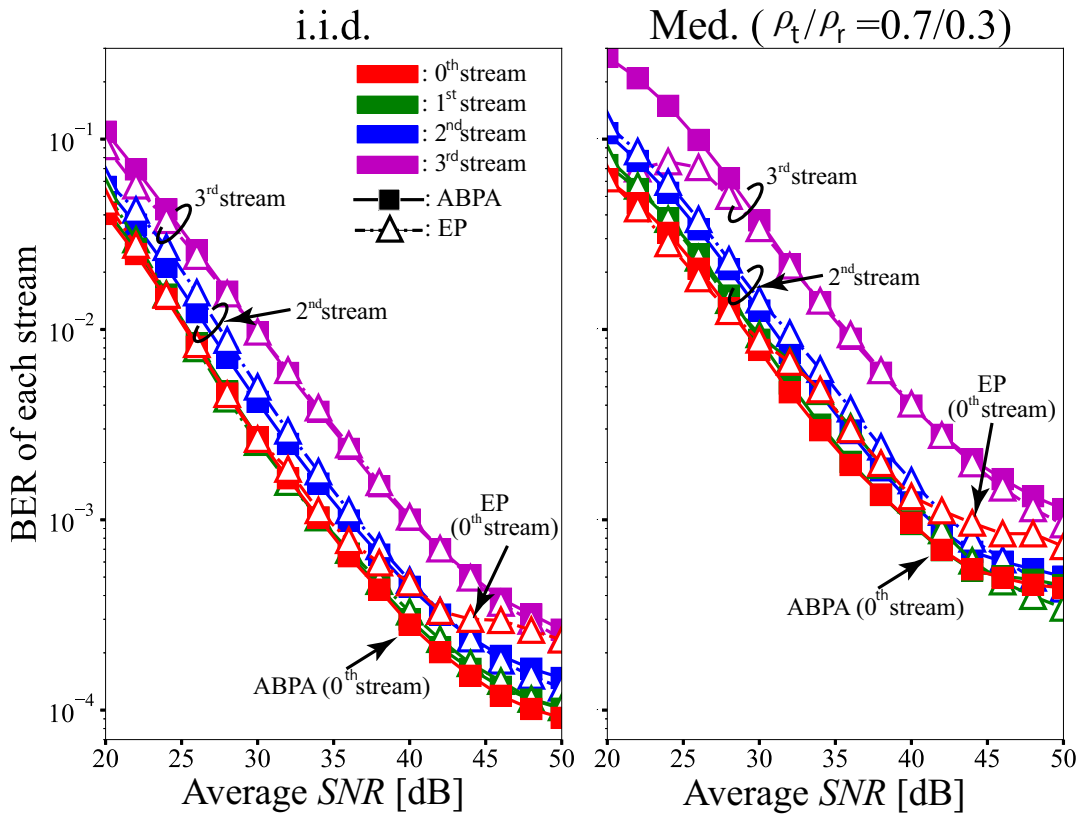

Figure 4.14: SNR-BER performances for each stream of the actual environment (Prop.). ©2023 IEICE, [4] Fig. 17

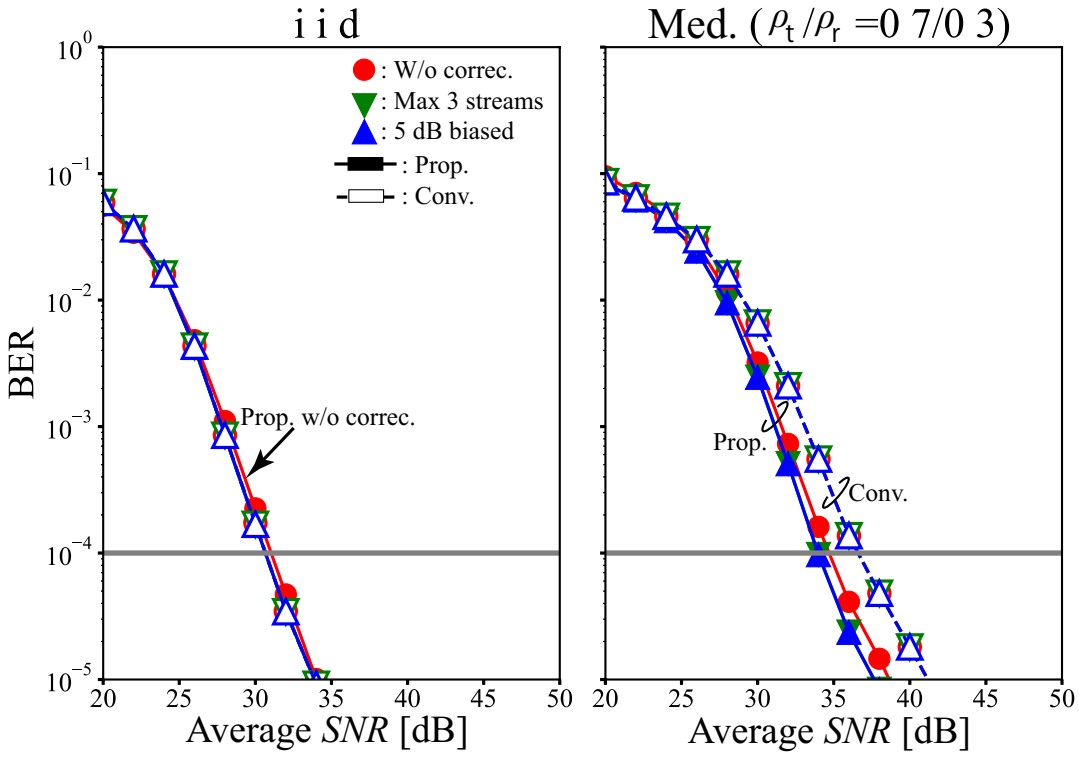

Figure 4.15: SNR-BER performances of the actual environment (ABPA with correction methods, $R = 0.92$). ©2023 IEICE, [4] Fig. 18

4.5.2 Overall Performance Evaluation

As an overall performance evaluation of the system model, this section evaluates SNR-BER for each correlation condition, each N^{mod}, and each coding rate. ABPA is used as the ATC algorithm, as mentioned earlier, and the evaluation targets are three types: the proposed method with 5 dB bias (Biased), the proposed method without correction (Prop.), and the conventional method (Conv.). Table 4.1 shows the required SNR and the lowest value under each condition is shown in bold. The values of Biased and Prop. compared with Conv. are written in parentheses. In addition, the transmission rate per N^{mod} and R (Rate in Mbps) is shown assuming the TDD frame configuration shown in Fig. 4.16.

First, this section compares and evaluates the performance in the i.i.d. environment using Table 4.1. Compared to Conv., Prop. slightly improves the required SNR by about 0.5–1.0 dB, except for some conditions. The reason why the amount of improvement is slight is thought to be that in i.i.d., the influence of $\boldsymbol{V}$ degradation is small in the first place. Biased is the same or slightly better than Conv., at 1.0 dB or less, but compared to Prop., the performance improvement is almost negligible. Moreover, it is partially degraded at high N^{mod}. In other words, in i.i.d., Prop. is generally the best method among the considered ones. This also confirms that even if there is a performance difference due to diversity order, there are some conditions where transmitting with four streams without correction is better than transmitting with three streams.

Next, the section compares and evaluates the performance at medium correlation using Table 4.1 and Fig. 4.16. Prop. improves performance by about 0.5–3.0 dB compared to Conv. except for some conditions. In particular, it improves by more than 2.0 dB at $R = 0.92$ with $N^{\mathrm{mod}} = 20, 24$. This is thought to be because the required SNR is high, and the influence of degradation due to correlation is significant, thus, the improvement effect is also significant. In particular, as shown in Fig. 4.15, compared to other conditions, the decrease of BER decreases against the SNR increase, and it approaches the floor error. Similar to Prop., Biased has a lower required SNR under almost all conditions than Conv., and lower by about 0–1.0 dB than Prop.. In other words, for medium correlation, all conditions using Biased show partial improvement, however, no degradation, compared to conditions using Prop.. This is because the difference in singular values is more significant in a correlated environment than in i.i.d.; thus, the benefits of transmitting four streams are relatively small, and the benefits of transmitting three streams outweigh the benefits, leading to improved performance. In the middle correlation environment, Biased is generally the best method among the considered ones.

Finally, the section compares and evaluates the performance at high correlation using Table 4.1. Prop. improves performance by about 0.5–5.5 dB compared to Conv. except for some conditions. In particular, it improves higher at a high coding rate. Biased improved under all conditions compared to Conv., and improved 0–1.5 dB compared to Prop. . From this, it is clear that high correlation has the same

overall tendency as medium correlation; however, the improvement effect from Prop. to Biased is limited. However, also in the high correlation environment, Biased is generally the best method among the considered ones.

From these results, the section confirmed that the proposed method (Prop./ Biased) works well regardless of correlation in the actual SVD-MIMO transmission, which uses degraded Tx/Rx weight matrices. In addition, by using a method that avoids using streams with poor specific MER margin-BER performance by giving a MER margin bias (Biased), further improvement was obtained compared to Prop. in medium and high correlation. On the other hand, since no improvement has been obtained in i.i.d., there is room for improvement by considering diversity order and interference rather than uniformly applying a 5 dB bias. Also, as shown in Table 4.1, the required SNR of Prop. for the transmission rate increases as the rate increases under most conditions. On the other hand, when comparing $N^{\mathrm{mod}} = 10$, $R = 0.71$ and $N^{\mathrm{mod}} = 20$, $R = 0.33$, the transmission rate is 62.3 Mbps and 57.9 Mbps, respectively. The required SNR is 17.5 dB and 17.0 dB for i.i.d., 17.5 dB and 18.0 dB for medium correlation, 22.5 dB and 23.0 dB for high correlation, thus $N^{\mathrm{mod}} = 10$, $R = 0.71$ is better. In other words, under these conditions, the total modulation order is relatively low, and the high coding rate yields the same or higher required SNR even at a high transmission rate. Although this is a comparison of specific conditions and cannot be considered a thorough study, it is expected that performance will be better if the total number of modulation orders is relatively lower and the coding rate is set higher under the same conditions.

4.6 Conclusion

In SVD-MIMO transmission that uses incomplete Tx and Rx weight matrices that have undergone various changes due to actual implementations, the thesis proposed a new transmission channel quality index that estimates the amount of noise enhancement and interference that has changed from ideal conditions and proposed the associated ATC methods. One proposed method estimates the actual transmission channel quality with high accuracy and an error of 2 dB or less within a practical SNR range. The other method improves the required SNR to achieve a required BER by up to 6 dB using a channel model assuming actual operation, high correlation, and high coding rate. These were confirmed by computer simulation.

Table 4.1: Required average SNR [dB] ($BER = 1.0 \times 10^{-4}$) ©2023 IEICE [4] Table 2

		Rate	i.i.d. ($\rho_t = \rho_r = 0$)			Med. corr. ($\rho_t = 0.7, \rho_r = 0.3$)			High corr. ($\rho_t = \rho_r = 0.7$)		
N^{mod}	R	(Mbps)	Biased	Prop.	Conv.	Biased	Prop.	Conv.	Biased	Prop.	Conv.
10	0.33	29.0	12.0 (0)	**11.5** (−0.5)	12.0	11.0 (−0.5)	11.5 (0)	11.5	**14.5** (−1.0)	15.0 (−0.5)	15.5
	0.71	62.3	**17.5** (−0.5)	**17.5** (−0.5)	18.0	**17.5** (−0.5)	**17.5** (−0.5)	18.0	**22.5** (−1.5)	**22.5** (−1.5)	24.0
	0.92	80.2	**22.0** (−1.0)	**22.0** (−1.0)	23.0	**22.5** (−0.5)	**22.5** (−0.5)	23.0	**28.5** (−2.5)	**28.5** (−2.5)	31.0
20	0.33	57.9	18.0 (0)	**17.0** (−1.0)	18.0	**18.0** (−0.5)	**18.0** (−0.5)	18.5	**23.0** (−0.5)	**23.0** (−0.5)	23.5
	0.71	125	24.5 (0)	**24.0** (−0.5)	24.5	**26.5** (0)	27.0 (+0.5)	**26.5**	**32.0** (−1.5)	32.5 (−1.0)	33.5
	0.92	160	**30.0** (0)	30.5 (+0.5)	**30.0**	**34.0** (−2.5)	34.0 (−2.0)	36.5	**40.5** (−6.0)	41.0 (−5.5)	46.5
24	0.33	69.5	20.0 (0)	**19.0** (−1.0)	20.0	**20.5** (0)	21.5 (+1.0)	**20.5**	**25.0** (−1.0)	26.5 (+0.5)	26.0
	0.71	150	28.0 (0)	**27.0** (−1.0)	28.0	**31.0** (0)	**31.0** (0)	**31.0**	**36.5** (−1.0)	**36.5** (−1.0)	37.5
	0.92	192	34.5 (0)	**34.0** (−0.5)	34.5	**39.5** (−3.0)	**39.5** (−3.0)	42.5	**46.0** (−6.0)	**47.0** (−5.0)	52.0

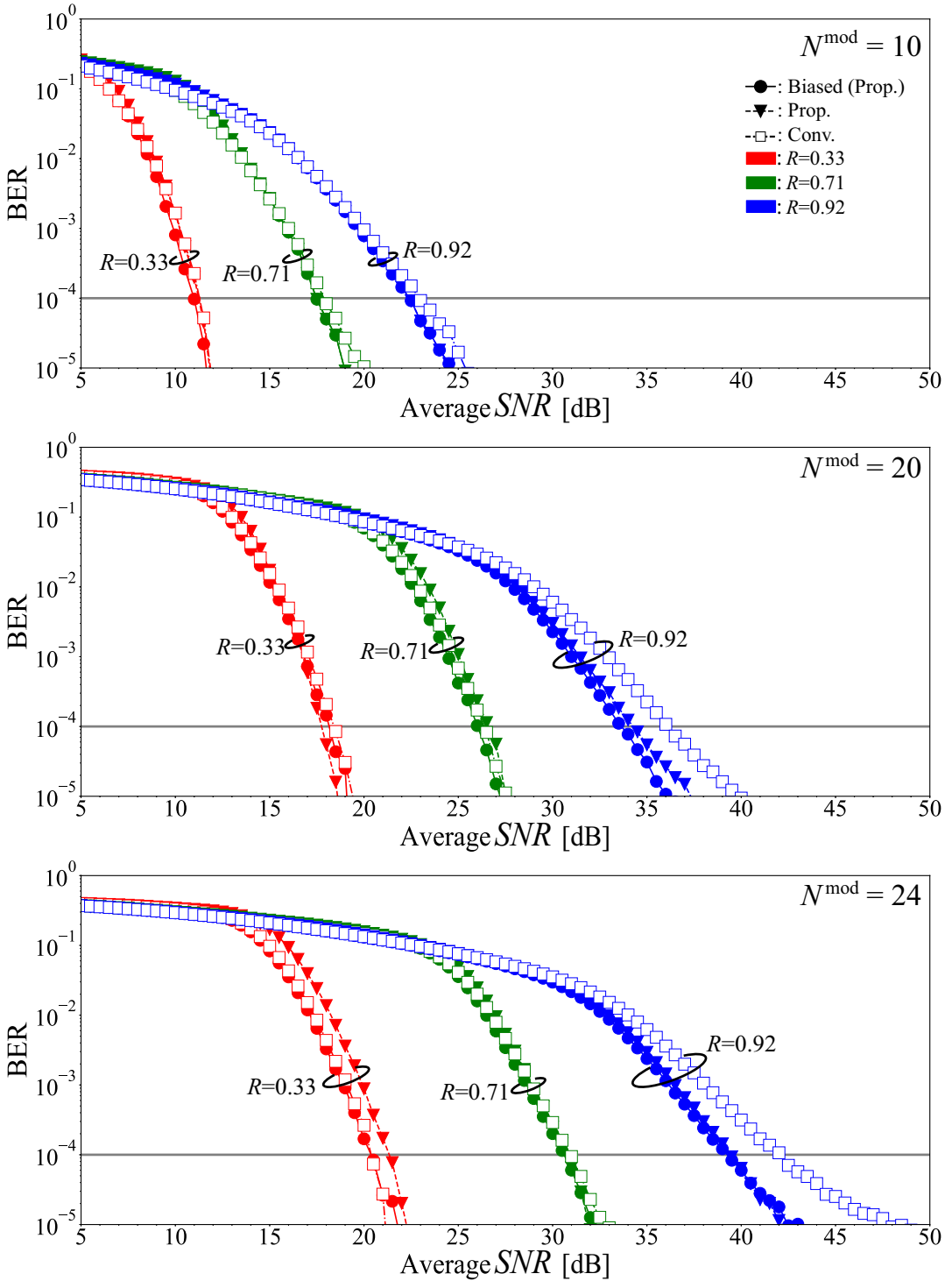

Figure 4.16: Comparison of SNR-BER performances (middle correlation). ©2023 IEICE, [4] Fig. 19

Chapter 5
ML-based Compensation Methods for SVD-MIMO

5.1 Introduction

This chapter proposes ML-based compensation methods using SVR for compensating the Tx weight matrices that are degraded from the ideal one. The compensation target is limited to the degradation that occurs when quantization is used to avoid bandwidth pressure with feedback of the Tx weight matrices. The training data were prepared by pairing ideal Tx weight matrices and deteriorated Tx weight matrices generated from many channel matrices created based on statistical distributions. This chapter also proposes simplified channel metrics to evaluate the attenuation in channel gain caused by the degraded matrices. The optimal parameters for the training data and learning kernels are determined using the simplified channel metrics. Moreover, the validity of using the simplified channel metrics for the determination and the compensation performance are evaluated. Finally, the overall performance of the compensation methods for the Tx weight matrices and the previously proposed ATC (P-ATC) algorithm [4] (Chapter 4) using the compensated matrices are evaluated.

The contributions of this chapter are as follows.

- Simplified channel metrics to evaluate compensation for degradation due to quantization (Section 5.2)
- ML-based compensation methods for the Tx weight matrices (Section 5.3)
- A method for creating training data based on statistical distributions in mobile communication environments (Section 5.3.1)
- A comparison of compensation methods using simplified channel metrics (Section 5.4)

This chapter is based on "Machine learning-based compensation methods of weight matrices for SVD-MIMO" [5], by the same author, which appeared in the IEICE Transactions on Communications,

- A computer simulation showing that the proposed ML-based methods are effective for quantization compensation and the simplified channel metrics are effective for selecting the optinum parameters (Sections 5.5.1 and 5.6.1)
- A computer simulation showing that the transmission using a combination of compensation and P-ATC methods has the highest performance in comparative methods (Sections 5.5.2 and 5.6.2)

5.2 Channel Metrics

As mentioned in Chapter 4, this thesis considered two types of MER for use in ATC. The MER of the ideal SVD-MIMO was calculated using the singular values ξ_i, and the MER of actual SVD-MIMO was calculated using the equivalent singular values ξ_i', as follows

$$MER_i^{\text{Conv.}} = SNR^{\text{Av.}} \xi_i^2 p_i, \tag{5.1}$$

$$MER_i^{\text{Prop.}} = \left[\left(SNR^{\text{Av.}} \xi_i'^2 p_i \right)^{-1} + \left(\Sigma_k \delta_{i,k}^2 p_k \right) \Big/ p_i \right]^{-1}. \tag{5.2}$$

As mentioned in Section 4.2, the conventional-calculated MER includes only the noise enhancement term ($SNR^{\text{Av.}} \xi_i^2 p_i$). On the other hand, the proposed-calculated MER includes the noise enhancement term ($SNR^{\text{Av.}} \xi_i'^2 p_i$) and interference term ($\Sigma_k \delta_{i,k}^2 p_k)/p_i$. The proposed-calculated MER is mainly affected by the noise enhancement and to a lesser extent by the channel estimation error and interference due to the weight matrix at reception. The effect of the ATC on the noise-enhancement term is the multiplications of power allocation term p_*, where $*$ represents i or k. On the other hand, ATC has a more complex effect on the interference term than it does on the noise enhancement term, because the interference term includes multiplications, summations, and divisions with p_*. As it stands, it is hard to evaluate the proposed-calculated MER because the interference term is so complexly related to the ATC through p_*. That is, calculating the ATC results needs p_*, but obtaining p_* requires the ATC to be calculated first.

5.2.1 Proposed Simplified Channel Metrics

This chapter proposes $met.^{\text{Ideal}} = \Sigma_i \xi_i^2$ and $met.^{\text{Quant.}} = \Sigma_i \xi_i'^2$ as metrics to evaluate the noise enhancement terms of Eqs. (5.1) and (5.2). $met.^{\text{Ideal}}$, which is the metric of the ideal SVD-MIMO, is the sum of the squares of the singular values ξ_i^2. It is known that $met.^{\text{Ideal}}$ always equals 16 (= 4×4) for 4×4 SVD-MIMO regardless of the correlation conditions [78]. $met.^{\text{Ideal}}$ is equivalent to the total channel gain over the transmission power of each stream when the transmission powers of each stream are equal in the ideal SVD-MIMO transmission. Similarly, $met.^{\text{Quant.}}$ is taken to be the

total channel gain when the transmission powers of each stream are equal in the actual SVD-MIMO transmissions. Therefore, it is possible to evaluate the attenuation of the channel gain by comparing $met.^{\text{Quant.}}$ with $met.^{\text{Ideal}} = 16$. Because these metrics are calculated from the amount of noise by using the weight matrix at reception (here, the signal detection matrix $\widetilde{\boldsymbol{W}}$), those metrics can be used for all MIMO transmissions using the Rx weight matrices.

Figure 5.1 plots $met.^{\text{Ideal}}$ and $met.^{\text{Quant.}}$ versus the number of quantization bits for the case of quantization degradation only. A plot of MIMO with ZF reception [72], "$met.^{\text{Quant.}}$ w/o precoding", is shown for comparison. The nearest correlation values $(\rho_{\text{t}}, \rho_{\text{r}})$ between the transmitting and receiving antennas are for four conditions, i.e., independent and identically distributed (i.i.d.: 0, 0), low correlation (Low cor.: 0.3, 0.3), medium correlation (Med. cor.: 0.7, 0.3) described in [46], and high correlation (High cor.: 0.7, 0.7). The method of creating the ML datasets is described in Section 5.3.1. The ML datasets created with these four types of correlation value are used as evaluation data.

The results confirm that the SVD-MIMO transmissions have advantages over MIMO transmissions without precoding, even when the Tx weight matrix is degraded. The advantage is regardless of the correlation or number of quantization bits. On the other hand, their quantization degradation is significant compared with the ideal SVD-MIMO transmission, increasing as the correlation increases. Especially in the case of the three-bit quantization used in the system model, the metrics decrease to 68 % (16⇒10.9) for i.i.d., 35 % (16⇒5.61) for medium correlation, and 17 % (16⇒2.72) for high correlation. In ML, it is desirable to use different data and metrics when selecting models/methods and when evaluating performance. Therefore, the optimal ML parameters would be determined by how well they compensated the degradation due to quantization by the simplified channel metrics in Section 5.4. On the other hand, a comprehensive transmission performance would be that of the SNR vs. BER in Section 5.5.

5.3 Compensation Methods for the Tx Weight Matrices using Machine Learning

This section describes the method for creating the training data, the training method, and the ML method for compensating the Tx weight matrices.

The Tx weight matrix $\boldsymbol{V} \in \mathbb{C}^{4\times4}$ has 32 elements, including real and imaginary parts. Since the Tx weight matrix is created from a single channel matrix, its elements are closely related. The Tx weight matrix $\boldsymbol{V}'$, in which each element is quantized to three-bit, has 2^{96} element patterns in total. The use of all elements should be able to compensate for the Tx weight matrices with higher precision than three-bit. However, attempting compensation by matching 2^{96} patterns is extremely difficult. Instead, the compensation can be treated as a regression problem in which the input is the Tx

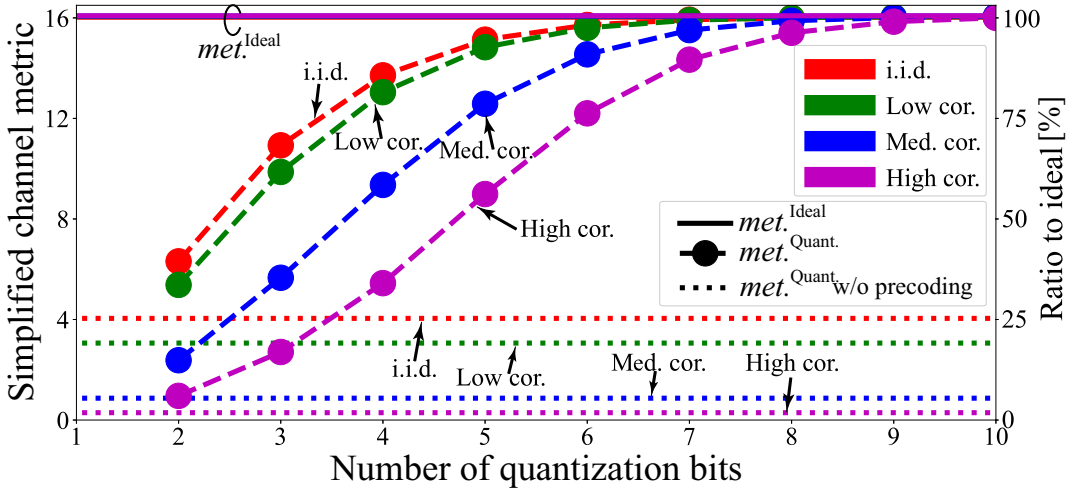

Figure 5.1: Simplified channel metric evaluation of degradation due to quantization. ©2023 IEICE, [5] Fig. 4

weight matrices $\boldsymbol{V}'$ and the output is each element of $\boldsymbol{V}$. Moreover, this chapter proposes to use ML, wherein the compensation is performed using computer-trained models during transmission. Considering the hardware implementation, this thesis chose to use SVR [79], which has a simplified test procedure and a high level of performance when there is a sufficient amount of training data.

5.3.1 Creation of Machine-learning Datasets

In ML, if the training data are biased to a specific condition, the performance will be strongly degraded under other conditions [80]. For this reason, creating a wide variety of conceivable channel environments is important. This section created statistical data for static fading channels without considering frequency selectivity or time-varying channels in order to compensate for the degradation due only to quantization. It is easy to create a large amount of data statistically as there is no need to acquire data in the field or by conducting a Monte Carlo simulation. On the other hand, data for dynamic fading channels would have to be created to compensate for the degradation described in Section 2.2.5.2.

Figure 5.2 shows the procedure for creating the training and validation datasets. First, the channel matrices $\boldsymbol{G} \in \mathbb{C}^{4\times4}$ based on the Rayleigh fading of i.i.d. channels were created. Since ideal Rayleigh fading affects the signal when both the real and imaginary parts of channels have an i.i.d. Gaussian distribution [76], $\boldsymbol{G}$ was calculated using $\boldsymbol{X}, \boldsymbol{Y} \in \mathbb{R}^{4\times4}$:

$$\boldsymbol{G} = \boldsymbol{X} + \mathrm{j}\boldsymbol{Y}. \tag{5.3}$$

Since $\boldsymbol{X}$ and $\boldsymbol{Y}$ are random numbers representing statistical properties, they can be used to make a wide variety of i.i.d. matrices. Subsequently, the channel matrices $\boldsymbol{H}$ that take account of correlation were defined using the Kronecker model [75], defined

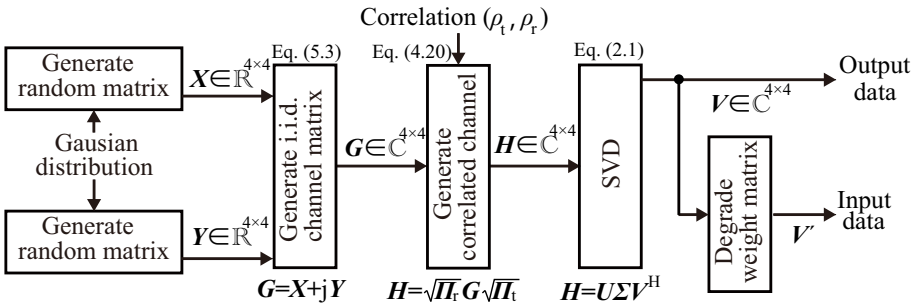

Figure 5.2: Process of creating training/validation datasets for ML. ©2023 IEICE, [5] Fig. 5

in Eq. (4.20). Two types of training data ρ_0 were used; static-medium correlation values, called "static correlations" and values drawn from a uniform distribution of $\rho_0 = [0, 1)$, called "uniformly distributed correlations". As described in Section 5.2.1, the evaluation data were made with the four types of correlation value. The creation method is the same as that of "static correlations".

Subsequently, ideal Tx weight matrices $\boldsymbol{V}$ were created from $\boldsymbol{H}$ by solving Eq. (2.1). Finally, the deteriorated Tx weight matrices $\boldsymbol{V}'$ (three-bit quantization is used) were created. Here, $\boldsymbol{V}'$ and $\boldsymbol{V}$ are the input and output in the training data.

5.3.2 Training Methods for Compensation

This section describes training methods for the models used in the Tx weight matrix compensation. The input is the Tx weight matrices $\boldsymbol{V}'$ after degradation and the Tx weight matrices $\boldsymbol{V}$ before degradation, and the output is the trained models.

SVR is an ML method for solving regression problems that takes vectors as input and outputs scalar values [79]. Here, $\boldsymbol{V}', \boldsymbol{V}$ of the training data were converted into $\boldsymbol{v}', \boldsymbol{v} \in \mathbb{R}^{32}$, as shown in Fig. 5.3. Next, as shown in Fig. 5.4, the elements of $\boldsymbol{v}$, i.e., the training data for the output, and $\boldsymbol{v}'$ were used as input for the SVR training; in total, 32 trained models were created.

5.3.3 Testing Methods for Compensation

This section describes the compensation methods for the Tx weight matrices using the trained models created in Section 5.3.2. The inputs were the deteriorated Tx weight matrices $\boldsymbol{V}'$ and trained models, and the output consisted of the compensated Tx weight matrices $\boldsymbol{V}''$. First, $\boldsymbol{V}'$ was converted into a 32-dimensional real vector $\boldsymbol{v}' \in \mathbb{R}^{32}$, as illustrated in Fig. 5.3. After that, the parameters were predicted using the trained SVR model, as in Fig. 5.5. Finally, $\boldsymbol{v}''$ was converted into $\boldsymbol{V}'' \in \mathbb{C}^{4\times4}$, as in Fig. 5.3.

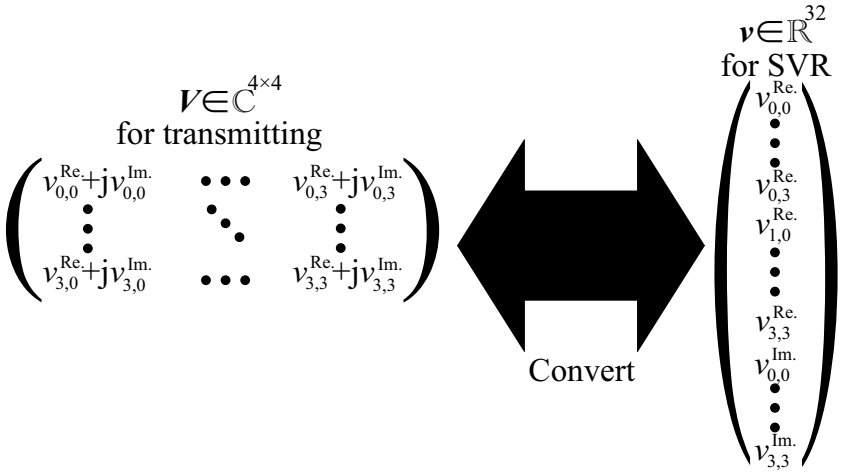

Figure 5.3: Converting a complex matrix into a vector. ©2023 IEICE, [5] Fig. 6

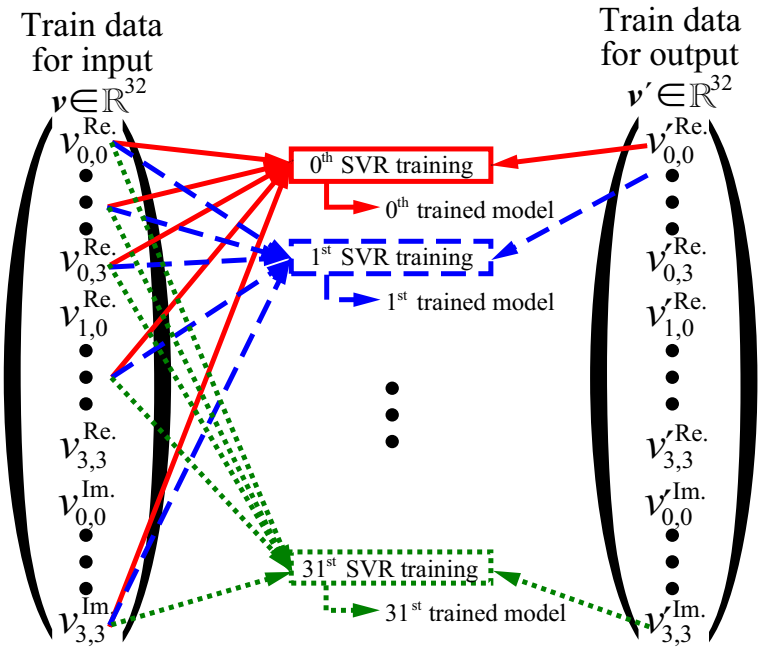

Figure 5.4: SVR training methods for compensation. ©2023 IEICE, [5] Fig. 7

5.3.4 Transmitting using Compensation Methods

This section describes the transmission using compensation methods for the Tx weight matrices. Figure 5.6 shows the block diagram. The MS (Tx-side) compensates the received Tx weight matrices $\boldsymbol{V}'$ to $\boldsymbol{V}''$ and uses them for the transmission. Similarly, BS (Rx-side) compensates the $\boldsymbol{V}'$ transmitted in the previous DL frame and uses them for signal detection.

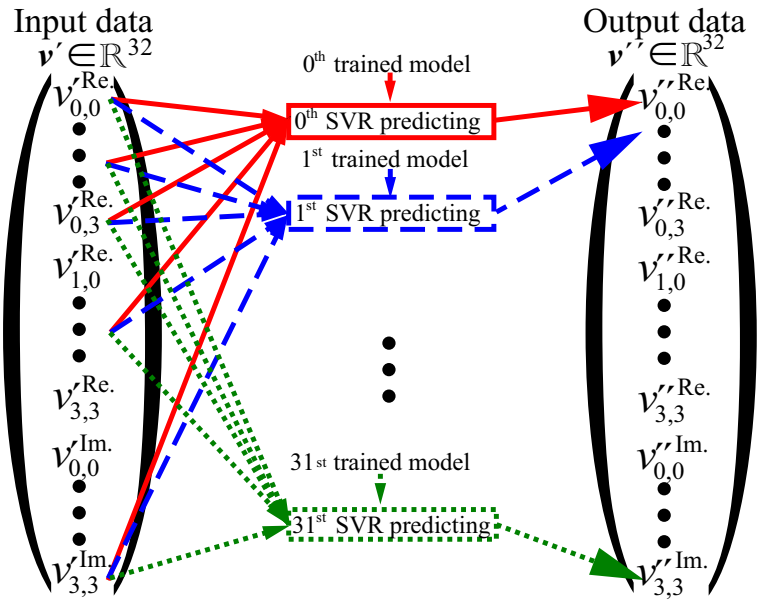

Figure 5.5: SVR testing methods for compensation. ©2023 IEICE, [5] Fig. 8

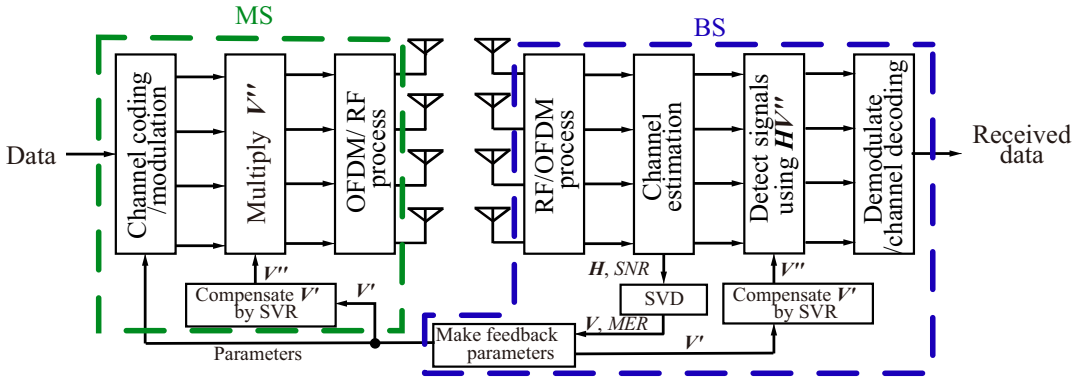

Figure 5.6: Block diagram of UL transmission with SVR compensation. ©2023 IEICE, [5] Fig. 9

5.4 Simplified Evaluation of Compensation Methods

This section evaluates the compensation methods for the Tx weight matrices by using the simplified channel metrics. Table 5.1 shows the parameters of the evaluation. Note that the SVR training included several other parameters besides the ones described in the table, such as epsilon, the number of support vectors used, and the number of power dimensions when using a polynomial kernel. A lot of research has been done on parameter optimization [81], but it is different from the purpose of this study. Thus, this thesis used only the default values of Scikit-learn [82].

Table 5.1: Training/ validation conditions. ©2023 IEICE, [5] Table 2

Implementation code	Python, scikit-learn, etc.
Regression method	SVR
Learning kernels	Linear, RBF, and polynomial
Number of train. data	10k (10,000), 30k, and 50k
Number of valid. data	2k
Correlation (for train.)	Static (medium cor.) and uniform dist. [0,1]
Correlation (for valid.)	i.i.d., low cor., medium cor., and high cor.
Evaluation metrics	Proposed simplified channel metrics

5.4.1 Simplified Comparison of Learning Kernels

Table 5.2 shows comparative results using the simplified metrics ($met.$) for each learning kernel. To evaluate the kernels fairly, the number of training data was set to 30k, and the correlation of the training data was set to the uniform distribution described in Section 5.3.1. "Ideal" means the ideal SVD-MIMO transmission performance without degradation, which is 16.0 regardless of the correlation, as described above. The other values are shown in parentheses as ratios based on 16.0. "W/o comp." is the transmission performance without compensation, which corresponds to the three-bit value in Fig. 5.1. Bold type indicates an improvement was obtained under the same correlation conditions. As can be seen, no improvement was obtained with the linear kernel. On the other hand, an improvement was had with the polynomial and RBF kernels for medium and high correlation. Moreover, the polynomial kernel showed an improvement even at low correlation. The polynomial kernel was thus used in the following evaluation.

5.4.2 Simplified Comparison of Training Data

Table 5.3 and Fig. 5.7 show comparative results using the simplified metrics ($met.$) for each training data condition. The two types of correlation condition described in Section 5.3.1 were used for the training data. The simplified channel metrics improved as the number of training data increased, regardless of whether the correlation of the training data followed a uniform distribution or was static. On the other hand, the difference between 30k and 50k was relatively small compared with the difference between 10k and 30k. In particular, the difference was up to 2% in the case of the uniform distribution for the correlation values of the training data.

In addition, given the same number of training data (for example, 30k), the uniform distribution outperformed the static correlation under the i.i.d. and low correlation conditions. In particular, the static correlation was much worse than the conventional method regardless of the number of training data. On the other hand, under the medium and high correlation conditions for evaluation, the static correlation had

Table 5.2: Simplified evaluation of leaning kernels (correlation: [0,1]). ©2023 IEICE, [5] Table 3

	i.i.d.	Low cor.	Med. cor.	High cor.
Ideal	16.0	16.0	16.0	16.0
W/o comp.	10.9 (68%)	9.82 (61%)	5.61 (35%)	2.72 (17%)
Linear	10.4 (65%)	9.51 (59%)	5.60 (35%)	2.72 (17%)
RBF	10.0 (63%)	9.37 (59%)	**6.02** (38%)	**2.95** (18%)
Polynomial	10.8 (68%)	**10.2** (64%)	**7.29** (46%)	**3.72** (23%)

Table 5.3: Simplified evaluation of training data (kernel: polynomial).©2023 IEICE, [5] Table 4

		i.i.d.	Low cor.	Med. cor.	High cor.
Ideal		16.0	16.0	16.0	16.0
W/o comp.		10.9 (68%)	9.82 (61%)	5.61 (35%)	2.72 (17%)
Static cor.	10k	3.28 (21%)	5.59 (35%)	**6.99** (44%)	**3.29** (21%)
(medium)	30k	4.97 (31%)	7.26 (45%)	**7.60** (48%)	**3.82** (24%)
for Train.	50k	5.94 (37%)	8.03 (50%)	**7.86** (49%)	**3.98** (25%)
Unif. dist.	10k	8.96 (56%)	9.16 (57%)	**6.70** (42%)	**3.20** (20%)
cor. [0,1]	30k	10.8 (68%)	**10.2** (64%)	**7.29** (46%)	**3.85** (24%)
for Train.	50k	**11.1** (69%)	**10.5** (66%)	**7.52** (47%)	**3.85** (24%)

slightly higher performance compared with the uniformly distributed correlations. Therefore, the training data with the static correlation are specialized for medium and high correlations, whereas the training data with the uniformly distributed correlations improves performance for a wide variety of correlation conditions.

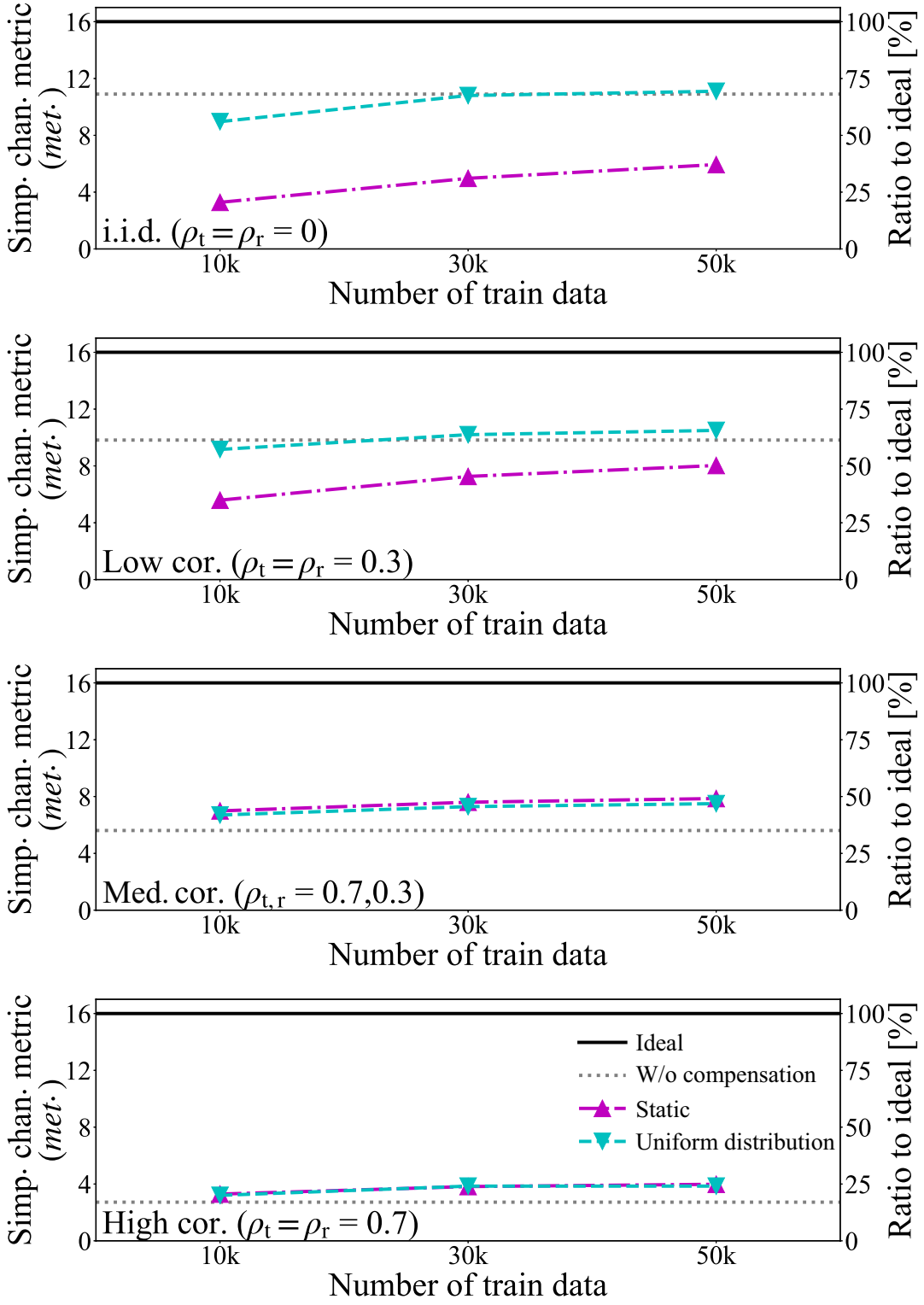

Figure 5.7: Simplified evaluation of training data (kernel: polynomial). ©2023 IEICE, [5] Fig. 10

5.4.2.1 Additional evaluation using the Coefficient of Determination r^2

For regression problems, the coefficient of determination r^2 is an index of accuracy, and it is generally used in evaluations [58]. This section describes the coefficient of determination and re-evaluates part of Section 5.4 with the coefficient of determination, and compares the results with Section 5.5.

The general coefficient of determination r^2 is defined as

$$r^2 = 1 - \frac{\sum_{i=0}^{N-1} v_i - \tilde{v}_i}{\sum_{i=0}^{N-1} v_i - \overline{v}}, \tag{5.4}$$

where $\{v_i\}$ is the correct data, $\{\tilde{v}_i\}$ is the data to be evaluated, N is the number of data, i is the data index, and $\overline{v}$ is the average value of the correct data.

Table 5.4 shows the evaluation results for the coefficient of determination under the same conditions as Table 5.3. First, the degradation from the Ideal case using w/o comp. is the same regardless of the correlation for evaluation. Since this result is different from Tables 5.3 and 5.5, the performance evaluation using the coefficient of determination does not accurately represent the transmission performance difference between correlations due to quantization degradation.

Next, the methods of giving the correlation value of the training data are examined. The static correlation (medium) is worse than the uniformly distributed correlations in the i.i.d. and low correlation evaluations but is slightly better in the medium and high correlation evaluations. This behavior is the same as in Tables 5.3 and 5.5.

Comparing the performance using SVR compensation for all numbers of training data (10k, 30k, 50k), medium correlation is the highest performance, followed by high correlation, low correlation, and i.i.d. This tendency is very different from what is shown in Table 5.5, and the performance evaluation based on the coefficient of determination does not correctly represent the transmission performance difference between correlations for SVR compensation.

For these reasons, the use of the coefficient of determination is inappropriate for the determination of this study.

5.4.3 Discussion on the Simplified Evaluation

This section discusses the above results of the simplified evaluation.

5.4.3.1 Determination of the optimal ML parameters

First, the results in Section 5.4.1 indicate that the amount of improvement (or degradation) differs for each kernel in SVR. In addition, the polynomial kernel seems to be ideal since it improved almost all of the evaluated correlation conditions. In SVR, the kernel to be used is determined on the basis of the comparative performance on each problem. It is known that non-linear (polynomial and RBF) kernels have complicated

Table 5.4: r^2 evaluation of training data (kernel: polynomial) [%].©2023 IEICE, [5] Table A·1

		i.i.d.	Low cor.	Med. cor.	High cor.
Ideal		100	100	100	100
W/o comp.		96.3	96.3	96.3	96.3
Static cor.	10k	78.4	88.7	96.3	95.8
(medium)	30k	85.9	92.6	**96.9**	**96.6**
for Train.	50k	88.7	93.9	**97.1**	**96.8**
Unif. dist.	10k	94.4	95.1	96.2	95.9
cor. [0,1]	30k	95.6	96.1	**96.9**	**96.7**
for Train.	50k	96.2	**96.5**	**97.0**	**96.9**

structures and higher performance than linear kernels [83]. On the other hand, since the RBF kernel has an incredibly complicated structure for solving complex problems, the trained models are easier to overfit the data for uncomplex problems [84]. Therefore, it seems that the polynomial kernel was the most effective because the quantization compensation was moderately complex.

Next, the results in Section 5.4.2 indicate that it is desirable to have as much training data as possible. On the other hand, the number of multiplications increases in proportion to the number of training data both during training and during testing in SVR. Therefore, there is a trade-off between transmission performance and hardware implementation scale.

Since data in i.i.d. channels were not included in the training data with the static correlation, the evaluation data were the outliers of the training data, and performance significantly deteriorated. On the other hand, since the training data with the static correlation were specialized for the correlated channels, performance significantly improved in the correlated channels (Med. cor. and High cor.). These results show that the training data with the static correlation made models overfit the correlated channels. On the other hand, the degradation was small when the models were trained with uniformly distributed correlations, regardless of the correlation of the evaluation data. A substantial improvement was obtained for evaluation data with the medium or high correlation. This is because the training data included a wide variety of correlation conditions from i.i.d. to high correlation, and the trained model was very robust. Furthermore, as shown in Table 5.3, when the training data with uniformly distributed correlations were used, 30k was 4–12% better than 10k. On the other hand, since the degradation in the case of 30k was only 2% less than that of 50k, it was concluded that about 30k is a reasonable amount of training data. These results indicate that the training data should have uniformly distributed correlations and a large amount of data (preferably 30k or more) should be used.

5.4.3.2 Additional Evaluation and Future Prospects

This chapter evaluated the performance while varying the number of training data for each learning kernel. The results were not much different from those in Tables 5.2 and 5.3, so their evaluation and discussion will be omitted. Similarly, I evaluated the performance of ridge regression or regression with three-layer neural networks [58]. Their performance did not exceed those of the methods using SVR, so the thesis will omit discussion of them as well.

This section discusses about evaluation using the coefficient of determination, shown in Section 5.4.2.1. It measures the rate of regression to statistically correct data. However, because the purpose of the proposed methods is to improve the channel quality, a discussion of this evaluation is not within the scope of this thesis.

On the other hand, the learning structure of SVR also aims at the regression approach to the correct data. Therefore, a learning structure that directly improves the simplified channel metrics is expected to enhance the performance of quantization compensation. In addition, a further performance improvement can be expected by performing a parameter optimization [81], even with the current learning structure.

5.5 Performance Evaluation of Compensation Methods

The validity of the simplified channel metrics and the transmission performance with proposed compensation methods were evaluated in a computer simulation. The evaluations were performed using the transmission configuration with the SVR compensation shown in Fig. 5.6. For the parts other than the SVR compensation, the SVD-MIMO system was implemented in python and numpy. The basic evaluation conditions such as the channel model are the same as the evaluation conditions in Section 4.5. Therefore, the evaluation in this chapter also uses the ATC algorithms. Unlike the data created for SVR in Section 5.3.1, $\boldsymbol{G}$ was a 4×4 i.i.d. fading channel matrix created by the Jakes model [76] having a time variation and frequency selectivity, same as Chapter 4. Therefore, an evaluation using this channel matrix would be affected by the degradations described in Section 2.2.5.2. On the other hand, since the compensation methods described in this study are only for degradation due to quantization, the performance would be degraded from the ideal SVD-MIMO transmission regardless of the method used.

5.5.1 Comparison of Compensation Conditions by Computer Simulation

This section compares transmission performances for some of the conditions in Table 5.3 in Section 5.4. The ATC method used in this section [43] did not consider

degradation.

Figure 5.8 shows the results for the ideal condition without quantization degradation (Ideal), the conventional method without compensation (W/o comp.), the proposed method with SVR compensation using 30k training data and static correlation (Static-30k), and the proposed method with SVR compensation using various numbers of training data and a uniformly distributed correlations (10k, 30k, 50k) in an i.i.d., medium correlation, or high correlation channel environments. Note that even Ideal is affected by the degradation described in Section 2.2.5.2. The required SNR is shown in Table 5.5, and the following performance comparisons were performed with those values. W/o comp. after degradation was used as the reference value, and the difference is shown in parentheses for each compensation method. The coding rate R was set to the maximum, 0.92.

First, in the i.i.d. environment, Static-30k significantly deteriorated and 10k slightly deteriorated. In particular, as shown in Fig. 5.8, the results for Static-30k had a larger and gentler slope than those of the other methods. On the other hand, 30k, 50k, and W/o comp. were equivalent in performance.

In the medium correlation environment, all of the methods with SVR compensation were better than W/o comp.. In particular, the improvement for Static-30k and 50k was more than 2.5 dB. The increase in the amount of training data (10k $\rightarrow$ 30k $\rightarrow$ 50k) led to the improvements.

Finally, in the high correlation environment, all of the methods with SVR compensation showed a significant improvement over W/o comp.. In particular, Static-30k and 50k had the largest improvement, 4.5 dB. The use of the uniformly distributed correlations for training and more training data led to the improvements.

In the following evaluation, the training data had uniformly distributed correlations and a size of 30k (30k).

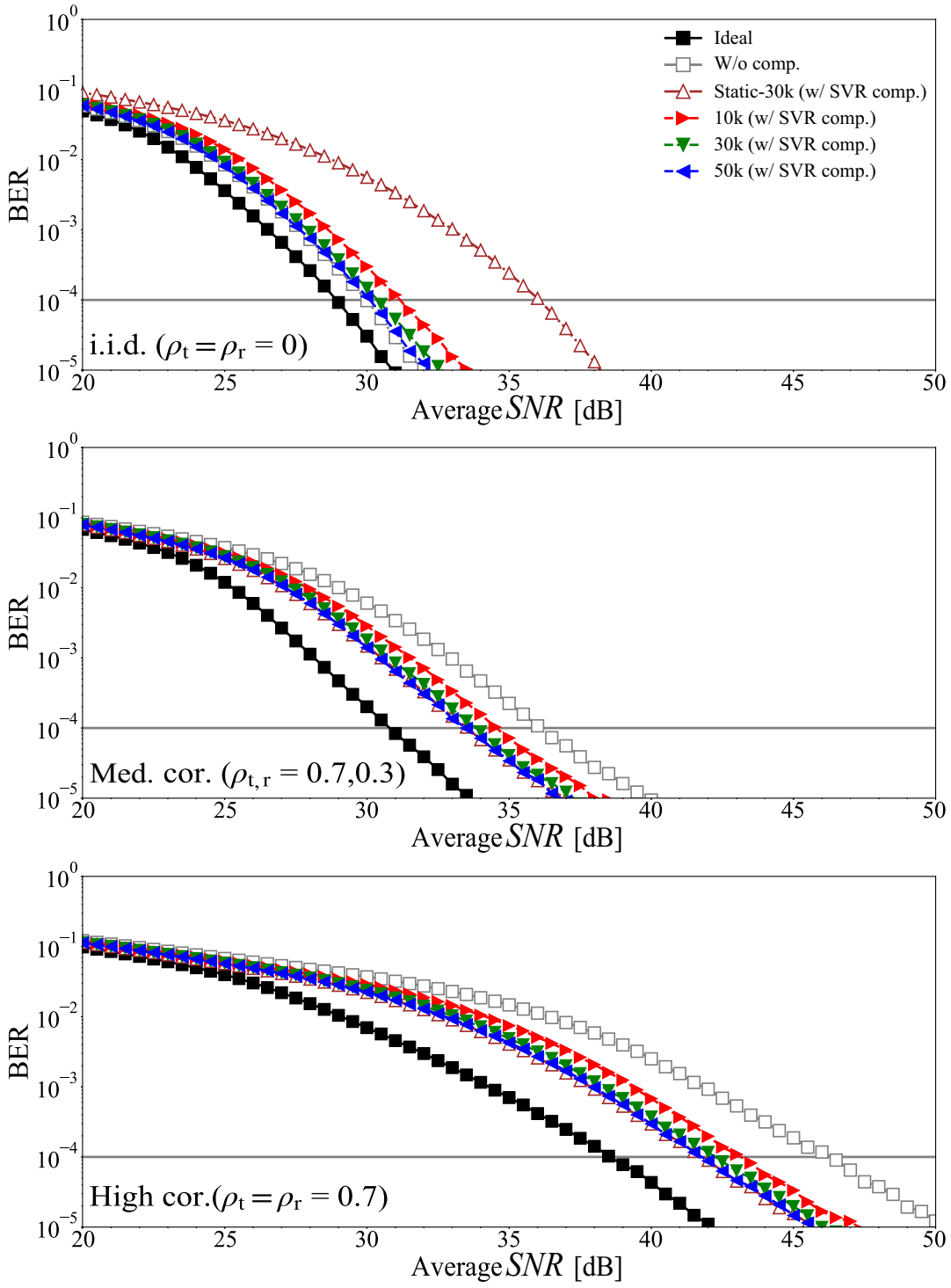

Figure 5.8: Performance evaluation for different SVR-compensation conditions (coding rate R=0.92). ©2023 IEICE, [5] Fig. 11

Table 5.5: Required SNR [dB] for different SVR-compensation conditions.©2023 IEICE, [5] Table 5

	i.i.d.	Med. cor.	High cor.
Ideal	29.0	31.0	39.0
W/o comp.	30.0	36.5	46.5
Static-30k (Med. cor.)	36.5 (+6.5)	**34.0** (−2.5)	**42.0** (−4.5)
10k (Unif. dist.)	31.5 (+1.5)	**35.0** (−1.5)	**43.5** (−3.0)
30k (Unif. dist.)	30.5 (+0.5)	**34.0** (−2.5)	**42.5** (−4.0)
50k (Unif. dist.)	30.5 (+0.5)	**33.5** (−3.0)	**42.0** (−4.5)

5.5.2 Comparison of ATC Conditions by Computer Simulation

The simulation examined different ATC methods in addition to the use of the SVR degradation compensations. An ATC method suitable for transmissions with deteriorated Tx weight matrices was described in 4.3.2.2; here, it is called P-ATC. Figure 5.9 shows the results for the conventional ATC without SVR compensation (W/o comp.) and P-ATC without SVR compensation (P-ATC), conventional ATC with degradation compensation (30k), and P-ATC with SVR compensation (30k+P-ATC). The required SNR is shown in Table 5.6, and the performance comparisons reported below were performed with those values. W/o comp. after degradation was used as the reference value, and the difference is shown in parentheses for each compensation condition.

In the i.i.d. environment, almost all methods were equivalent in performance (the difference is up to 1.0 dB). In the medium correlation environment, for $R = 0.33$ and $R = 0.71$, almost all methods were equivalent in performance (the difference is up to 0.5 dB). For $R = 0.92$, P-ATC, 30k, and 30k+P-ATC improved by 2.0–3.5 dB. In the high correlation environment, P-ATC, 30k, and 30k+P-ATC improved by 1.0–7.0 dB for all variations of R.

Moreover, 30k+P-ATC improved by up to 0.5 dB in the i.i.d. and medium correlation environments and by up to 1.5 dB in the high correlation environment compared with P-ATC.

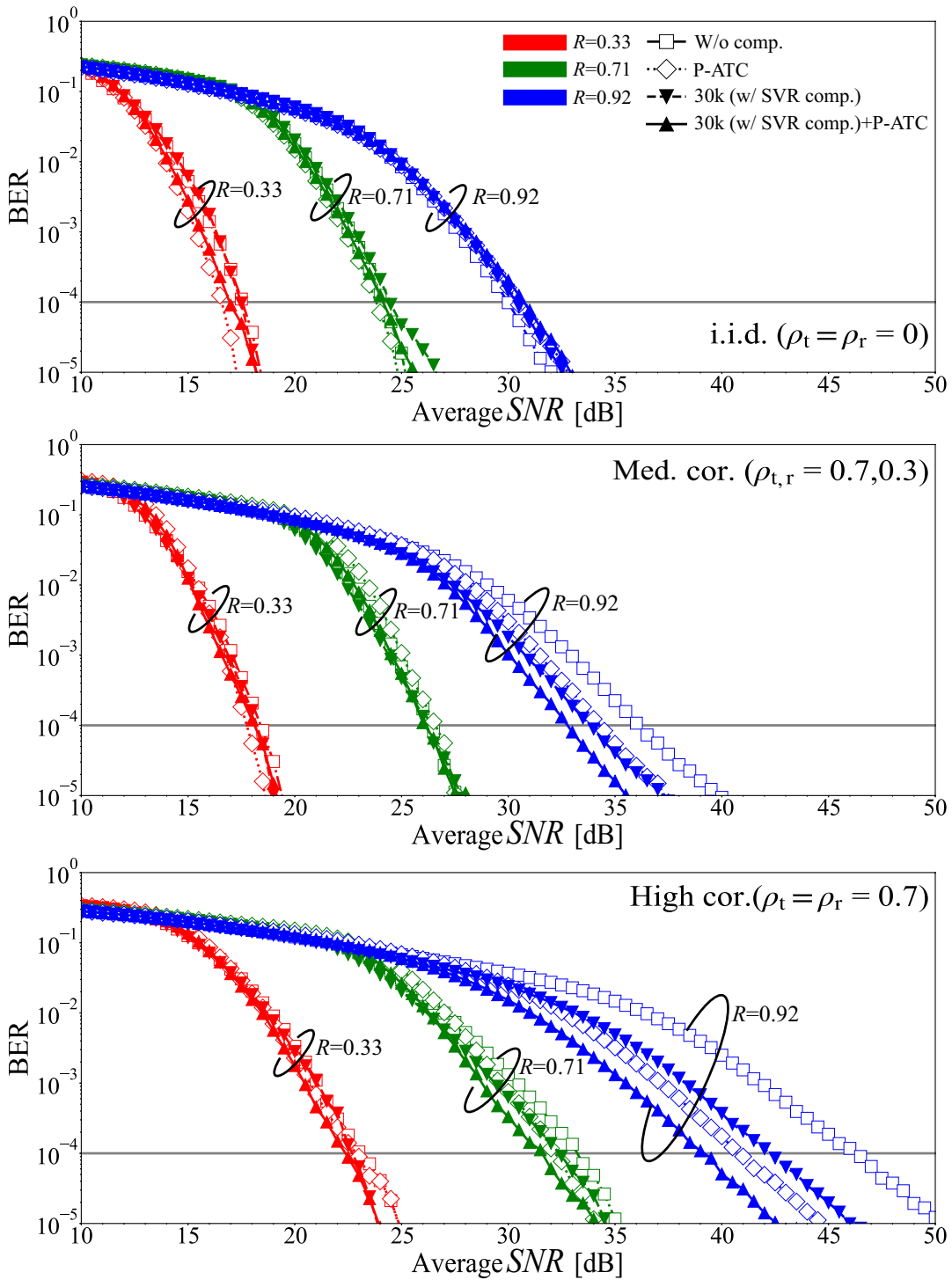

Figure 5.9: Performance evaluation for different correlations (ρ_t, ρ_r) and coding rates (R). ©2023 IEICE, [5] Fig. 12

Table 5.6: Required SNR [dB] for different correlations (ρ_t, ρ_r) and coding rates (R).©2023 IEICE, [5] Table 6

	Compensation (SVR)	Proposed-ATC [4]	R=0.33	R=0.71	R=0.92	Name
i.i.d. $\rho_t = \rho_r = 0$	without	without	18.0	24.5	30.0	W/o comp.
	without	with	**17.0** (−1.0)	**24.0** (−0.5)	30.5 (+0.5)	P-ATC [4]
	with (30k)	without	**17.5** (−0.5)	24.5 (0)	30.5 (+0.5)	30k
	with (30k)	with	**17.0** (−1.0)	24.5 (0)	31.0 (+1.0)	30k+P-ATC
Medium correlation $\rho_t = 0.7, \rho_r = 0.3$	without	without	18.5	26.5	36.5	W/o comp.
	without	with	**18.0** (−0.5)	27.0 (+0.5)	**34.5** (−2.0)	P-ATC [4]
	with (30k)	without	18.5 (0)	26.5 (0)	**34.0** (−2.5)	30k
	with (30k)	with	18.5 (0)	26.5 (0)	**33.0** (−3.5)	30k+P-ATC
High correlation $\rho_t = \rho_r = 0.7$	without	without	23.5	33.5	46.5	W/o comp.
	without	with	**23.0** (−0.5)	**32.5** (−1.0)	**41.0** (−5.5)	P-ATC [4]
	with (30k)	without	**23.0** (−0.5)	**32.5** (−1.0)	**42.5** (−4.0)	30k
	with (30k)	with	**22.5** (−1.0)	**32.0** (−1.5)	**39.5** (−7.0)	30k+P-ATC

5.6 Discussion

This section discusses the results shown in Sections 5.4 and 5.5.

5.6.1 Validity of Simplified Channel Metrics

The results in Table 5.5 indicate that the method using the uniformly distributed correlations for the training data has high robustness: it did not cause much degradation in the i.i.d. evaluation and showed a large improvement in the medium and high correlation evaluation. On the other hand, the method using the static correlation had poor robustness and was overfitted to the correlation channels. It caused a large degradation in the i.i.d. evaluation. In addition, the use of uniformly distributed correlations for the training data led to the transmission performance increasing with the amount of training data. In particular, the performance difference between 10k and 30k (1.0 dB) was larger than that between 30k and 50k (0–0.5 dB). Therefore, to improve the overall performance while suppressing the degradation in the i.i.d. environment, it is desirable to use a large amount of training data (more than 30K if possible) with uniformly distributed correlations. This conclusion is similar to those on Table 5.3 that were discussed in Section 5.4.3.1. Accordingly, the simplified channel metrics proposed in Section 5.2 appropriately expresses the degradation in transmission performance due to the degradation of the Tx weight matrices.

5.6.2 Comparison of ATC Conditions

This section discusses the evaluation results in Table 5.6 in Section 5.5.2. First, in the i.i.d. environment, the improvements or degradations are only about $\pm$1.0 dB at maximum. Even when $R = 0.92$, since the degradation compared with the ideal is only about 1.0 dB in Table 5.5, the amount of improvement is also small. When a low coding rate is used ($R = 0.33, 0.71$) in the medium correlation environment, the degradation or improvement stays within the range of $\pm$0.5 dB regardless of the method. There was almost the same performance as in the i.i.d. environment. On the other hand, in the medium correlation environment with $R = 0.92$ and in the high correlation environment for all values of R, the improvement had by the combination (30k+P-ATC) was 1.3–2.0 times (0.5–5.5 dB$\Rightarrow$1.0–7.0 dB) that of the SVR compensation method (30k) and P-ATC method (P-ATC). For this reason, neither method alone is deemed insufficient when it is used alone. On the other hand, a significant performance improvement of up to 7.0 dB can be obtained by using the Tx weight matrices compensated by SVR together with an ATC suitable for the compensated Tx weight matrices.

5.6.3 Overall Discussion and Future Prospects

As an overall trend, performance improvement was relatively higher in higher-correlation environments. The reason is that the channel gain is more strongly affected by the compensation (and degradation) performance of the Tx weight matrix in a higher-correlation environment. Explanations for this are given below.

First, this section compares the channel gain of W/o comp. relative to Ideal. As shown in Fig. 5.1, the quantization degradation of the Tx weight matrix reduced the channel gain (the simplified metrics) in the higher-correlation environment. This result makes sense from the point of view of wireless communications, because it is more difficult to create streams (equivalent independent channels) in MIMO in a higher-correlation environment. Since the channel gain is directly linked to the SNR-BER performance, the degradation of the required SNR of W/o comp. is more significant in a higher-correlation environment than that of Ideal (as shown in Table 5.5, i.i.d.: 1.0 dB, Med. cor.: 5.5 dB, High cor.: 7.5 dB at R = 0.92).

Next, the section describes the channel gains of compensation methods in comparison with w/o comp. As shown in Fig. 5.7 and Table 5.3, the simplified channel metrics were 0.99 times (10.9→10.8) for i.i.d., 1.30 times (5.61→7.29) for Med. cor., and 1.41 times (2.72→3.85) for High cor. with uniformly distributed correlations and 30k compared to w/o comp. That is, the improvement of the channel gain was higher in the high correlation environment. As a result, in a high correlation environment, the improvement in required SNR due to the compensation methods is more significant than that of W/o comp. (For example, as shown in Table 5.6, i.i.d.: −0.5 dB, Med. cor.: 2.5 dB, High cor.: 4.0 dB at 30k and R=0.92).

Tables 5.5 and 5.6 at $R = 0.92$ show the results of the evaluation for the same coding rate but different compensation conditions. Here, 30k+P-ATC is 31.0 dB versus the 29.0 dB of Ideal in the i.i.d. environment, 33.0 dB versus 31.0 dB in the medium correlation environment, and 39.5 dB versus 39.0 dB in the high correlation environment. The amount of degradation is 0.5–2.0 dB. These values are the limit to the improvement that can be achieved using the training data created in Section 5.3.1. More improvements to the ATC or ML methods will be needed in order to reduce the degradation further.

On the other hand, as described in Section 2.2.5.2, the Tx weight matrices also suffer degradation from channel estimation errors and the use of precoding blocks. To compensate for these degradations, it is necessary to use the Tx weight matrices of the previous frame and adjacent precoding blocks. Therefore, not only statistically created training data (Section 5.3.1) but also data based on the Jakes model used in computer simulations or data obtained in actual channel environments are needed as training data. In addition, the machine-learning method must account for these degradations. Thus, while the evaluation showed there is a possibility of achieving a level of performance beyond Ideal, investigations of these issues will have to be conducted in future research.

Moreover, I evaluated the feasibility of the proposed compensation method in

another research [85]. I proposed a method to reduce the computation for the compensation and evaluated the circuit scale and processing time when implementing the one to an FPGA board. As a result, the results showed that it is expected to be realized within the processing time available for actual transmission. In addition, as a result of a performance evaluation using a combination of computer simulation and FPGA board, evaluation results equivalent to the results in this chapter were obtained. It is possible to further evaluate the feasibility by implementing the method on the prototype [5] and conducting experiments.

5.7 Conclusion

This chapter proposed and evaluated machine-learning-based compensation methods for the Tx weight matrices used in actual SVD-MIMO transmissions. It also proposed simplified channel metrics based on the channel quality to evaluate compensation performance and methods for creating training data based on statistical distributions. The simplified channel metrics enabled the learning kernel, number of training data, and correlations for the training data to be examined under many conditions. Furthermore, the results of a computer simulation evaluation indicated that the metrics could be used for selecting the optimum machine-learning parameters. Finally, a computer simulation of transmissions with SVR compensation using a polynomial kernel and 30k of training data with uniformly distributed correlations was conducted in different correlation environments and for different coding rates. It was found that the proposed SVR compensation method improved the SNR to achieve the required BER by a maximum of 4.0 dB. Furthermore, the maximum performance improved by 7.0 dB when the proposed compensation method was combined with a previously proposed ATC method suitable for transmissions with deteriorated weight matrices.

Chapter 6
Prospects for Platforms of Various Applications

This chapter describes the prospects for platforms toward the use of various applications. There is a need to realize various services by communicating between devices and servers in fields and objects where wireless communication (or wired communication) has not been used until now. However, when installing such services in a new field, it isn't easy to install the communication method to be introduced from scratch. For these reasons, there is a need for a platform that users in other fields can easily install, which can be used in various areas. To achieve this, I envision expanding each private communication system mentioned in this thesis into a separate platform. The following part describes the prospects for each.

6.1 CPS Platforms Using WRAN

The implementation of CPS platforms has significantly improved various applications in recent years. As shown in Fig. 2.1, CPS is a system that uses various communication methods to transmit data from physical space to cyberspace, analyze it, and feed it back to physical space. The target applications are diverse. For example, it is expected to be used in various fields such as agriculture and disaster prevention. I will discuss the prospects for introducing it into each field.

- Agriculture

  In the field of agriculture, R&D of smart agriculture, where ICT is used to efficiently carry out agriculture, is being conducted [86, 87]. For example, it is expected to be used by collecting data from meters such as thermometers and water level gauges when automating cultivation on farms such as robot farming. Various wireless communication technologies, such as LPWA and cellular communication as shown in Table 1.1 are used as WSN. However, each communication method has various issues such as limited coverage, data rate, and band license. For example, WATARAS, a water management system for rice fields, has introduced equipment using LoRa or LTE-M [88]. No matter which communication method is used, the data rate according to the standard is several hundred kbps or less. Furthermore, LoRA has issues with the coverage and LTE-

M has issues with usage fees (and being a public communication). Because farms can be vast, ultra-wide-area WRAN communications that support both wide area and high data rate of several Mbps or more are suitable. In WRAN, since the UL data rate can be set at 6 Mbps or higher, it is possible to install 30 times more sensors than LoRA or LTE-M. On the other hand, since each meter transmits data intermittently and with a small capacity, it is not good to install RS and MS of WRAN to all meters. Therefore, as shown on the right side of Fig. 2.1, it is assumed that some meters will be connected to other communication systems, such as Wi-SUN, and connected to WRAN via MGW.

It is also expected to be used in the automatic operation of agricultural machinery, etc. Even now, some agricultural machinery is equipped with public communication functions, and it is possible to use WRAN for agricultural machinery. Usage fees are required when using public communications, however there are no usage fees when using WRAN. Depending on the application, it is also possible to build a closed network within the farm without connecting to the Internet. Both use cases can be implemented using public communications; however, there is a usage charge, and communication is impossible outside the area.

- Disaster prevention

  In the field of disaster prevention, it is expected to be used for collecting information on water disasters caused by rainfall. It is necessary to collect information quickly when a river floods. Due to the characteristics of this information, it is necessary to collect large amounts of data continuously; however, it is often located outside public communication areas, such as in mountainous areas. Another issue is cases where power supply and wired lines do not reach the surrounding areas, making it challenging to select the installation area. Though IoT monitoring systems for river water levels are provided by various manufacturers, they are connected to cellular networks [89, 90]. For these reasons, ultra-wide-area WRAN communications are suitable in the disaster prevention field, as in the agricultural field. However, even with ultra-wide area WRAN, power supply is an issue; thus, considering installation in conjunction with private power generation equipment is also an issue. Although it is possible to provide the acquired water disaster information as a service directly, there are issues, such as legal requirements for such use.

In addition, it is important to have a common platform that can be easily introduced in various fields.

6.2 Program Production Platforms Using Next-generation FPU

I consider an integrated program production platform using next-generation FPUs, wired lines, and others. In the field of TV program production, efforts of remote program production using IP lines have begun [91]. Previously, switching and camera operations were performed in environments extremely close to the filming location, such as in the same studio or inside a relay car. As part of remote program production, it is considered to perform program production, such as switching at home far away from the studio or at a studio far away from the broadcast site. Experiments using wired lines such as dark fiber have already begun.

In conventional broadcast program production, since the video was transmitted to the broadcasting station's studio after switching and other processing was performed at the relay destination, it was sufficient to transmit the video material for one camera (line). However, in remote program production, because switching and other operations are performed remotely, it is necessary to transmit video material from all cameras, and the required transmission capacity is enormous. As mentioned above, although there are remote program production [91] using wired lines and wireless remote production using FPU for fixed use [35], there are no examples of implementation using mobile relay. As part of R&D, experiments have been conducted on the remote control and switching of cameras installed on camera relay cars using next-generation FPUs, and it has been confirmed that they work normally [66]. The next-generation FPU has ultra-high capacity and is capable of bidirectional transmission, making it a suitable system for remote program production. For 2K video, it is possible to transmit program material video over several lines even at the minimum transmission rate of 40 Mbps. However, transmitting multiple 4K video lines requires even higher capacity. For these reasons, the challenge is to increase the capacity as much as possible using the various methods proposed in this thesis.

Additionally, efforts to migrate program master equipment to the cloud are being considered worldwide [92, 31]. In addition, research is being conducted to utilize data such as river information distributed on the web and social media posts in program production [93, 94]. In this way, the number of program productions performed on the cloud/Internet is increasing, and it is expected that the number of program productions completed on IP systems will increase more than ever before. As a means to achieve this, there is a need to realize an integrated program production platform that uses a combination of next-generation FPUs, wired lines, cellular lines, etc.

Chapter 7
Conclusions

This thesis described the design of communication networks for an era where devices with various uses are connected. To achieve this, it is essential to build private communication systems with features tailored to the purpose, in addition to the already widely used general-purpose public wireless communication systems. This thesis proposed and evaluated various methods for installing two types of private communications, each with the characteristics of "wide-area" and "wide-band."

Chapter 2 described use cases and specifications for the wide-area WRAN system and the next-generation FPU system that uses wide-band. WRAN systems are expected to be used in various situations, including IoT communications, mobile communications, and V2X communications. It is a method that has all the characteristics of wide-area, mobile, multi-hop, and relatively high-speed transmission. The aim is high throughput and wide coverage area transmission with the same transmission power. Furthermore, the base system is standardized both domestically and internationally, and R&D is being conducted based on this standard. That chapter described an overview of transmitters based on that standard. The next-generation FPU system is expected to be used for mobile relay programs of high-definition video, such as 4K/8K. In particular, the aim is to achieve both stable and high-speed transmission by dramatically changing the transmission rate according to the channel quality changes during movement. The base system is also standardized domestically, and R&D is being conducted based on this standard. Furthermore, that chapter described the system model and detailed the degradation and changes in the weight matrices, which was a research topic.

Chapter 3 proposed single-hop and multi-hop methods for realizing a WRAN system and evaluated their performance. For single-hop transmission, the chapter designed the receivers, including a comparative study of channel estimation methods, and evaluated the performance through computer simulation and laboratory experiments using a prototype. The results showed that even using single-hop transmission, transmitting 10 km is possible at transmission speeds of several hundred kbps to several Mbps. For multi-hop transmission, the chapter evaluated the expansion of the coverage area and the throughput when simply relaying in multiple stages based on the results of single-hop transmission. The results showed that 50 km transmission is possible with a throughput of 1/6 to 1/2 compared to single-hop transmission.

Chapter 4 proposed a channel quality estimation method and an ATC method based on it and evaluated the performance through computer simulations to realize a next-

generation FPU system. That chapter showed that a method for estimating changes in channel quality by using degraded or changed weight matrices can suppress the error in channel quality estimation to within 2 dB. Furthermore, that chapter showed that ATC using this estimation method significantly improves the required SNR by up to 6 dB, leading to the expansion of the transmission area coverage at the same throughput.

Chapter 5 proposed simplified channel metrics for the degradation of the Tx weight matrix, proposed a compensation method for the degradation using machine learning, and evaluated performance for the realization of next-generation FPU systems. That chapter proposed metrics for simply calculating the gain part of the channel quality estimation results described in Chapter 4 and demonstrated through computer simulation that the evaluation results are valid. That chapter also proposed a learning data creation method and learning/compensation structure for compensating degradation using machine learning and evaluated the performance through computer simulations. It was shown that by combining this method with the ATC method proposed in Chapter 4, it improved by up to 7.0 dB, leading to the expansion of the transmission area coverage at the same throughput.

Chapter 6 described the prospects for realizing platforms that support various applications using two private communication systems. For the WRAN system, the assumptions and challenges involved in realizing a CPS platform used in various fields, such as agriculture and disaster prevention, were described. For the next-generation FPU system, the challenges in realizing a program production platform for remote program production were described.

Future research topics for the WRAN system include outdoor mobile transmission experiments using a prototype. As a result, it is possible to evaluate whether stable transmission over a communication distance of 10 km or more is achievable. Furthermore, regarding multi-hop, it is expected that the transmission distance will be further extended by considering a hop that transmits data at multiple hops at the same time rather than a simple multi-hop relay design.

Future research topics for the next-generation FPU include hardware implementation of each function and evaluation through mobile transmission experiments. Although the proposed method in this thesis is not implemented, a prototype based on the system model has been created and evaluated through mobile transmission experiments. Furthermore, since quantization compensation technology has been installed on FPGAs, there is hope for realization to operate in a time that does not affect real-time processing. It is expected that it will be possible to further evaluate the feasibility of each proposed method by installing it in a prototype and assessing its performance through mobile transmission experiments.

Bibliography

[1] M. Agiwal, A. Roy, and N. Saxena, "Next Generation 5G Wireless Networks: A Comprehensive Survey," *IEEE Commun. Surv. Tutor.*, vol. 18, no. 3, pp. 1617-1655, 2016, DOI: 10.1109/COMST.2016.2532458.

[2] W. Jiang, B. Han, M. A. Habibi, and H. D. Schotten, "The Road Towards 6G: A Comprehensive Survey," *IEEE OJ-COMS*, vol. 2, pp. 334-366, 2021, DOI: 10.1109/OJCOMS.2021.3057679.

[3] K. Makino, K. Mizutani, T. Matsumura, and H. Harada, "Super-large-coverage standardized wireless communication system and its implementation in VHF Band for IoT and V2X," *IEEE Open J. Veh. Technol.*, vol. 4, pp. 667-680, Sept. 2024, DOI: 10.1109/OJVT.2023.3311544.

[4] K. Makino, T. Sato, F. Ito, T. Nakagawa, and N. Iai, "Methods of adaptive transmission control for SVD-MIMO using incomplete weight matrices," *IEICE Trans. Commun. (Japanese Edition)*, vol. J106-B, no. 2, pp. 1-16, Feb. 2023. DOI: 10.14923/transcomj.2022JBP3019

[5] K. Makino, T. Nakagawa, and N. Iai, "Machine learning-based compensation methods of weight matrices for SVD-MIMO," *IEICE Trans. Commun.*, vol. E106-B, no. 12, pp. 1441-1454 Dec. 2023, DOI: 10.1587/transcom.2023EBP3033.

[6] K. Makino, T. Sato, F. Ito, T. Nakagawa, and N. Iai, "Field experiment with FPUs for mobile relay programs with automatic switching of total modulation orders," *ITE Trans. MTA*, vol. 11, no. 4, pp. 164-175, Oct. 2023, DOI:10.3169/mta.11.164.

[7] Wu, S. Luo, S. Wang, and H. Wang, "NLES: A Novel Lifetime Extension Scheme- for Safety-Critical Cyber-Physical Systems Using SDN and NFV," *IEEE Internet Things J.*, vol. 6, no. 2, pp. 2463-2475, Apr. 2019, DOI: 10.1109/JIOT.2018.2870294.

[8] *IEEE Standard for Information technology-Local and metropolitan area networks-Specific requirements-Part 22: Cognitive Wireless RAN Medium Access Control (MAC) and Physical Layer (PHY) specifications: Policies and procedures for operation in the TV Bands*, IEEE Standard 802.22TM-2011, IEEE, NJ, USA, Jul. 2011, DOI: 10.1109/IEEESTD.2011.5951707.

[9] K. Hasegawa, M. Takekawa, T. Keat-Beng, K. Yanagisawa, S. Sasaki, and M. Asano, "IEEE 802.22-based WRAN system for disaster-resistant network

systems," in *Proc. 2013 IEEE R10 HTC 2013*, pp. 264-269, Aug. 2013, DOI: 10.1109/R10-HTC.2013.6669053.

[10] K. Ishizu, K. Hasegawa, K. Mizutani, H. Sawada, K. Yanagisawa, T. Keat-Beng, T. Matsumura, S. Sasaki, M. Asano, H. Murakami, and H. Harada, "Field experiment of long-distance broadband communications in TV white space using IEEE 802.22 and IEEE 802.11af," in *Proc. WPMC 2014*, pp. 468-473, Sept. 2014, DOI: 10.1109/WPMC.2014.7014864.

[11] R. Ouyang, T. Matsumura, K. Mizutani and H. Harada, "Software-Defined Radio-Based Evaluation Platform for Highly Mobile IEEE 802.22 System," *IEEE Open J. Veh. Technol.*, vol. 3, pp. 167-177, Apr. 2022, DOI: 10.1109/OJVT.2022.3164461.

[12] *IEEE Standard for Local and metropolitan area networks Part 16: Air Interface for Broadband Wireless Access Systems*, IEEE Standard 802.16-2009, IEEE, NJ, USA, Mar. 2009, DOI: 10.1109/IEEESTD.2009.5062485.

[13] B. Li, Y. Qin, C. P. Low and C. L. Gwee, "A Survey on Mobile WiMAX," *IEEE Commun. Mag.*, vol. 45, no. 12, pp. 70-75, Dec. 2007, DOI: 10.1109/MCOM.2007.4395368.

[14] M. F. Mohamad, M. A. Saeed, and A. U. Priantoro, "Downlink channel estimation and tracking in mobile WiMAX systems," in *Proc. ICCCE 2008*, pp. 1340-1343, May 2008, DOI: 10.1109/ICCCE.2008.4580823.

[15] S. Galih, R. Karlina, F. Nugroho, A. Irawan, T. Adiono, and A. Kurniawan, "High mobility data pilot based channel estimation for downlink OFDMA system based on IEEE 802.16e standard," in *Proc. ICEEI '09*, vol. 02, pp. 478-483, Aug. 2009, DOI: 10.1109/ICEEI.2009.5254688.

[16] S. Su, Y. Lin, Ch. Hsu, and G. C. H. Chuang, "A DFT-based channel estimation scheme for IEEE 802.16e OFDMA systems," in *Proc. ICACT 2010*, Feb. 2010, pp. 775-779.

[17] K. Makino, K. Mizutani, T. Matsumura, and H. Harada, "A transceiver design of VHF band standardized broadband mobile communications systems," in *Proc. WPMC 2017*, pp. 87-93, Dec. 2017, DOI: 10.1109/WPMC.2017.8301895.

[18] *200 MHz-band broadband wireless communication systems between portable BS and MS*, ARIB STD-T103, ARIB, Tokyo, Japan, Mar. 2011.

[19] M. Oodo and H. Harada, "Current status of 200 MHz-band public broadband wireless communication system," in *Proc. IEEE WPMC 2014*, pp. 759-764, Sept. 2014, DOI: 10.1109/WPMC.2014.7014917.

[20] *IEEE Standard for Air Interface for Broadband Wireless Access Systems-Amendment 2: Higher Reliability Networks*, IEEE Standard 802.16n-2013, IEEE, NJ, USA, Mar. 2013, DOI: 10.1109/IEEESTD.2013.6530596

[21] Y. Li, L. Yang, S. Han, X. Wang, and F.-Y. Wang, "When LPWAN Meets ITS: Evaluation of Low Power Wide Area Networks for V2X Communications," in *Proc. 2018 ITSC*, pp. 473-478, 2018, DOI: 10.1109/ITSC.2018.8569320.

[22] S. Popli, R. K. Jha, and S. Jain, "A Survey on Energy Efficient Narrowband Internet of Things (NBIoT): Architecture, Application and Challenges," *IEEE Access*, vol. 7, pp. 16739-16776, Nov. 2019, DOI: 10.1109/ACCESS.2018.2881533.

[23] G. Stanco, A. Botta, F. Frattini, U. Giordano, and G. Ventre, "On the performance of IoT LPWAN technologies: the case of Sigfox, LoRaWAN and NB-IoT," in *Proc. IEEE ICC 2022*, pp. 2096-2101, 2022, DOI: 10.1109/ICC45855.2022.9839078.

[24] D. Abada, A. Massaq, A. Boulouz, and M. B. Salah, "An Adaptive Vehicular Relay and Gateway Selection Scheme for Connecting VANETs to Internet via 4G LTE Cellular Network," in *Proc. 2019 ICCSRE*, pp. 1-8, 2019, DOI: 10.1109/ICCSRE.2019.8807536.

[25] *IEEE Standard for Information technology-Local and metropolitan area networks-Specific requirements-Part 11: Wireless LAN Medium Access Control (MAC) and Physical Layer (PHY) Specifications Amendment 6: Wireless Access in Vehicular Environments*, IEEE Standard 802.11pTM-2010, IEEE, NJ, USA, Jul. 2010, DOI: 10.1109/IEEESTD.2010.5514475.

[26] R. Atallah, M. Khabbaz, and C. Assi, "Multihop V2I Communications: A Feasibility Study, Modeling, and Performance Analysis," *IEEE Trans. Veh. Technol.*, vol. 66, no. 3, pp. 2801-2810, Jun. 2016, DOI: 10.1109/TVT.2016.2586758.

[27] Ministry of Land, Infrastructure, Transport and Tourism. "MLIT Public Broadband Mobile Communication System Standard Specifications (in Japanese)," Ministry of Land, Infrastructure, Transport and Tourism (Japan), 2016, https://www.mlit.go.jp/tec/it/denki/kikisiyou/kokudenntsushi56.pdf, (Data accessed Oct. 29, 2023).

[28] Shizuoka-shi. "[Press release] Social experiments to strengthen Construction Bureau disaster prevention capabilities using public broadband (in Japanese)," Shizuoka-shi (Japan), 2021, https://www.city.shizuoka.lg.jp/000920269.pdf, (Data accessed Oct. 29, 2023).

[29] H. Harada, K. Makino, K. Mizutani and T. Matsumura, "A TV white space wireless broadband prototype for wireless regional area network," in *Proc. WPMC 2018*, pp. 206-211, Nov. 2018, DOI: 10.1109/WPMC.2018.8713057.

[30] *Parameter values for ultra-high definition television systems for production and international programme exchange*, Rep. ITU-R BT.2020, ITU-R, Geneva, Switzerland, Aug. 2012.

[31] S. Asakura, H. Nagata, R. Kabutomori, M. Onishi, K. Kambara, K. Otsuki, and K. Tsuchida, "End-to-end Verification of the Advanced Broadcasting System," *ITE Trans. MTA*, vol. 11, no. 3, pp. 113-122, Jul. 2023, DOI:10.3169/mta.11.113.

[32] LiveU Inc. "LU6000 HEVC," LiveU (USA) https://cdn-liveutv.pressidium.com/wpcontent/uploads/2021/07/LU600_HEVC_Datasheet .pdf, (Data accessed Oct. 29, 2023).

[33] T. Hiraguri, T. Ogawa, T. Shindo, F. Uzawa, and K. Mitsuyama, "High Efficiency Retransmission Control for Bidirectional Field Pick-up Unit Systems", *ITE Trans. MTA*, vol. 3, no. 3, pp. 206-213, Jul. 2015, DOI: 10.3169/mta.3.206.

[34] T. Yoshida, K. Saito, K. Ito, and M. Takahashi, "The Specific Absorption Rate Evaluation of 1.2 GHz Band Wireless Camera by a Thermographic Method", *ITE Trans. MTA*, vol. 4, no. 3, pp. 269-276, Jul. 2016, DOI: 10.3169/mta.4.269.

[35] T. Yamaguchi, F. Ito, T. Nakagawa, T. Nakatogawa, T. Kurakake, and K. Imamura, "FPU Wireless Transmission System for IP Remote Production That Enables PTP Time Synchronization between Equipment in Each Venue (in Japanese)", *Journal of ITE*, vol. 77, 2 pp. 253-261, Mar. 2023, DOI: 10.3169/itej.77.253.

[36] *Tuning Ranges and Operational Characteristics of Terrestrial Electronic News Gathering (ENG), Television Outside Broadcast (TVOB) and Electronic Field Production (EFP) systems*, Rep. ITU-R BT.2069, ITU-R, Geneva, Switzerland, 2006.

[37] J. Ma, N. J. Karl, S. Bretin, G. Ducournau, and D. M. Mittleman, "Frequency-division Multiplexer and Demultiplexer for Terahertz Wireless Links", *Nat. Commun.*, no. 8: 72, Sept. 2017, DOI: 10.1109/TBC.2013.2273598.

[38] J. Kim, Y. Tian, S. Mangold, and A. F. Molisch, "Joint Scalable Coding and Routing for 60 GHz Real-time Live HD Video Streaming Applications", *IEEE Trans. Broadcast.*, vol. 59, no. 3, pp. 500-512, Sept. 2013, DOI: 10.1109/TBC.2013.2273598.

[39] T. Nakagawa and T. Ikeda, "A 64-State 16-QAM Space-Time Trellis Code for Television Program Material Transmission (in Japanese)", *Journal of ITE*, vol. 68, no. 5, pp.J184-J191, 2014, DOI: 10.3169/itej.68.J184.

[40] J. Tsumochi, S. Okabe, F. Suginoshita, J. Takeuchi, and A. Hirata, "120-GHz-Band SHV-FPU for UHDTV Broadcasting Program Transmission (in Japanese)", *IEICE Trans. Electro. (Japanese Edition)*, vol. J99-C, no. 8, pp.382-392, Aug. 2016.

[41] J.Tsumochi, K. Murase, Y.Matsusaki, F. Ito, H. Kamoda, H. Kamoda, N. Iai, K.Imamura, H. Hamazumi, and K. Shibuya : "Wireless Links For 8K Super Hi-Vison Program Production", *IBC 2017 Conference*, Oct. 2017.

[42] *1.2GHz/2.3GHz-band Portable OFDM Digital Transmission System for Television Program Contribution*, ARIB STD-B57, ARIB, Tokyo, Japan, Dec. 2013.

[43] K.Mitsuyama and N. Iai, "Adaptive bit and power allocation algorithm for SVD-MIMO system with fixed transmission rate," in *Proc. IEEE WiMob*, pp. 455-460, Oct. 2014, DOI: 10.1109/WiMOB.2014.6962210.

[44] F. Ito, F.Uzawa, T. Sato, T. Nakagawa, and N. Iai, "Performance Analysis of 4×4 TDD-SVD-MIMO System in Suburban Field Trial", in *Proc. IEEE GLOBECOM 2020*, Dec. 2020, DOI: 10.1109/GLOBECOM42002.2020.9348151.

[45] F. Ito, T. Sato, K. Makino, T. Nakagawa, and N. Iai, "Switching Algorithm of Total Number of Modulation Bits for SVD-MIMO System (in Japanese)", in *Proc. 2021 ITE Winter Annual Convention*, 11B-3, Dec. 2021.

[46] *Semi-microwave band portable OFDM digital transmission system for ultra high definition television*, ARIB STD-B75, ARIB, Tokyo, Japan, Oct. 2021.

[47] J. Choi, J. Park and B. L. Evans, "Spectral Efficiency Bounds for Interference-Limited SVD-MIMO Cellular Communication Systems," *IEEE Wireless Commun. Lett.*, vol. 6, no. 1, pp. 46-49, Feb. 2017, DOI: 10.1109/LWC.2016.2629474.

[48] K. J. Lee and I. Lee, "Diversity analysis of coded SVD schemes for MIMO spatial multiplexing systems," in *Proc. IEEE ICC 2008*, pp. 4703-4707, May 2008, DOI: 10.1109/ICC.2008.881.

[49] F. Uzawa, F. Ito, K. Mitsuyama, and N. Iai, "A Rate-matching Method Applicable to 4×4 TDD-SVD-MIMO System with Adaptive Transmission Control (in Japanese)", *ITE Tech. Rep.*, BCT2017-83, vol. 41, no. 35, pp.9-12, Oct. 2017.

[50] *H.266 : Versatile video coding*, Rec. ITU-T H.266, ITU-T, Geneva, Switzerland, Apr. 2022.

[51] C. Bonnineau, W. Hamidouche, J. Fournier, N. Sidaty, J. -F. Travers, and O. Déforges, "Perceptual Quality Assessment of HEVC and VVC Standards for 8K Video," *IEEE Trans. Broadcast.*, vol. 68, no. 1, pp. 246-253, March 2022, DOI: 10.1109/TBC.2022.3140710.

[52] G. Lebrun, J. Gao and M. Faulkner, "MIMO transmission over a time-varying channel using SVD," *IEEE Trans. Wirel. Commun.*, vol. 4, no. 2, pp. 757-764, Mar. 2005, DOI: 10.1109/TWC.2004.840199.

[53] K. Miyashita, T. Nishimura, T. Ohgane, Y. Ogawa, Y. Takatori, and K. Cho, "High data-rate transmission with eigenbeam-space division multiplexing (E-SDM) in a MIMO channel," in *Proc. IEEE VTC*, vol. 3, pp. 1302-1306, Dec. 2002, DOI: 10.1109/VETECF.2002.1040426.

[54] See Ho Ting, K. Sakaguchi, and K. Araki, "A robust and low complexity adaptive algorithm for mimo eigenmode transmission system with experimental validation," *IEEE Trans. Wirel. Commun.*, vol. 5, no. 7, pp. 1775-1784, Jul. 2006, DOI: 10.1109/TWC.2006.1673089

[55] F. Ito, F. Uzawa, T. Sato, T. Nakagawa and N. Iai, "Performance analysis of 4×4 TDD-SVD-MIMO system in suburban field trial," in *Proc. IEEE GLOBECOM 2020*, pp. 1-7, Dec. 2020, DOI: 10.1109/GLOBECOM42002.2020.9348151.

[56] Y. Seki and F. Adachi, "Adaptive MMSE-SVD for OFDM downlink MU-MIMO in a high mobility environment," *IEICE ComEx*, vol. 7, no. 6, pp. 195-200, 2018, DOI: 10.1587/comex.2018XBL0028.

[57] T. Nechiporenko, K. T. Phan, C. Tellambura, and H. H. Nguyen, "On the capacity of Rayleigh fading cooperative systems under adaptive transmission," *IEEE Trans. Wirel. Commun.*, vol. 8, no. 4, pp. 1626-1631, Apr. 2009, DOI: 10.1109/T-WC.2008.071098.

[58] M. Fernández-Delgado, M. S. Sirsat, E. Cernadas, S. Alawadi, S. Barro, and M. Febrero-Bande, "An extensive experimental survey of regression methods," *Neural Networks*, vol. 111, pp. 11-34, 2019, DOI: 10.1016/j.neunet.2018.12.010.

[59] P. Dong, H. Zhang, and G. Y. Li, "Machine learning prediction based CSI acquisition for FDD massive MIMO downlink," in *Proc. IEEE GLOBECOM 2018*, pp. 1-6, 2018, DOI: 10.1109/GLOCOM.2018.8647328.

[60] Q. Mao, F. Hu, and Q. Hao, "Deep learning for intelligent wireless networks: a comprehensive survey," *IEEE Commun. Surv. Tutor.*, vol. 20, no. 4, pp. 2595-2621, 2018, DOI: 10.1109/COMST.2018.2846401.

[61] T. Ohtsuki, "Machine learning in 6G wireless communications," *IEICE Trans. Commun.*, vol. E106-B, no. 2, pp. 75-83, Feb. 2023, DOI: 10.1587/transcom.2022CEI0002.

[62] T. Peken, S. Adiga, R. Tandon, and T. Bose, "Deep learning for SVD and hybrid beamforming," *IEEE Trans. Wirel. Commun.*, vol. 19, no. 10, pp. 6621-6642, Oct. 2020, DOI: 10.1109/TWC.2020.3004386.

[63] H. Harada, K. Mizutani, J. Fujiwara, K. Mochizuki, K. Obata, and R. Okumura, "IEEE 802.15.4g Based Wi-SUN Communication Systems," *IEICE Trans. Commun.*, vol. E100-B, no. 7, pp. 1032-1043, Jul. 2017, DOI: 10.1587/transcom.2016SCI0002.

[64] R. Molina-Masegosa and J. Gozalvez, "LTE-V for Sidelink 5G V2X Vehicular Communications: A New 5G Technology for Short-Range Vehicle-to-Everything Communications," *IEEE Veh. Technol. Mag.*, vol. 12, no. 4, pp. 30-39, Dec. 2017, DOI: 10.1109/MVT.2017.2752798.

[65] NEC. "VC-8900/VD-8900 For 8K Video Material Transmission H.265 CODEC (in Japanese)," NEC(Japan), 2019, https://jpn.nec.com/bv/hoso/pdf/vcvd-8900.pdf, (Data accessed Oct. 13, 2023).

[66] T. Sato, K. Makino, F. Ito, T. Nakagawa, and N. Iai , "A Study on Remote Production using Next Generation Mobile Relay FPU (in Japanese)," *ITE Tech. Rep.*, BCT2021-43, vol. 45, no. 27, pp.23-28, Sept. 2021.

[67] S. Yang and L. Hanzo, "Fifty years of MIMO detection: The road to large-scale MIMOs," *IEEE Commun. Surv. Tutor.*, vol. 17, no. 4, pp. 1941-1988, Sep. 2015, DOI: 10.1109/COMST.2015.2475242.

[68] W.C. Jakes, "A Comparison of Specific Space Diversity Techniques for Reduction of Fast Fading in UHF Mobile Radio Systems," *IEEE Trans. Veh. Technol.*, vol. 20, pp. 81-92, Nov. 1971, DOI: 10.1109/T-VT.1971.23485.

[69] H. Harada and R. Prasad, "Simulation and software radio for mobile communications," Artech House, 2002.

[70] J. Cho and Z. J. Haas, "On the Throughput Enhancement of the Downstream Channel in Cellular Radio Networks Through Multi-hop Relaying," *IEEE J. Sel. Areas in Commun.*, vol. 22, no. 7, pp. 1206-1219, Sept. 2004, DOI: 10.1109/JSAC.2004.829340.

[71] *Monte Carlo simulation methodology for the use in sharing and compatibility studies between different radio services or systems*, Rep. ITU-R SM.2028, ITU-R, Geneva, Switzerland, Jan. 2001.

[72] K. Zheng, L. Zhao, J. Mei, B. Shao, W. Xiang and L. Hanzo, "Survey of Large-Scale MIMO Systems," *IEEE Commun. Surv. Tutor.*, vol. 17, no. 3, pp. 1738-1760, Apr. 2015, DOI: 10.1109/COMST.2015.2425294.

[73] W. Yu and J. M. Cioffi, "On constant power water-filling," in *Proc. IEEE ICC 2001*, pp. 1665-1669 vol. 6, Jun. 2001, DOI: 10.1109/ICC.2001.937077.

[74] A. Liu, Y. Liu, H. Xiang and W. Luo, "Polite water-filling for weighted sum-rate maximization in MIMO B-MAC networks under multiple linear constraints," *IEEE Trans. Signal Process.*, vol. 60, no. 2, pp. 834-847, Feb. 2012, DOI: 10.1109/TSP.2011.2173334.

[75] K. I. Pedersen, J. B. Andersen, J. P. Kermoal, and P. Mogensen, "A stochastic multiple-input-multiple-output radio channel model for evaluation of space-time coding algorithms," in *Proc. IEEE VTC Fall 2000*, Sep. 2000, DOI: 10.1109/VETECF.2000.887129.

[76] W. C. Jakes, "Microwave mobile communications," John Wiley & Sons Inc., 1975.

[77] *Evolved Universal Terrestrial Radio Access (E-UTRA); User Equipment (UE) Radio Transmission and Reception*, 3GPP TS 36.101, 3GPP; TSG RAN, Sophia Antipolis, France, Sep. 2008.

[78] Y. Karasawa, "MIMO propagation channel modeling," *IEICE Trans. Commun.*, vol. E88-B, no. 5, pp. 1829-1842, May 2005, DOI: 10.1093/ietcom/e88-b.5.1829.

[79] A. J. Smola and B. Schölkopf, "A tutorial on support vector regression," *Statistics and Computing*, vol. 14, no. 3, pp. 199-222, 2004, DOI: 10.1023/B:STCO.0000035301.49549.88.

[80] B. Kim, H. Kim, K. Kim, S. Kim, and J. Kim, "Learning not to learn: Training deep neural networks with biased data," in *Proc. CVPR 2019*, pp. 9004-9012, 2019, DOI: 10.1109/CVPR.2019.00922.

[81] W. Cao, X. Liu, and J. Ni, "Parameter optimization of support vector regression using Henry gas solubility optimization algorithm," *IEEE Access*, vol. 8, pp. 88633-88642, 2020, DOI: 10.1109/ACCESS.2020.2993267.

[82] F. Pedregosa et al., "Scikit-learn: machine learning in python," *J. Mach. Learn. Res.*, pp. 2825-2830, Nov. 2011, DOI: 10.5555/1953048.2078195.

[83] Y. W. Chang, C. J. Hsieh, K. W. Chang, M. Ringgaard, and C. J. Lin, "Training and testing low-degree polynomial data mappings via linear SVM," *J. Mach. Learn. Res.*, vol. 11 no. 48, pp. 1471-1490, 2010, DOI: 10.5555/1756006.1859899.

[84] R. Izmailov, V. Vapnik, and A. Vashist, "Multidimensional splines with infinite number of knots as SVM kernels," in *Proc. IJCNN 2013*, pp. 1-7, Aug. 2013, DOI: 10.1109/IJCNN.2013.6706860.

[85] K. Makino and T. Nakagawa, "FPGA implementation of ML-compensation for SVD-MIMO weight matrices (in Japanese)," *IEICE Tech. Rep.*, vol. 123, no. 108, RCS2023–99, pp. 103–108, July 2023.

[86] O. Elijah, T. A. Rahman, I. Orikumhi, C. Y. Leow, and M. N. Hindia, "An Overview of Internet of Things (IoT) and Data Analytics in Agriculture: Benefits and Challenges," *IEEE Internet Things J.*, vol. 5, no. 5, pp. 3758-3773, Oct. 2018, DOI: 10.1109/JIOT.2018.2844296.

[87] Ministry of Agriculture, Forestry and Fisheries “Regarding the situation surrounding smart agriculture (in Japanese),” Ministry of Agriculture, Forestry and Fisheries (Japan), Nov. 2023, https://www.maff.go.jp/j/kanbo/smart/attach/pdf/index-128.pdf, (Data accessed Dec. 23, 2023).

[88] KUBOTA-CHEMIX .Co ., LTD. “Field management system: WATARAS (in Japanese),” KUBOTA-CHEMIX .Co ., LTD (Japan), June 2023, https://agriculture.kubota.co.jp/img_sys/catalog/7-00-2-0017-04.pdf, (Data accessed Dec. 23, 2023).

[89] NEC Platforms, Ltd. “NEC Platforms launches ”IoT Monitoring Package for River Water Level” that visualizes and shares water level information in real-time (in Japanese),” NEC Platforms, Ltd (Japan), June 2020, https://www.necplatforms.co.jp/press/202006/20200617_01.html, (Data accessed Dec. 23, 2023).

[90] Denshin. Co Ltd.“IoT ultrasonic river water level monitoring sensor (in Japanese),” Denshin. Co Ltd (Japan), June 2020, https://www.densin.co.jp/product_iot/3486/, (Data accessed Dec. 23, 2023).

[91] R. Shirato, J. Kawamoto, T. Nakatogawa, and T. Kurakake, “Multiformat Transmission System Using Video Decomposition for Remote Professional Media Production,” *ITE Trans. MTA*, vol. 10, no. 4, pp. 243-253, Oct. 2023, DOI:10.3169/mta.10.243.

[92] Study group on the state of the broadcasting system in the digital age. “Summary of the future vision and system of broadcasting in the digital age (in Japanese),” Ministry of Internal Affairs and Communications (Japan), 2019, https://www.soumu.go.jp/main_content/000831138.pdf, (Data accessed Oct. 29, 2023).

[93] J. Goto, T. Miyazaki, Y. Takei, and K. Makino, “Automatic tweet detection based on data specified through news production,” in *Proc. IUI 2018*, pp. 1-2, Mar. 2018, DOI: 10.1145/3180308.3180309.

[94] T. Miyazaki, Y. Takei, and K. Makino, “Social Media Analysis System on NHK STRL, and its usage in TV Programs (in Japanese),” *Journal of ITE*, vol. 74, no. 1, pp. 169-173, Feb. 2020 , DOI: 10.3169/itej.74.169.

Author's Publication List

Journal Papers

1. **K. Makino**, T. Sato, F. Ito, T. Nakagawa, and N. Iai, "Methods of adaptive transmission control for SVD-MIMO using incomplete weight matrices ," *IEICE Trans. Commun. (Japanese Edition)*, vol. J106-B, no. 2, pp. 62–77, Feb. 2023, DOI: 10.14923/transcomj.2022JBP3019.

2. **K. Makino**, K. Mizutani, T. Matsumura, and H. Harada, "Super-large-coverage standardized wireless communication system and its implementation in VHF Band for IoT and V2X," *IEEE Open J. Veh. Technol.*, vol. 4, pp. 667-680, Sept. 2023, DOI: 10.1109/OJVT.2023.3311544.

3. **K. Makino**, T. Sato, F. Ito, T. Nakagawa, and N. Iai, "Field experiment with FPUs for mobile relay programs with automatic switching of total modulation orders," *ITE Trans. MTA*, vol. 11, no. 4, pp. 164-175, Oct. 2023, DOI:10.3169/mta.11.164.

4. **K. Makino**, T. Nakagawa, and N. Iai, "Machine learning-based compensation methods of weight matrices for SVD-MIMO," *IEICE Trans. Commun.*, vol. E106-B, no. 12, pp. 1441-1454, Dec. 2023, DOI: 10.1587/transcom.2023 EBP3033.

International Conference Papers

1. **K. Makino**, K. Mizutani, T. Matsumura, and H. Harada, "A transceiver design of VHF band standardized broadband mobile communications systems," in *Proc. 2017 20th International Symposium on Wireless Personal Multimedia Communications (WPMC)*, Bali, Indonesia, Dec. 2017, pp. 87-93, DOI: 10.1109/WPMC.2017.8301895.

2. T. Miyazaki*, **K. Makino***, Y. Takei, H. Okamoto, and J. Goto, "NHK STRL at TREC 2018 Incident Streams track," in *Proc. Twenty-Seventh Text REtrieval Conference (TREC 2018)*, Gaithersburg, Maryland, USA, Nov. 2018.

3. **K. Makino**, Y. Takei, T. Miyazaki, and J. Goto, "Classification of tweets about reported events using neural networks," in *Proc. 2018 EMNLP Workshop W-NUT: The 4th Workshop on Noisy User-generated Text*, Brussels, Belgium, Nov. 2018, pp. 153-163, DOI: 10.18653/v1/W18-6121.

*These two authors contributed equally.

4. J. Goto, T. Miyazaki, Y. Takei, and **K. Makino**, "Automatic tweet detection based on data specified through news production," in *Proc. 23rd ACM International Conference on Intelligent User Interfaces Companion (IUI 2018)*, New York, NY, USA, Mar. 2018, pp. 1-2, DOI: 10.1145/3180308.3180309.

5. H. Harada, **K. Makino**, K. Mizutani, and T. Matsumura, "A TV white space wireless broadband prototype for wireless regional area network," in *Proc. 2018 21st International Symposium on Wireless Personal Multimedia Communications (WPMC)*, Chiang Rai, Thailand, Nov. 2018, pp. 206-211, DOI: 10.1109/WPMC.2018.8713057.

6. T. Miyazaki, **K. Makino**, Y. Takei, H. Okamoto, and J. Goto, "Label Embedding using Hierarchical Structure of Labels for Twitter Classification," in *Proc. 2019 Conference on Empirical Methods in Natural Language Processing and the 9th International Joint Conference on Natural Language Processing (EMNLP-IJCNLP)*, Hong Kong, China, Nov. 2019, pp. 6318-6323, DOI: 10.18653/v1/D19-1660.

Technical Reports and Local Conference Papers

1. **K. Makino**, K. Mizutani, and H. Harada, "Receiver design for VHF broadband mobile communication systems," *IEICE Tech. Rep.*, vol. 114, no. 490, RCS2014–333, pp. 189–194, Mar. 2015 (in Japanese).

2. **K. Makino**, K. Mizutani, and H. Harada, "Performance evaluation of ARIB STD-T103 VHF broadband mobile communication systems," *IEICE Tech. Rep.*, vol. 115, no. 113, RCS2015–95, pp. 287–292, June 2015 (in Japanese).

3. **K. Makino**, K. Mizutani, and H. Harada, "Experimental evaluation of ARIB STD-T103 VHF broadband mobile communication systems," *IEICE Tech. Rep.*, vol. 115, no. 472, RCS2015–362, pp. 175–180, Mar. 2016 (in Japanese).

4. **K. Makino**, Y. Takei, T. Miyazaki, and J. Goto, "Classification of reported tweets using neural networks," in *Proc. Twenty-fourth Annual Meeting of the Association for Natural Language Processing (NLP2018)*, pp. 1143–1146, Mar. 2018 (in Japanese).

5. **K. Makino**, Y. Takei, H. Okamoto, T. Miyazaki, and J. Goto, "A study on multitask learning methods for extracting important tweets," *ITE Winter Annual Convention 2018*, 12C-3, Dec. 2018 (in Japanese).

6. **K. Makino**, R. Endo, T. Mochizuki, S. Takebe, and G. Koshii, "Campaign posters detection for TV program production," in *Proc. Forum on information technology 2020*, no. 3, pp. 127–128, Mar. 2020 (in Japanese).

7. **K. Makino**, T. Sato, F. Ito, T. Nakagawa, and N. Iai, "Estimation method for channel quality of TDD SVD-MIMO," *IEICE Tech. Rep.*, vol. 121, no. 103, RCS2021–85, pp. 39–44, July 2021 (in Japanese).

8. **K. Makino**, T. Nakagawa, and N. Iai, "Compensation method for transmission weight matrix of SVD-MIMO using machine learning," *IEICE Tech. Rep.*, vol. 122, no. 106, RCS2022–73, pp. 26–31, July 2022 (in Japanese).

9. **K. Makino**, T. Sato, F. Ito, T. Nakagawa, and N. Iai, "Laboratory experiments of SVD-MIMO with automatic change in the total number of modulation indices," *ITE Tech. Rep.*, vol. 46, no. 25, BCT2022–49, pp. 5–8, Sept. 2022 (in Japanese).

10. **K. Makino**, T. Sato, F. Ito, T. Nakagawa, and N. Iai, "Field trial of SVD-MIMO transmission with automatic change in the total number of modulation indices," *ITE Tech. Rep.*, vol. 47, no. 2, BCT2023–17, pp. 63–66, Jan. 2023 (in Japanese).

11. **K. Makino**, T. Nakagawa, and N. Iai, "Machine-learning based compensation and adaptive transmission control for SVD-MIMO," in *Proc. 2023 IEICE general conference*, no. 1, B-5-6, pp. 251, Mar. 2023 (in Japanese).

12. **K. Makino** and T. Nakagawa, "FPGA implementation of ML-compensation for SVD-MIMO weight matrices," *IEICE Tech. Rep.*, vol. 123, no. 108, RCS2023–99, pp. 103–108, July 2023 (in Japanese).

13. T. Miyazaki, **K. Makino**, Y. Takei, K. Miura, H. Sumiyoshi, and J. Goto, "Extraction system of important tweets for news program production," in *Proc. ITE Annual Convention 2017*, 32B-1, Sept. 2017 (in Japanese), DOI: 10.11485/iteac.2017.0_32B-1.

14. J. Goto, **K. Makino**, Y. Takei, T. Miyazaki, and H. Sumiyoshi, "Automatic manuscript generation for news production," in *Proc. ITE Winter Annual Convention 2017*, 13B-5, Dec. 2017 (in Japanese), DOI: 10.11485/itewac.2017.0_13 B-7.

15. T. Miyazaki, **K. Makino**, Y. Takei, H. Sumiyoshi, and J. Goto, "TV program retrieval from tweets for supporting TV program creation,", in *Proc. ITE Annual Convention 2018*, 32B-1, Aug. 2018 (in Japanese).

16. Y. Takei, **K. Makino**, T. Miyazaki, H. Sumiyoshi, and J. Goto, "Social Media Analysis System for news gathering support," in *Proc. Forum on information technology 2018*, no. 2, E-015, pp. 177–178, Sept. 2018 (in Japanese).

17. Y. Yasuda, **K. Makino**, H. Okamoto, T. Miyazaki, and J. Goto, "Study of multi-Label text classification focusing on the relationship between input sentence and label structure," in *Proc. Forum on information technology 2020*, no. 2, E-011, pp. 133–134, Sept. 2020 (in Japanese).

18. T. Sato, **K. Makino**, F. Ito, T. Nakagawa, and N. Iai, "A study on remote production using next generation mobile relay FPU," *ITE Tech. Rep.*, vol. 45, no. 27, BCT2021–43, pp. 23–28, Oct. 2021 (in Japanese).

19. F. Ito, T. Sato, **K. Makino**, T. Nakagawa, and T. Nakatogawa, "Field Trial of Wireless IP Remote Production using TDD-based FPU," *ITE Tech. Rep.*, vol. 47, no. 11, BCT2023-41, pp. 45-48, Mar. 2023 (in Japanese).

Invited Papers and Lectures

1. T. Miyazaki, Y. Takei, and **K. Makino**, "[Invited Paper] Social Media Analysis System on NHK STRL, and its usage in TV Programs," *The Journal of The Institute of Image Information and Television Engineers*, vol. 74, no. 1, pp. 169-173, Feb. 2020 (in Japanese), DOI: 10.3169/itej.74.169.

2. T. Miyazaki, **K. Makino**, Y. Takei, N. Fujimori, I. Yamada, H. Sumiyoshi, and J. Goto, "Social media analysis using deep learning technology," *ConnecTech Asia 2018*, Singapore, T3-3, June 2018.

3. N. Fujimori, T. Miyazaki, Y. Takei, **K. Makino**, T. Mochizuki, and J. Goto, 'Application of AI image classification technology to news gathering support system based on social media analysis," *NAB Broadcast Engineering and Information Technology Conference 2019 (NAB 2019)*, Washington DC, Apr. 2019, p.183-187

4. T. Miyazaki, Y. Takei, and **K. Makino**, "Social media analysis system on NHK STRL, and its usage in TV programs," *ITE Winter Annual Convention 2019*, Special session 4-5, Dec. 2019 (in Japanese).

5. H. Okamoto, T. Miyazaki, N. Fujimori, **K. Makino**, Y. Yasuda, and J. Goto, "Social big data analysis for TV program production," *ABU Digital Broadcasting Symposium 2020 (ABU DBS 2020)*, Session 8: no. 1, Kuala Lumpur, Malaysia, Mar. 2020.

6. T. Sato, **K. Makino**, F. Ito, F. Uzawa, T. Nakagawa, N. Iai, K. Hatano, T. Ono, H. Sugiyama, H. Saito, and Y. Iwadate, "[Memorial Lecture] Field trial of MIMO system with adaptive transmission control for next generation mobile relay FPU," *ITE Tech. Rep.*, vol. 46, no. 11, BCT2022-30, pp. 37, Mar. 2022 (in Japanese).

Organ Magazines

1. K. Makino, "High-capacity mobile transmission technology for high-quality mobile live program production," *Broadcast Technology*, Japan: NHK, no. 90,

Autumn 2022, ISSN: 1345-4099.

2. **K. Makino**, T. Sato, F. Ito, T. Nakagawa, and N. Iai, "Advancement of Bidirectional-wireless Transmission using Adaptive Control (in Japanese)," *NHK Giken R&D*, Japan: NHK, no. 193, Spring 2023, pp. 32-47, Jan. 2023, ISSN: 0914-7535.

Granted Patents

1. H. Harada, K. Mizutani, and **K. Makino**, PROPAGATION PATH ESTIMATION METHOD, JP.6632364, Jan. 2020.

2. **K. Makino**, T. Miyazaki, J. Goto, and Y. Takei, NEWS MATERIAL CLASSIFICATION APPARATUS, PROGRAM AND LEARNING MODEL, JP.7181693, Dec. 2022.

3. **K. Makino**, T. Miyazaki, and J. Goto, THE TEXT CLASSIFICATION APPARATUS, LEARNING APPARATUS, AND PROGRAM, JP.7186591, Dec. 2022.

Awards

1. Distinguished Service Award, Presented by the IEICE Kansai Student branch, Feb. 2017.

2. Technology Promotion Award (Content Technology Award): T. Miyazaki, **K. Makino**, Y. Takei, Presented by the ITE, May 2019.

Scholarships and Financial Support

1. Category 1 scholarship from JASSO, Apr. 2015-Mar. 2017.